Kobe University Repository : Kernel

PDF issue: 2025-02-11

Optical properties of Si nanocrystal based photonics materials

Imakita, Kenji

(Degree)
博士（理学）
(Date of Degree)
2009-09-25
(Date of Publication)
2014-04-11
(Resource Type)
doctoral thesis
(Report Number)
甲4758
(URL)
https://hdl.handle.net/20.500.14094/D1004758

※ 当コンテンツは神戸大学の学術成果です。無断複製・不正使用等を禁じます。著作権法で認められている範囲内で、適切にご利用ください。

Doctoral Dissertation

Optical properties of Si nanocrystal based photonics materials

July, 2009

Graduate School of Science and Technology
Kobe University

Kenji Imakita

Doctoral Dissertation

Optical properties of Si nanocrystal based photonics materials

Si ナノ結晶をベースとする
フォトニクス材料に関する研究

July, 2009

Graduate School of Science and Technology
Kobe University

Kenji Imakita

Contents

Chapter 1 Introduction **1**
1.1 Needs of Si nanocrystals for Si photonics 1
1.2 Preparation of Si nanocrystals 2
1.2.1 Porous Si 2
1.2.2 Si nanocrystals doped SiO_2 prepared by deposition-based method . 3
1.2.3 Si nanocsrystals doped SiO_2 prepared by sol-gel method 4
1.3 Luminescence properties of Si nanocrystals 5
1.3.1 Luminescence properties of bulk Si 5
1.3.2 Luminescence properties of Si nanocrystals 6
1.3.3 Luminescence properties of P- or/and B-doped Si nanocrystals . . . 9
1.3.4 EL and LED devices made of Si nanocrystals-based materials . . . 10
1.4 Si nanocrystal as a photo-sensitizer of Er ions 12
1.4.1 Er ions 12
1.4.2 Er doped bulk Si 13
1.4.3 Er and Si nanocrystals co-doped SiO_2 14
1.4.4 Optical amplifier made of Er and Si-ncs codoped SiO_2 15
1.5 Nonlinear optical properties of Si nanocrystals 16
1.6 Chapter Overview and Goal of this thesis 19

Chapter 2 Coexistence of two different energy transfer processes from Si nanocrystals to Er ions in SiO_2 **27**
2.1 Introduction 27
2.2 Experimental details 28
2.3 Results and discussions 28
2.4 Conclusion 34

Chapter 3 Spectrally resolved energy transfer from excitons in Si nanocrystals to Er ions **37**
3.1 Introduction 37
3.2 Experimental details 39
3.3 Results and discussions 40
3.4 Conclusion 46

Chapter 4 Interaction between Er ions and shallow impurities in Si nanocrystals **49**

4.1 Introduction 49
4.2 Experimental details 52
4.3 Results and discussions 53
4.3.1 P or B doping 53
4.3.2 P and B doping 60
4.4 Conclusion 64

Chapter 5 Enhancement of radiative recombination rate of excitons in Si nanocrystals on a Au film **67**

5.1 Introduction 67
5.2 Experimental details 68
5.3 Results 69
5.4 Discussions 75
5.5 Conclusion 77

Chapter 6 Nonlinear optical properties of Si nanocrystals embedded in SiO_2 prepared by a co-sputtering method **81**

6.1 Introduction 81
6.2 Experimental details 82
6.3 Results and discussions 83
6.4 Conclusion 90

Chapter 7 Nonlinear optical properties of Phosphorous-doped Si nanocrystals embedded in phosphosilicate glass thin films **93**

7.1 Introduction 93
7.2 Experimental details 94
7.3 Results and discussion 95
7.4 Conclusion 101

Chapter 8 Conclusion **107**

Acknowledgment **111**

List of Publications **113**

Chapter 1

Introduction

1.1 Needs of Si nanocrystals for Si photonics

Si photonics is an emerging field of research and technology, in which various kinds of photonics devices are tried to be integrated on a single Si chip [1–11]. If this is realized, that is, if photons can be generated, guided, amplified, switched, modulated and detected on a single Si chip, this newly developed photonics device can be hybridized with today's microelectronics devices, and will solve a number of problems [12–15]. For example, electrical interconnections based on metal lines widely spread today is the most important limitation on the performances of Si-based microelectronic devices [16, 17]. If we realize optical interconnections for the transfer of information inside a chip, this limitation will be defeated [14, 15].

In order to be integrated on Si substrates, photonics devices are required to be made of Si-based materials. This is because the integration of the different kinds of materials causes some difficulty in manufacturing due to the lattice mismatch and hence results in high-cost [18]. The realization of photonics devices by Si-based materials which can be easily integrated on Si substrates is thus a topic of great interest today [4, 7, 8]. The most challenging and interesting issue is how we realize the active photonics devices, such as light source [8, 10], otical amplifier [20, 21], and optical switching system [2], by Si-based materials. It is generally well known that Si has indirect band structure and is not suitable for the active photonics devices [27]; Since phonons should be involved for its band-edge transitions, the oscillator strength is rather small, resulting in relatively poor optical properties needed for photonics devices. For example, first, they have small radiative transition rate of the band-egde transition and hence long radiative lifetime. Since the lifetime is so long, before the excitons recombine radiatively, they move around the crystals, encounter the non-radiative centers, and then finally recombine non-radiatively. After a great effort on the improvement of photo-luminescence (PL) and electro-luminescence (EL) of Si, the quantum efficiencies are still less than ∼0.1% [22–26]. Second, they show relatively small

nonlinear optical responses. Due to its inversion symmetry of the crystal structure, second order nonlinearity is zero. Furthermore, the third order nonlinearity is rather small because of the small oscillator strength [28, 29]. This small nonlinear optical responses is not suitable for the realization of highly efficient Si-based optical switching system. Further improvements of these optical properties are strongly needed for the realization of Si photonics.

Decreasing the size of Si into nanometer scale (Si nanocrsytals) is the most promising approach for the improvement of these properties [30–38]. Due to confinement of electrons and holes in a space smaller than the exciton Bohr radius of bulk Si crystals (∼4.2 nm), non-phonon transitions are partially allowed and hence oscillator strength is improved. Furthermore, the confinement of electron and holes in a small space suppress their probability of encounter with non-radiative centers. Indeed, light emitting diode made of Si nanocrystals (Si-ncs) doped SiO_2 have been reported to show strong luminescence at room temperature. The nonlinear optical response of Si-ncs has been also reported to be enhanced several orders of magnitudes compared to that of bulk Si, suggesting that Si-ncs are also promising for the realization of the Si-based optical switching systems. Furthermore, Si-ncs based materials in the above reports can be fabricated by conventional CMOS (Complementary Metal-Oxide Semiconductor) technology used for Si based microelectronics with regard to the techniques in their synthesis (chemical vapor deposition,sputter deposition, ion implantation) and in processing (conventional dry and wet etchin g processes). With the aid of CMOS technology, Si-ncs based materials will realize very compact, low-cost, and high-efficiency photonics devices.

Although there are numerous reports on Si-ncs in the view point of both fundamental [41–45] and applied physics [39, 40, 47, 48], the mechanisms of the improved optical properties are still controversial. To further improve these properties and to realize photonics devices with high efficiency, more detailed investigations are definitively necessary. This chapter summarizes the optical properties of Si-ncs based materials revealed by past reports, and then describes the purpose of this thesis.

1.2 Preparation of Si nanocrystals

1.2.1 Porous Si

Porous Si is nano-structured Si obtained by an anodic-reaction-etching of Si substrate in hydrogen fluoride (HF) solution [49]. An anodic reaction is depicted as below.

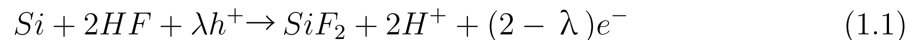

$$Si + 2HF + \lambda h^{+} \rightarrow SiF_2 + 2H^{+} + (2 - \lambda)e^{-} \quad (1.1)$$

Here, h^+ and e^- denote a hole and an electron in Si substrate. Figure 1.1(a)-(c) show the TEM images of Porous Si [49]. We can see that all the samples comprise nano-structured

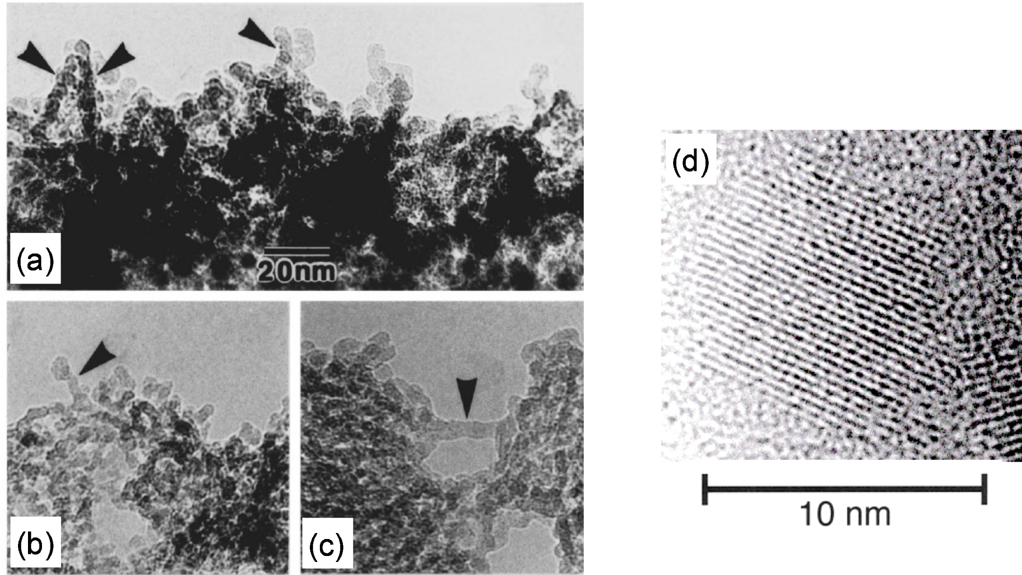

Figure 1.1: (a)-(c) TEM images of Porous Si prepared by a chemical etching of Si wafer, with different preparation conditions [49]. (d) TEM images of Si nano-crystals doped SiO_2 prepared by a reactive sputtering followed by thermal annealing [55].

undulating rod-like Si columns with a diameter of about 3 nm. These porous Si samples are completely crystalline, evidenced by clear transmission electron diffraction patterns. In this preparation method, it is easily possible to control the size of nano-structure by controlling the concentration of HF, the etching time, and the anode current. Since the strong room temperature PL from porous Si was firstly reported [54], many authors have investigated PL properties of Porous Si [50–53]. However, porous Si samples are unstable both chemically and physically. Their surfaces are usually H-terminated and can be easily oxidized in air. Furthermore, they are fragile due to their high porosity (usually higher than 50%). These instability is not suitable for the realization of Si-based photonics devices and even not for elucidating the mechanism of the improved optical properties.

1.2.2 Si nanocrystals doped SiO_2 prepared by deposition-based method

Si-ncs can be fabricated within SiO_2 matrix by following two steps. First, Si-rich SiO_2 (or SiO_x) thin films are formed by some techniques such as sputtering deposition [55, 56], chemical vapor deposition [57], and ion implantation [58, 59]. Second, the obtained SiO_x thin films are treated at or above $1000^O C$ to induce the nucleation, growth and

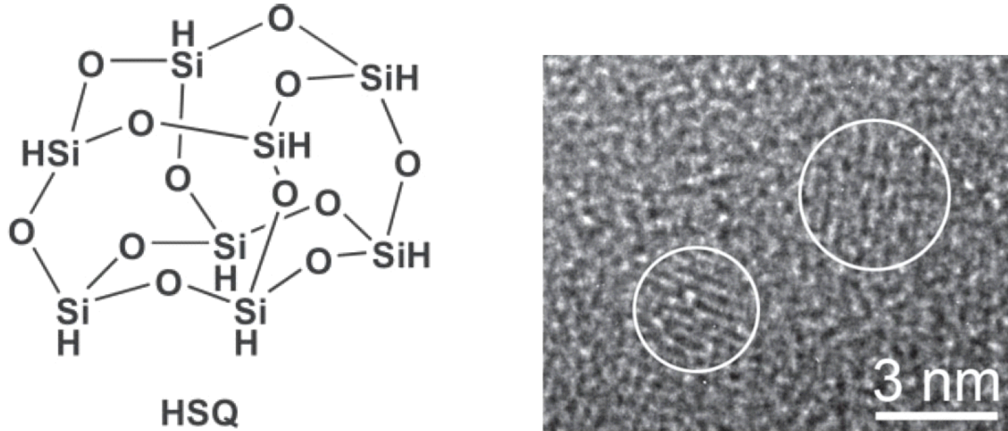

Figure 1.2: (a) Structre of hydrogen silsesquioxane (HSQ). (b) TEM image of Si nanocrystal doped SiO_2 formed by spin coating of HSQ and following thermal treatment [60].

crystallization of Si-ncs within amorphous SiO_2, as shown in the follwoing equation.

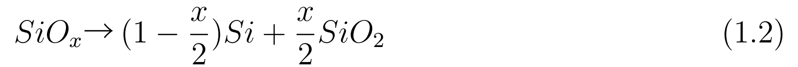

$$SiO_x \rightarrow (1-\frac{x}{2})Si + \frac{x}{2}SiO_2 \tag{1.2}$$

In this method, the size of Si-ncs can be controlled by Si concentration in SiO_x and also by annealing temperature. Compared to porous Si, the obtained Si-ncs samples are stable both chemically and physically, because they are embedded in SiO_2. Furthermore, since the matrix is SiO_2, optical and mechanical coupling with conventional SiO_2 fiber is rather good. In addition, Si-ncs doped SiO_2 can be synthesized and processed with conventional CMOS technology. Thus Si-ncs doped SiO_2 fabricated by these methods is believed to be promising for realizing low-cost high-efficiency compact Si-based photonics devices. Figure 1(d) shows a TEM image of the Si-ncs doped SiO_2 prepared in our laboratory [55] by a sputtering deposition followed by thermal annealing. We can see clear lattice stripes whose spaces corresponding to (111) plane of Si. The average size of Si nano-crystals is about 2.5 to 8.0 nm in diameter, depending on sample preparation conditions. The standard deviation is about 1.0 nm. In this thesis, our discussion will be focused on the Si-ncs based materials prepared by the sputtering methods.

1.2.3 Si nanocsrystals doped SiO_2 prepared by sol-gel method

Recently, C. M. Hessel et al. have succeeded in preparing Si-ncs doped SiO_2 by sol-gel method [60]. In this method, Si-ncs can be formed within SiO_2 just by heating hydrogen silsesquioxane (HSQ, see figure 2(a)). Figure 2(b) shows a TEM image of Si-ncs prepared by this method. Being similar to that prepared by deposition-based method (figure 1(d)), we can see clear lattice stripes corresponding to Si-ncs. HSQ is

a versatile, commercially available compound which is used as high-resolution e-beam resist. Unlike deposition-based methods, macroscopic quantities of Si-ncs doped SiO_2 can be readily produced by this method. Furthermore, since HSQ is an electron beam resist, it is possible to straightforwardly pattern the structures with sub-100 nm dimensions (No separate resist and etching procedures are needed). Thus this method has been attracting much attentions. However, this method is still in the early stage and further fundamental research will be needed to be applied for Si-based photonics.

1.3 Luminescence properties of Si nanocrystals

1.3.1 Luminescence properties of bulk Si

Before understanding the luminescence properties of Si-ncs, we are going to see briefly those of bulk Si. It is well known that bulk Si shows strong temperature quenching of PL and EL [22–24]. It is very important to understand the mechanism of the temperature quenching and to know how we can improve these optical properties. Figure 1.3 shows the schematics of the luminescence mechanism of bulk Si. When electrons are excited by

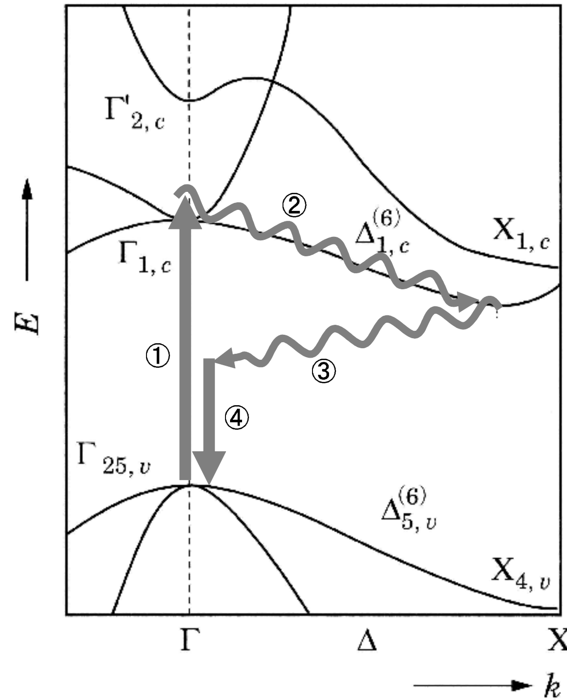

Figure 1.3: The mecahnism of band-edge photo-luminescence of bulk Si. The straight and the wavy line arrows denote photon-involved and phonon-involved transitions, respectively.

photons or carrier injection, in the conduction band, they are readily de-excited to the bottom of the conduction (valence) band with emitting phonons. Then the de-excited electrons form the excitons with holes, and finally they recombine with emitting photons, whose energy corresponds to the band gap of bulk Si (∼1.1eV). The most important feature of bulk Si is in its indirect type band structure. Whereas the top of the valence band is located at the center of Brilluan zone (Γ point), the bottom of the conduction band is at the Δ point near the end of Brilluan zone in the [100] direction [27]. This in-coincidence between the valence top and the conduction bottom in k-space require the involvement of phonons for the radiative recombination of excitons; If no phonons are involved, the recombination cannot conserve momentum(k), because photons have negligibly small momentum. This radiative recombination process is a weak second-order process and its rate is rather small, compared to other compound semiconductor with direct type band structure.

Generally, the quantum efficiency of luminescence (η) is determined by the ratio of the radiative (ω_r) to nonradiative recombination rate(ω_{nr}), as below.

$$\eta = \frac{\omega_r}{\omega_r + \omega_{nr}} \tag{1.3}$$

In addition to the small radiative recombination rate, relatively large non-radiative recombination rate is known to be responsible for the small quantum efficiency of bulk Si. Two dominant origins of the non-radiative recombination processes are known in bulk Si. One is the non-radiative recombination center such as defects or impurities in bulk Si [61]. Before excitons recombine radiatively, they move around in bulk Si crystals, then encounter these non-radiative centers, and finally they recombine non-radiatively via these centers. The other is the thermal dissociation of excitons [62]. Before the excitons recombine radiatively, they dissociate by obtaining thermal energy, and become free carriers, finally loosing their opportunities to recombine radiatively. At room temperatures, these non-radiative recombination processes are much dominant to the radiative recombination process. Thus photo- or electro-luminescence of bulk Si shows strong temperature quenching.

1.3.2 Luminescence properties of Si nanocrystals

Since the strong PL was observed in porous Si in 1990 [54], the origin of the PL from Si-ncs has been intensively studied by both experimentally [30–33] and theoretically [41–44]. It has been reported by several authors that the reduction of the size of Si leads to the enhancement of the radiative recombination rate [53, 63]. Figure 1.4 shows the theoretical calculation of optical band gap (•, left axis) and oscillator strength (×, right axis) of Si-ncs as a function of the size [63]. The optical band gap increases with decreasing

the size of Si-ncs, according to a simple quantum confinement model. We can also see smaller Si-ncs have larger oscillator strength. With decreasing the size, according to the uncertainty principle, the wave-functions of electrons and holes are de-localized in the quasi momentum space. This partially allows zero phonon optical transitions, and thus results in the enhancement of the oscillator strength.

The reduction of the size is also well known to suppress the non-radiative transition rate of Si-ncs [53, 64]. In Si-ncs, carriers are confined in small spatial region. This suppress their probability of encouner with non-radiative recombination centers. Furthermore, thermal dissociation of excitons is also suppressed in Si-ncs. In bulk Si, excitons can become free carriers by the thermal dissociation. This results in the lost of their opportunities to recombine radiatively. However, in Si-ncs, excitons (or electron-hole pairs) cannot become free carriers due to the spacial confinement. Thus the reduction of the size of Si-ncs significantly suppress the nonradiative recombination rate. By the combination of the enhancement of radiative recombination rate and the suppression of the nonradiative recombination rate, Si-ncs show the strong PL and EL even at room temperature.

Figure 1.5(a) shows the PL spectra of porous Si [49]. The PL intnsity of porous Si increases with increasing the etching time. The blue shift of the spectra by the etching can be qualitatively explained by simple quantum size effect. The PL spectra are inhomogeneously broadened due to their large size- and shape-distributions. Due to this inhomogeneity, the origin of the strong PL sometimes become obscure; sometimes PL

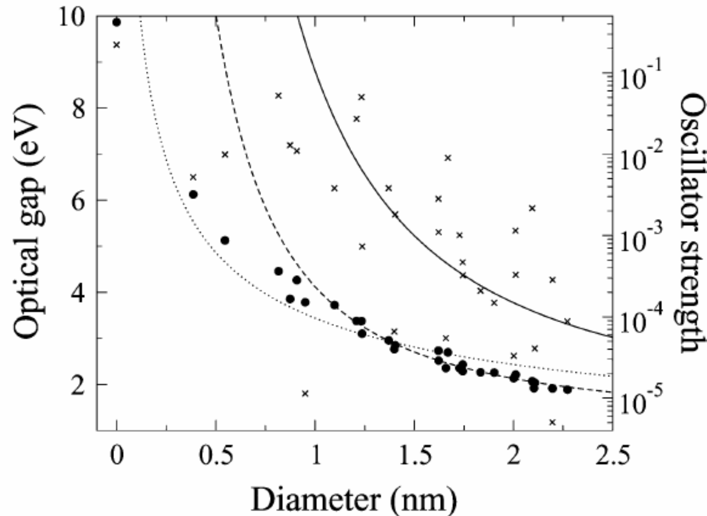

Figure 1.4: Optical gaps (•, in eV) and oscillator strengths (×) for silicon clusters of different size as a function of the cluster diameter calculated at the BP TDDFT level using the def2-SV(P) basis set [63].

from defects in the matrix at the surface of Si-ncs or are mixed in the broad spectra. One possible way to lift the inhomogeneous broadening is the resonantly excited PL spectra at low temperature [65]. When the photon energy of the excitation source is inside the emission band of Si-ncs, only the larger Si-ncs, i.e. smaller band gap ones, are excited, thus size-selectd excitation is possible. Figure 5(b) shows the result of the resonantly excited PL [65]. We can see that inhomogeneous broadening is partially lifted and that periodical structure appears in the spectra. This structure implies the involvement of phonons in the radiative recombination processes in Si-ncs. Since the phonons should be emitted to meet the momentum conservation rule, Si-ncs show PL at the energies coinciding with the excitation energy minus integer number of the phonon energies. This result also suggests that Si-ncs strongly inherit the indirect band structure and the radiative recombination rate is not so enhanced, in spite that the PL at room temperature is strongly enhanced compared to that of bulk Si; the suppression of non-radiative recombination rate is more responsible for the improved PL of Si-ncs than the enhancement of radiative recombination rate. The further improvement of radiative recombination rate of Si-ncs has been a topic of great interest today.

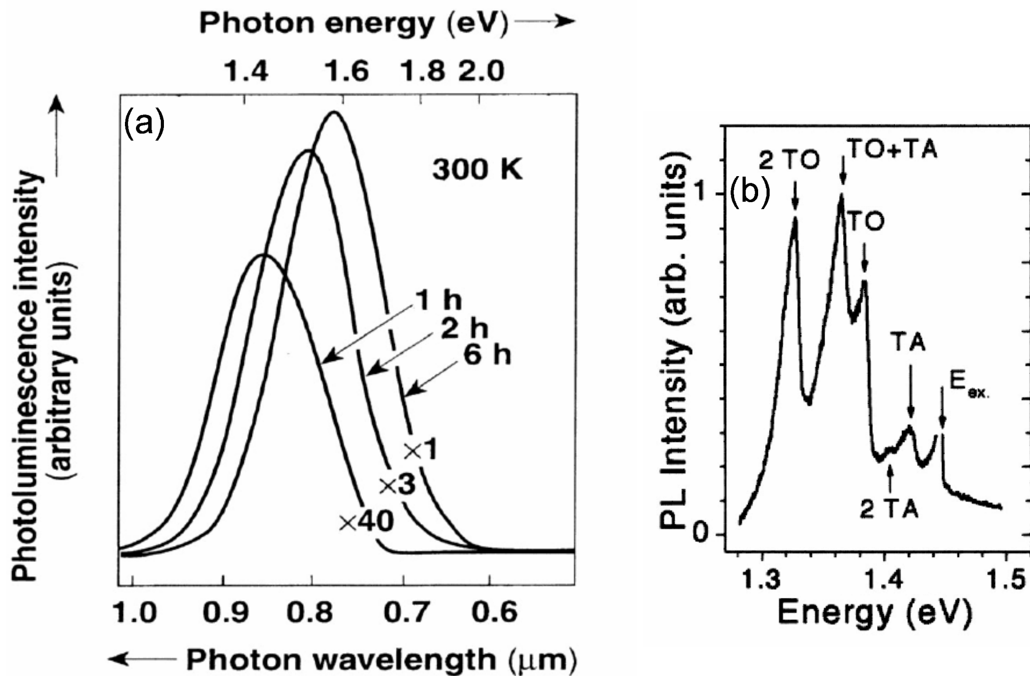

Figure 1.5: (a)PL spectra of Porous Si reported by Chanham et al., the PL energy can be controlled by the porosity (or size) of nanostructured Posous Si [49]. (b)Resonantly excited PL spectra of Porous Si at low temperature reported by Kovalev et al. Clear phonon structures can be seen in the spectra [65].

It should be noted here that some authors suggest that defect-related state is responsible for the strong PL of Si-ncs. The theoretical calculation revealed that Si=O bonds at the surface of Si-ncs form the energy level at 1.6 eV [42]. The electron-hole pairs are suggested to recombine via this energy level [66]. However, this model cannot explain the phonon structure shown in figure 1.5(b). In this thesis, the discussion on the defect-related PL shall be excluded out because our sputter-deposited samples studied in this thesis show phonon structure in the resonantly excited PL spectra, being similar to that observed in porous Si [67].

1.3.3 Luminescence properties of P- or/and B-doped Si nanocrystals

In bulk Si, it is generally known that doping impurities strongly change its electronic band structure and its electronic transport properties. The technology of controlling the doping is key technology of today's Si-based microelectoronics. The effect of doping on the Si-ncs is studied both experimentally [68, 71, 72] and theoretically [69, 70]. Fujii et. al. have firstly succeeded in preparing Si-ncs with electrically active carriers, evidenced by the appearance of infrared absorption which is very similar to free carrier absorption in bulk Si, and by the ESR signal peaked at g=1.98 which can be assigned to free electron within Si-ncs [71, 72].

Figure 1.6(a) demonstrate the effect of B-doping on the PL properties of Si-ncs [73]. With increasing B concentration, PL intensity decreases. The origin of this quenching of the PL intensity is suggested to be the non-radiative Auger interactions between photo-

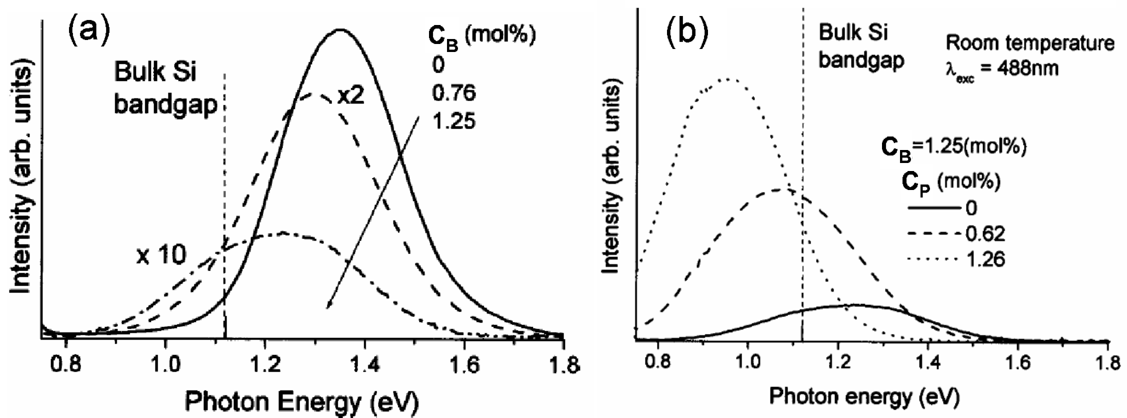

Figure 1.6: (a)PL spectra of B-doped Si nanocrsytals. B-doping results in the quenching of PL from Si nanocrystals. (b)PL spectra of P- and B-doped Si nanocrystals. The simultaneous co-doping results in the recovery of the PL intensiry of Si nanocrystals [73].

excited electron-hole pairs and impurity-supplied holes (three body Auger interaction). This model is validated by P and B co-doping. By the co-doping, P-supplied electrons and B-supplied holes are compensated within Si-ncs. Thus the three body Auger interaction can be inhibited. In Figure 1.6(b), the PL spectra of the co-doped Si-ncs are shown. We can see that the suppressed PL intensity of B-doped Si-ns can be recovered by the additional P-doping. This suggest that the electrons and holes are compensated within Si-ncs. The P and B co-doping accompanies the redshift of PL as shown in figure 1.6(b). The PL peak energy reaches $\sim$0.9eV, which is smaller than the band gap of bulk Si. This redshift can be attributed to the impurity levels formed inside the band gap of Si-ncs. Photo-excited electrons (holes) are trapped at the P- (B-) related levels below (above) the conduction (valence) band, and then the electrons and holes recombine via impurity levels. Since the energy gap between P- and B-related levels is smaller than band gap of Si-ncs, the PL of the co-doped Si-ncs is red-shifted. Furthermore, the oscillator strength of Si-ncs may be enhanced due to the co-doping. By localizing electrons and holes in real space at impurities sites, the wavefunctions of them are delocalized in the quasi momentum space. This allows the zero-phonon recombination processes, resulting in the enhancement of the oscillator strength. These results suggest that in addition to size, impurity doping can ba another parameter to control the optical properties of Si-ncs. It is definitely worth studying in more detail the optical properties of doped Si-ncs.

1.3.4 EL and LED devices made of Si nanocrystals-based materials

The main problem to realize the efficient EL or LED devices made of Si-ncs based materials is the efficient carrier injection. Since the SiO_2 is, unfortunately, the good insulating material, Si-ncs doped SiO_2 was considered not to be suitable for the EL devices. Porous Si is more suitable for carrier injection than Si-ncs doped SiO_2. However, as mentioned in the section 1.2.1, it is chemically and physically unstable, and not suitable for the realization of practical devices. The first breakthrough was reported by N. Lalic et. al. for the Si-ncs doped SiO_2 prepared by ion-implantation [74]. By confining Si-ncs in a ultra thin SiO_2, they have succeeded in the observation of the room temperature EL. After this discovery, a number of successful results have been reported. In most of the reported devices the EL is produced by impact excitation where energetic electrons which can penetrate through the insulating matrix were used for the excitation of electron-hole pairs within the Si-ncs [36, 75]. Although the strong emission at room temperature has been observed, the impact excitation was still inefficient and also it induced damage in the SiO_2 matrix due to the energetic electron flow. Very recently, to overcome this problem, R. J. Walters et al. applied a FET (Field Emission Transistor) structure where the gate

dielectric is a thin oxide with a layer of Si-ncs [76]. By changing the sign of the gate bias, separate injection of electrons (Figure 1.7(a)) and holes (Figure 1.7(b)) in the Si-ncs is achieved. Luminescence is observed only when both electrons and holes are injected into Si-ncs (Figure 1.7(c)). By using this pulsing bias technique, alternate charge carrier injection is achieved. This will lead to high efficiency in the emission of the LED, and will open the new bright possibility in this field .

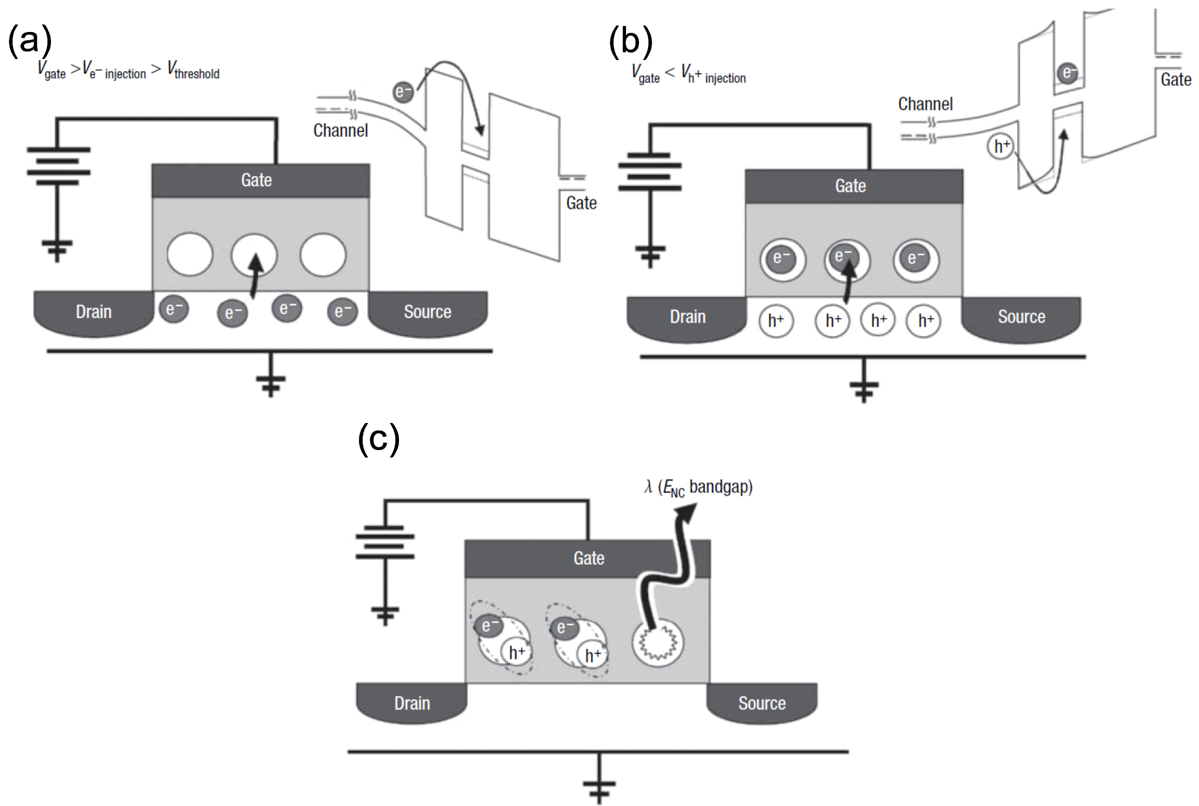

Figure 1.7: Schematic of the field-effect electroluminescence mechanism in a silicon nanocrystal floating-gate transistor structure. Inset band diagrams depict the relevant tunneling processes. The array of silicon nanocrystals embedded in the gate oxide of the transistor can be sequentially charged with electrons (a) by Fowler-Nordheim tunneling, and holes (b) via Coulomb field-enhanced Fowler-Nordheim tunneling to prepare excitons that radiatively recombine (c) [76].

1.4 Si nanocrystal as a photo-sensitizer of Er ions

1.4.1 Er ions

Erbium ion (Er^{3+}) is one of the rare earth ions. Being similar to other rare earth ions, this ion shows photo-luminescence arising from intra-4f shell transitions. This is parity- and spin-forbidden transition and thus the oscillator strength is rather small. However, in oxide matrix such as SiO_2, it shows strong luminescence at room temperature, because the non-radiative transition rate is relatively small in these matrices. Furthermore, since the intra-4f shells are surrounded by more external 5d-shell and not affected by the surrounding matrix, they show atomic-like sharp luminescence. In addition, fortunately, this sharp luminescence appears at 1.5μm, which is used as standard wavelength in the optical telecommunication. Due to the above reasons, Er^{3+} doped SiO_2 is generally used for the fiber-type optical amplifier operating at 1.5μm, which is called EDFA(Er-Doped Fiber Amplifier).

Although EDFA is now used as a standard in the field of optical telecomunication, further improvement of their properties are strongly required. For example, Er^{3+} show very sharp absorption spectra with very small absorption coefficient, reflecting the discrete energy levels and small oscillator strength. Therefore, high-cost and high power laser whose lasing wavelength is finely tuned to the sharp absorption peak of Er ions (980nm or 1.5μm) are required for EDFA. Furthermore, since the oscillator strength of the intra-4f shell transitions are very small, fibers as long as several tens of meters are needed to obtain the enough signal-gain for practical use. The one approach to obtain larger gain is to increase the concentration of Er ions in EDFA. However, higher Er concentration is

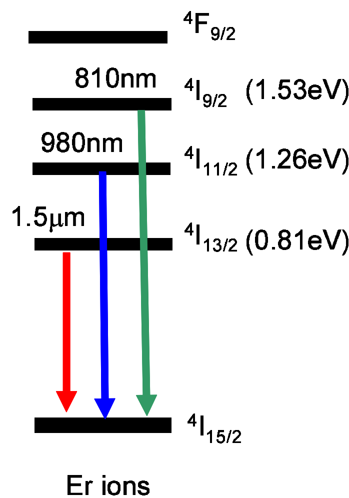

Figure 1.8: Energy diagram of intra-4f shell of Er ions.

known to result in less gain due to the increase of the Er-Er interactions (this is called concentration quenching) [77]. Another way to get larger gain is to use photo-sensitizers of Er^{3+}. For example, Ytterbium ions (Yb^{3+}) were found to act as a photo-sensitizers of Er^{3+} [78, 79]. In the case of Yb^{3+} and Er^{3+} co-doped SiO_2, Yb^{3+} efficiently absorb the excitation light at 980 nm, instead of the non-efficient absorber of Er^{3+}. Then Yb^{3+} efficiently transfer the excitation energy to Er^{3+}. Concequently, the effective excitation cross section of Er^{3+} can be significantly enhanced (about one order of magnitude). This is the great improvement, however, Yb^{3+} are also rare earth ions, and show sharp absorption spectra, like Er^{3+}. Therefore, high-cost laser whose lasing wavelength is finely tuned to the discrete energy levels of Yb^{3+} is needed for EDFA even if Yb ions are co-doped. More efficient photo-sensitizer is needed for the further improvement of EDFA properties.

1.4.2 Er doped bulk Si

In 1980, Ennen et al. reported that, in bulk Si, Er^{3+} show strong PL at low temperature [80]. It was found that in this material, Er^{3+} are excited by energy transfer from excitons in bulk Si. Figure 1.9(a) shows the schematics of the excitation mechanism of Er^{3+} in bulk Si [81, 82]. First, exciton is excited in bulk Si by photons or carrier injection. Second, the exciton is trapped at the Er-related levels formed 0.15 eV below the band edge of bulk Si. Finally, the excitation energy is transfered to the first excited state of Er^{3+} ($^4I_{13/2}$) via Auger-like interaction. (Note that energy transfer to the second excited state ($^4I_{11/2}$) is impossible because the energy of $^4I_{13/2}$ state is lager than band-gap of bulk Si.) Since bulk Si have large abrosption coefficient in whole visible range, low-cost and low-power light

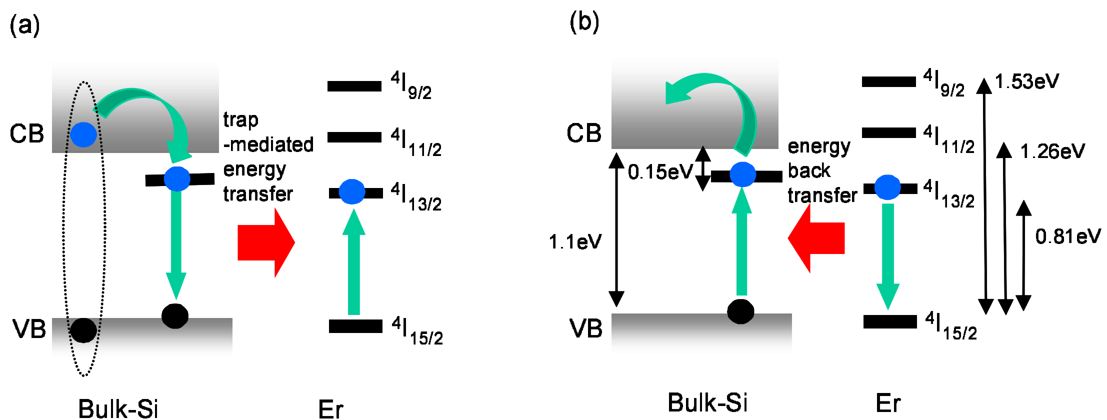

Figure 1.9: (a)Excitation and (b)De-excitation mechanisms of Er ions doped in bulk Si. Er ions are excited by energy-transfer from excitons trapped at Er-related levels, and de-excited by its reverse process, which called energy-back-transfer process.

source such as LED chip or flash lamp can be used for the excitation of Er^{3+}. Furthermore, in bulk Si, the excitation of Er^{3+} by carrier injection is also easily achieved by forming p-n junctions. Thus Er^{3+} doped bulk Si had attracted much attentions.

However, PL or EL of Er^{3+} in bulk Si was known to show strong temperature quenching and show no luminescence at room temperature. Figure 1.9(b) shows the mechanism of the temperature quenching, i.e., the de-excitation mechanism. Since the energy of Er-related energy level inside bulk Si band gap is comparable to that of the $^4I_{13/2}$ state of Er^{3+}, excited Er^{3+} again transfer their energy back to the bulk Si, i.e., electrons are excited to the Er-related level in bulk Si by energy transfer from Er^{3+}. Then, the electron trapped at the Er-related level dissociate by obtaining the thermal energy. Thus Er^{3+} in bulk Si show strong temperature quenching. The overcome of this temperature quenching is necessary and great effort have been devoted for this.

1.4.3 Er and Si nanocrystals co-doped SiO_2

Er^{3+} and Si-ncs co-doped SiO_2 (Er:Si-ncs:SiO_2) is now the most promising material for the realization of the high-efficiency and low-cost Si-based optical amplifier operating at $1.5\mu m$ [83–88]. In Er:Si-ncs:SiO_2, Er^{3+} are excited by the energy transfer from photo-excited electron-hole pairs within Si-ncs, being similar to the case of Er doped bulk Si (Er:bulk-Si). The effective excitation cross section of Er^{3+} is enhanced more than 4 orders of magnitudes compared to that of Er^{3+} in SiO_2 (Er:SiO_2). Furthermore, in this material, Er^{3+} show no temperature quenching. This is remarkable and in a sharp contrast with the strong temperature quenching observed in Er:bulk-Si. The strong luminescence of Er^{3+} can be observed even at room temperature.

Figure 1.11(a) shows typical PL spectra of Er:Si-ncs:SiO_2 prepared in our laboratory. The PL peak at around 1.5 eV is assigned to the recombination of electron-hole pairs within Si-ncs, and that at around 0.81 eV is to the infra-4f shell transition of Er^{3+}. With increasing Er ions, the PL of Si-ncs decreases and that of Er^{3+} increases. This suggests that excitation energy of Si-ncs is transfered to Er^{3+}. Figure 1.11(b) shows PL excitation (PLE) spectra of Er^{3+} in Er:Si-ncs:SiO_2 and in Er:SiO_2. PL intensities of Er^{3+} at 0.81 eV (or 1.5μm) are plotted as a function of the excitation wavelength. We can see the significant enhancement of PLE spectra of Er^{3+} by the presence of Si-ncs in whole visible range.

Due to this promising feature, the mechanisms of the interaction between Er^{3+} and Si-ncs has been intensively studied. The strong coupling between Er^{3+} and Si-ncs are generally observed for Er:Si-ncs:SiO_2 prepared by various kinds of preparation method. such as ion CVD [83], sputtering [84, 85], ion implantation [86, 87], sol-gel [60], and so on. However, the microscopic mechanisms of the coupling are still not clear. For example,

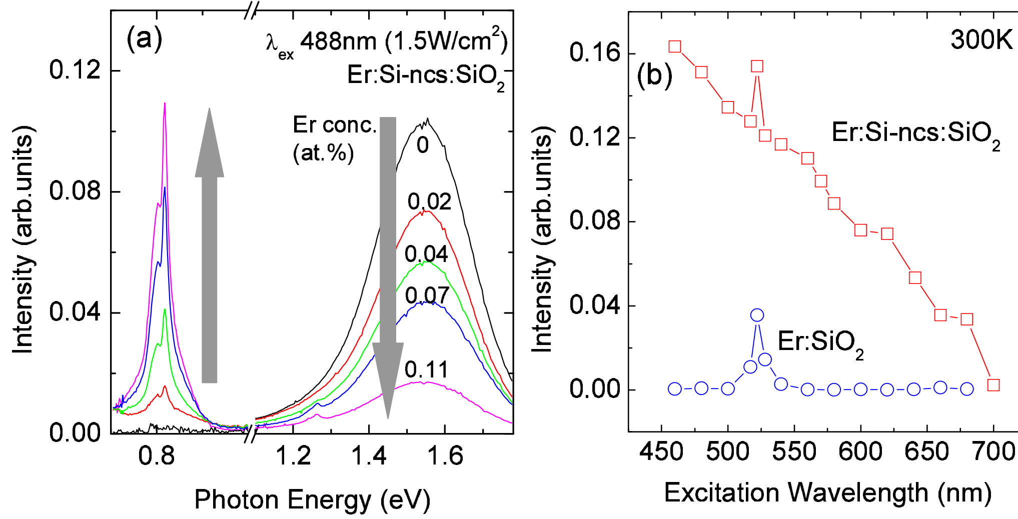

Figure 1.10: (a)Er concentration dependence of PL spectra of Er:Si-nc:SiO$_2$. With increasing Er concentration, the PL of Si-ncs is supressed and that of Er ions is enhanced. (b)PLE spectra of Er:Si-nc:SiO$_2$ and Er:SiO$_2$ with the detection of Er-PL. By the additon of Si-ncs, the PL intensity of Er ions is significantly enhanced in visible range excitation.

first, it is not clear which states of Er^{3+} are excited by the energy transfer. In Er:bulk-Si, the first excited state of Er^{3+} ($^4I_{13/2}$) is excited. This is very clear because the energy of the second excited state of Er^{3+} ($^4I_{11/2}$) is larger than the band gap of bulk Si. On the other hand, in Er:Si-nc:SiO$_2$, The band gap Si-ncs are enlarged due to quantum confinement effect. Therefore, the energy transfer to the second or third excited states of Er^{3+} ($^4I_{11/2}$ or $^4I_{9/2}$) seems to be also possible. Second, it is not clear whether or not the Er related level is formed inside Si-ncs, and whether or not this level participate in the enegy transfer. If the Er^{3+} are doped into Si-ncs, Er-related state should be formed inside the bandgap of Si-ncs. However, Er^{3+} may be located outside Si-ncs. In this case, Er-related energy level may not be formed inside the band gap of Si-ncs, and thus the energy transfer mechanism is considered to be different from that of bulk Si systems. The elucidation of these essential issues are of great interests today.

1.4.4 Optical amplifier made of Er and Si-ncs codoped SiO$_2$

Although the microscopic mechanism of the energy transfer is still skeptical, the large optical gain have been reported by using this material. The first observation of the optical gain is made by J. H. Shin et al. [20]. Figure 1.11 show the signal enhancement

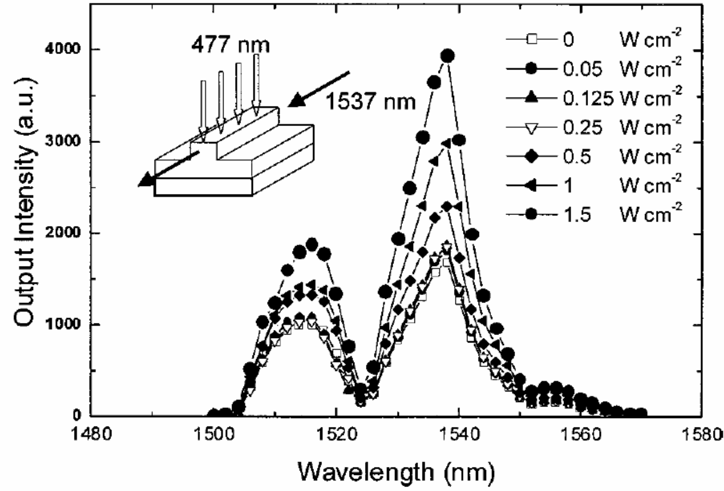

Figure 1.11: The spectra of the external signal from a 1537 nm laser after being transmitted through the waveguide. The experimental setup used to measure the spectra is shown schematically in the inset. Note the increase in the transmitted signal as the pump power is increased beyond 0.25W/cm^2 [20].

at 1.5μm in an Er-coupled Si-nc ridge-type waveguide versus the pumping power density using top pumping as shown in the inset. The excitation wavelength is 477 nm, which coincides with no energy levels of Er^{3+}. Thus Er^{3+} are considered to be excited by energy transfer from Si-ncs. The deduced internal gain was as large as 7 dB/cm. After this succesful reports, low-cost and small-chip LED was demonstrated to be used to obtain the optical gain instead of high-cost and high-power laser [21]. On the other hand, another reports showed no or weak signal enhancement with similar experiment [89]. As possible mechanisms of the small gain, propagation losses, saturation of Er ions, up-conversion of the pumpled light, and confined carrier absorption have been proposed. The machinsims of the optical gains and losses are still now controversial. In order to obtain larger optical gain, detailed mehcanism of the excitation and de-excitation in this material are strongly required to be elucidated.

1.5 Nonlinear optical properties of Si nanocrystals

Nonlinear optics is a field of optics which describe materials in which the dielectric polarization (P) responds nonlinearly to the electric field (E) of the light. In relatively weak or normal E conditions, P responds linearly to E. All of the optical phenomena such as refraction, reflection, and absorption, observed in daily life can be well explained by this linear response. On the other hand, in extremely strong E conditions, for example,

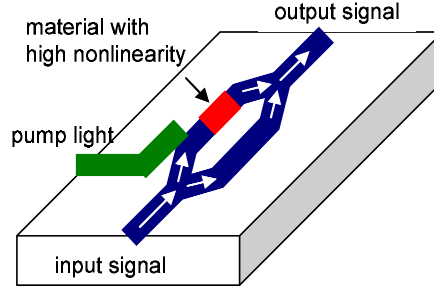

Figure 1.12: Schematic of Machzehnder type optical switching system. The control of the interference by the nonlinear optical response realizes the all optical switching systems.

in those generated by very high-power laser, P responds nonlinearly to E as below.

$$P = \epsilon_0(\chi^{(1)}E + \chi^{(2)}E^2 + \chi^{(3)}E^3 + \cdots).$$

Here, $\chi^{(1)}$ and $\chi^{(n)}$ $(n \geq 2))$ are linear and n^{th} order nonliniear susceptibility of materials. ϵ_0 is permittivity in vacuum. Materials with inversion symmetry have no second order nonlinearity. Thus, $\chi^{(2)}$ is zero and $\chi^{(3)}$ plays a most important role in the nonlinear optical response of Si-ncs doped SiO_2. The third order optical nonlinearity, or $\chi^{(3)}$, is known to cause intensity-dependent refractive index and absorption as below.

$$n = n_0 + n_2 \cdot I$$
$$\alpha = \alpha_0 + \beta \cdot I$$

Here, n_0 and α_0 are linear refractive index and absorption coefficient, n_2 and β are nonlinear refractive index and nonlinear absorption coefficient (or two photon absorption). I is the intensiy of incident light. Strong I causes the refractive index and absorption change due to the third order nonlinear response. By using this phenomena, Machzehnder type optical switching system (see figure 1.12) can be realized. One input light signal diverges into two chanels, and then the two diverged signals again converges into one chanel in this system. The convergence accompanies the interference of the two signals. If we embedd high-nonlinear materials in one chanel, we can cause a pahse-shift in this chanel by inducing strong E generated by pump laser. This enable us to control the strength of the interference and consequently the intensity of the output signal.

In addition to the large nonlinearity, small linear refractive index and very fast time response of the nonlinearity are required for the high-nonlinear materials in optical switching system. The small linear refractive index minimizes the optical coupling loss with the conventional SiO_2 fiber and the fast time response helps to realize the ultra-fast optical switching system . In these points, Si-ncs doped SiO_2 is a very promising material. Firstly, n_2 and β of Si-ncs has been reported to be enhanced more than one orders of

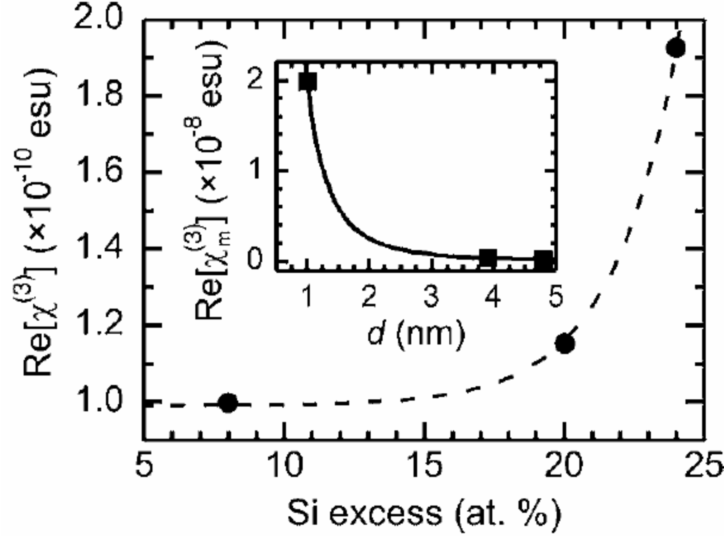

Figure 1.13: Real part of the electronic susceptibility vs Si excess at 1.5 eV; the dashed line is a guide to the eye. In the inset, the real part of the microscopic susceptibility at the same excitation energy has been represented as a function of the Si nanocrystal size; the solid line represents the best fit to $1/d^3$ *[93].*

magnitudes than that of bulk-Si, and three orders of magnitudes larger than SiO_2 in a relatively transparent energy range. Secondly, whereas the linear refractive index of bulk Si is about as large as 3.5 in visible or near infrared region, that of Si-ncs doped SiO_2 is small and typically less than 1.8. Thirdly, since the large nonlinearity arises from bound electrons, the time response of the nonlinearity is very fast (in the order of several tens *psec*).

Motivated by these promising features, there have been many reports on nonlinear optical response of various forms of Si-ncs, such as porous Si [90, 91], Si-ncs doped SiO_xN_y deposited by CVD [92, 93], Si-ncs doped SiO_2 prepared by a sol-gel method [94], and so on. All of the reports observed a significant enhancement of n_2, compared to bulk-Si. However, the magnitudes of the enhancement strongly depend on the preparation method. The reported values of n_2 varied from $\sim 10^{-7}$cm^2/W to $\sim 10^{-13}$cm^2/W, and both positive and negative n_2 were reported for various forms of Si-ncs. Due to these confusing results, the origin of the large n_2 is still not clear.

There are two possible origins of this large nonlinear optical response. One is quantum size effect. The modification of the electronic band structure of electron-hole pairs within Si-ncs causes the size-dependent $\chi^{(3)}$ enhancement. The inset of Fig. 1.13 shows the size dependence of $\chi^{(3)}$ of Si-ncs doped SiO_2 prepared by PECVD [93]. We can see that $\chi^{(3)}$ is significantly enhanced with decreasing the size of Si-ncs (d), followed by the $1/d^3$

dependence (solid line in the inset) predicted by a simple quantum confinement model. The other possible origin is that surface defect. The theoretical calculation revealed that Si=O bonds at the surface of Si-ncs form the energy level at 1.6 eV [42]. Some authors suggest the this state is responsible for the n_2 enhancement of Si-ncs [95]. At present, no definite conclusion is obtained on the origin of the large n_2 and further intensive research is required to clarify the origin.

1.6 Chapter Overview and Goal of this thesis

The final goal of this thesis is to contribute to the realization of Si-based photonics. To achieve this goal, the author aimed to clarify the optical properties of various kinds of Si-ncs based materials, elucidate some important mechanisms, and explore new Si-ncs based photonics materials. Topics of this thesis can be categorized into three groups. First one is photo-sensitized PL from Er in Er:Si-ncs:SiO_2. The goal this topic is the elucidation of energy exchange mechanism between Er and Si-ncs in Er:Si-ncs:SiO_2. Second one is PL from Si-ncs in SiO_2. The goal of this topic is to enhance the radiative transition rate of Si-ncs. Third one is the nonlinear optical properties of Si-ncs. The goal of this topic is to investigate the nonlinear optical properties of Si-ncs and explore new Si-ncs based materials for nonlinear photonics. Hereafter we are going to see the overview of each chapter.

Elucidation of energy exchange mechanism between Er and Si-ncs (chapter 2-4)

In chapter 2, the mechanism of energy transfer from Si-ncs to Er is studied by analyzing delayed infrared luminescence from Er after short-pluse photo-excitation of Si-ncs sensitizer. From the analysis of the delayed luminescence, the author propose, that there are two different energy transfer processes, i.e., fast and slow processes occuring simultaneously in Er:Si-ncs:SiO_2. The analysis also enable us to estimate the ratio of slow to fast processes, and energy transfer time of the slow process. The ratio and the energy transfer time is shown to depend on the Si-nc size and Er concentration. These give us a deep insight that the the fast energy transfer is bulk-Si:Er-like, i.e., a trap-mediated energy transfer, and the slow one is a characteristic process occurring only in Er:Si-ncs:SiO_2 system. In chapter 3, the energy transfer from Si-ncs to Er^{3+} is studied spectroscopically. At low temperatures, inhomogeneously broadened PL bands of Si-ncs are partially quenched and some dips are observed. The energy in which dips appear coincides with discrete energy levels of Er^{3+}. The author suggests that this is the direct evidence that there occurs a resonant energy transfer process from electron-hole pairs within Si-ncs to Er^{3+}

in Er:Si-ncs:SiO_2. This process is considered to be characteristic process occurring only in Er:Si-ncs:SiO_2 system. This result is consistent with the conclusion of chapter 1.

In chapter 4, the interaction between Er^{3+} and shallow impurities in Si-ncs is studied for Er:Si-ncs:SiO_2. The author shows the luminescence property of Er^{3+} is strongly modified by shallow impurities in Si-ncs. The formation of excess carriers in Si-ncs by P or B doping results in the quenching of infrared luminescence of Er^{3+}, while the compensation of the carriers by P and B co-doping recover the quenched PL. The author propose that the Auger interaction between Er^{3+} and the impurity-supplied carriers in Si-ncs is responsible for the quenching and recovering of the PL. It is also shown that the estimated Auger coefficient is much smaller than that of Er doped bulk Si. This small Auger coefficient is probably responsible for the small temperature quenching of PL of Er in Er:Si-ncs:SiO_2 systems.

Control of photonic mode density for the improvement of the radiative transition rate of Si-ncs (chapter 5)

In chpater 5, the author try to enhance the radiative transition rate of Si-ncs by controlling the the local photonic mode density (PMD). As one approach to enhance PMD, assymetric Au half-mirror cavity is applied, i.e., Au mirror just depositted on the Si-ncs:SiO_2 thin films. Time-resolved photoluminescence (PL) spectra of Si-ncs:SiO_2 on Au thin films demonstrates the enhancement of the radiative transition rate of Si-ncs. The semi-classical calculation of PMD can qualitatively explain the observed wavelength-dependent enhancement.

Investigation of nonlinear optical properties of Si nanocrystals (chapter 6-7)

In chapter 6, nonlinear optical properties of Si-ncs:SiO_2 are studied by z-scan technique in a femtosecond regime at around 1.6 eV. The nonlinear refractive index (n_2) and nonlinear absorption coefficient (β) are strongly enhanced compared to those of bulk Si. In the diameter range of 2.7 to 5.4 nm, the size dependence of n_2 coincided well with that calculated by a pseudoptential approach. The author suggests that the discrete energy states of Si-ncs are responsible for the observed enhanced optical nonlinearity. In chapter 7, nonlinear optical properties of phosphorus (P) -doped silicon (Si) nanocrystals are studied. n_2 and β of Si-ncs are significantly enhanced by P-doping. The enhancement of n_2 is accompanied by the increase of the linear absorption in the same energy region. The author suggests that impurity-related energy states are responsible for the enhancement of the nonlinear optical response.

References

[1] L. Pavesi and D. J. Lockwood, Materialstoday, **7**, 53 (2004).

[2] T. Tanabe, M. Notomi, S. Mitsugi, A. Shinya, and E. Kuramotchi, Appl. Phys. Lett., **87**, 151112 (2005).

[3] H. Yamada, T. Shu, S. Ishida, and Y. Arakawa, IEEE J. Sel. Top. Quantum Electron. **12**, 1371 (2006).

[4] V. R. Almeida, C. A. Barrios, r. R. Panepucci, and M. Lipson, Nature, **431**, 1081 (2004).

[5] V. R. Almeida, C. A. Barrios, r. R. Panepucci, M. Lipson, M. A. Foster, D. G. Ouzounov, and A. L. Gaeta, Opt. Lett., **29**, 2867 (2004).

[6] B. Jalali, and S. Fathpour, J. Lightw. Technol., **24**, 4600 (2006).

[7] Graham T. Reed, Nature, **427**, 595 (2004).

[8] H. Rong, R. Jones, A. Liu, O. Cohen, D. Hak, A. Fang, and M. Paniccia, Nature**433**, 725 (2005).

[9] L. Pavesi, Materialstoday, **8**, 18 (2005).

[10] L. Pavesi, L. Dal Negro, C. Mazzoleni, G. Franzo, and F. Priolo, Nature, **408**, 23 (2000).

[11] Leigh Canham, Nature, **408**, 312 (2000).

[12] Jahns J. Proc. IEEE, **82**, 1623 (1994).

[13] M. R. Feldman, S. C. Esener, C. C. Guest, and S. H. Lee, Applied optics, **27**, 1742 (1988).

[14] Goodman J.W., Leonberger F.J., Sun-Yuan Kung, and Athale R.A., Proc. IEEE, **72**, 850 (1984).

[15] Nordin R. A., Holland, W. R., Shahid, M. A., J. Lightw. Technol., **13**, 987 (1995).

[16] E. D. Kyriakis, N. Haralabidis, M. Lagadas, A. Georgakilas, Y. Moisiadis, and G. Halkias, J. Lightw. Technol., **19**, 1532 (2001).

[17] J. A. Davis, R. Venkatesan, A. Kaloyeros, M. Beylansky, S. Souri, K. Banerjee, K.C. Sarawat, A. Rahman, R. Reif, and J. D. Meindl, Proc. IEEE, **89**, 305 (2001).

[18] G. Roelkens, J. Van Campenhout, J. Brouckaert, D. Van Thourhout, R. Baets, P. Rojo Romeo, P. Regreny, A. Kazmierxzak, C. Seassal, X. Letartre, G. Hollinger, J. M. Fedeli, L. Di Cioccio, and c. Lagahe-Blanchard, Materialstoday, **10**, 36 (2007).

[19] Soref, R. A., Proc. IEEE, **81**, 1687 (1993).

[20] Hak-Seung Han, Se-Young Seo, and Jun H. shin, Appl. Phys. Lett., **79**, 4568 (2001).

[21] Jinku Lee, Jun H. shin, and Namkyoo Park, J. Lightwave Technology, **23**, 19 (2005).

[22] E. O. Sveinbjornsson, J. Weber, Appl. Phys. Lett., **69**, 2686 (1996).

[23] V. V. Kveder, E. A. Steinman, S. A. Shevchenko, H. G. Grimmeiss, Phys. Rev. B, **51**, 10520 (1995).

[24] W. L. Ng, M. D. Lourenco, R. M. Gwilliam, S. Ledain, G. Shao, K. P. Homewood, Nature, **410**, 192 (2001).

[25] M. A. Green, J. Zhao, A. Wang, P. J. Reece, M. Gal, Nature, **412**, 805 (2001).

[26] J. M. Sun, T. Dekorsy, W. Skorupa, B. Schmidt, M. Helm, Appl. Phys. Lett., **83**, 3885 (2003).

[27] E. O. Kane, Phys. Rev. B, **146**, 558 (1966).

[28] H. Fukuda, K. Yamada, T. Shoji, M. Takahashi, T. Tsuchizawa, T. Watanabe, J. Takahashi, and S. Itabashi, Optics. Express, **13**, 4629 (2005).

[29] M. Dinu, F. Quochi, and H. Garcia, Appl. Phys. Lett., **82**, 2954 (2003).

[30] M. Zacharias, J. Heitmann, R. Scholz, U. Kahler, M. Schumidt, and J. Blasing, Appl. Phys. Lett., **80**, 661 (2002).

[31] P. Mutti, G. Ghislotti, S. Bertoni, L. Bonoldi, G. F. Cerofolini, L. Meda, e. Grilli, and M. Guzzi, Appl. Phys. Lett., **66**, 852 (1995).

[32] D. Kovalev, H. Heckler, G. Polisski, J. Diener, and F. Koch, Optical Materials, **17**, 35 (2001).

[33] G. Ledoux, O. Guillois, D. Porterat, C. Reynaud, F. Huisken, B. Kohn, and V. Paillard, Phys. Rev. B, **62**, 15942 (2000).

[34] V. Vinciquerra, G. Franzo, F. Priolo, F. Lacona, and C. Spinella, J. Appl. Phys. **87**, 8165 (2000).

[35] Kwan. Sik. Cho, Nae-Man Park, Tae-Youb Kim, Kyung-Hyun Kim, Gun Young Sung, and Jung H. Shin, Appl. Phys. Lett., **86**, 071909 (2005).

[36] A. Irrera, D. Pacifici, M. Miritello, G. Franzo, and F. Priolo, F. Iacona, D. Sanfilippo, G. Di Stefano, and P. G. Fallica, Appl. Phys. Lett. **81**, 1866 (2002).

[37] Liang-Yih Chen, Wen-Hua Chen, and Franklin Chau-Nan Hong, Appl. Phys. Lett., **86**, 193506 (2005).

[38] A. Irrera, D. Pascifici, M. Miritello, G. Franzo, F. Priolo, F. Iacona, D. Sanfilippo, G. Di Stefano, and P. G. Fallica, Physica E, **16**, 395 (2003).

[39] G. Ledoux, J. Gong, and F. Huisken, Appl. Phys. Lett., **79**, 4028(2001).

[40] M. Lopez, B. Garrido, C. Garcia, P. Pellegrino, A. Perez-Rodriguiz, J. R. morante, C. Bonafos, M. Carrada, and A. Claverie, Appl. Phys. Lett., **80**, 1637 (2002).

[41] Nicola, A. Hill, and K. Birgitta Whaley, Phys. Rev. Lett, **75**, 1130 (1995).

[42] N. Daldosso, M. Luppi, S. Ossicini, E. Degoli, R. Magri, G. Dalba, P. Fornasini, R. Grisenti, F. Rocca, L. Pavesi, S. Bonineli, F. Priolo, C. Spinella, and F. Iacona, Phys. Rev. B, **68**, 085327 (2003).

[43] A. Puzder, A. J. Williamson, J. c. Grossman, and G. Galli, J. Am. Chem. Soc., **125**, 2786 (2003).

[44] P. E. Batson, and J. R. Heath, Phys. Rev. Lett., **71**, 911 (1993).

[45] M. Luppi, and S. Ossicini, Phys. Rev. B, **71**, 035340 (2005).

[46] K. Leung, K. B. Whaley, Phys.Rev. B, **56**, 7455 (1997).

[47] M. Dovrat, Y. Goshen, J. Jedrzejewski, I. Balberg, and A. Saar, Phys. Rev. B, **69**, 155311-1 (2004).

[48] Y. Kanemitsu and S. Okamoto, Phys. Rev. B, **58**, 9652 (1998).

[49] A. G. Cullis, L. T. Canham, and P. D. J. Calcott, J. Appl. Phys. **82**, 909 (1997).

[50] S. Shih, C. Tsai, K.-H. Li, K. H. Jung, J. C. Campbell, and D. L. Kwong, Appl. Phys. Lett., **60**, 633 (1992).

[51] T. Maruyama, and S. Ohtani, Appl. Phys. Lett., **85**, 1348 (1994).

[52] M. V. Wolkin, J. Jorne, P. M. Fauchet, G. Allan, and C. Delerue, Phys. Rev. Lett., **82**, 197 (1999).

[53] D. Kovalev, H. Heckler, G. Polisski, and F. Koch, Phys. Status Solidi B, **215**, 871 (1999).

[54] L. T. Canham, Appl. Phys. Lett., **57**, 1046 (1990).

[55] S. Takeoka, M. Fujii, and S. Hayashi, Phys. Rev, B, **62**, 16820 (2000).

[56] Y. Kanzawa, T. Kageyama, S. Takeoka, M. Fujii, S. Hayashi, and K. Yamamoto, Solid State Commun. **102**, 533 (1997).

[57] F. Iacona, G. Franzo, and C. Spinella, J. Appl. Phys., **87**, 1295 (2000).

[58] S. Guha, J. Appl. Phys. **84**, 5210 (1998).

[59] M. L. Brongersma, A. Polman, K. S. Min, E. Boer, T. Tambo, and H. A. Atwater, Appl. Phys. Lett., **72**, 2577 (1998).

[60] C. M. Hessel, M. A. Summers, A. meldrum, M. Malac, and J. G. V. Veinot, Advanced Materials, **19**, 3513 (2007).

[61] M. Lannoo, C. Delerue, and G. Allan, J. Lumin., **70**, 170 (1996).

[62] G. Davies, Physics Reports, **176**, 83 (1989).

[63] O. Lehtonen, D. Sundholm, and T. Vanska, Phys. Chem. Chem. Phys., **10**, 4535 (2008).

[64] S. Miura, T. Nakamura, M. Fujii, M. Inui, and S. Hayashi, Phys. Rev. B, **73**, 245333 (2006).

[65] D. Kovalev, H. Heckler, M. Ben-Chroin, G. Polisski, M. Schwartzkopff, and F. Koch, Phys. Rev. Lett., **81**, 2803 (1998).

[66] V. I. Klimov, Ch. J. Schwarz, and D. W. McBranch, and C. W. White, Appl. Phys. Lett., **73**, 2603 (1998).

[67] M. Fujii, D. Kovalev, J. Diener, and F. Koch, S. Takeoka, and S. Hayashi, J. Appl. Phys., **88**, 5772 (2000).

[68] M. Fujii, Y. Yamaguchi, Y. Takase, K. Ninomiya, and S. Hayashi, Appl. Phys. Lett., **85**, 1158 (2004).

[69] G. Cantele, E. Degoli, E. Luppi, R. Magri, D. Ninno, G. Iadonisi, and S. Ossicini, Phys. Rev. B, **72**, 113303-1 (2005).

[70] G. Allan, C. Delerue, M. Lannoo, and E. Martin, Phys. Rev. B, **52**, 11982 (1995).

[71] M. Fujii, A. Mimura, and S. Hayashi, Phys. Rev. B, **89**, 206805-1 (2002).

[72] A. Mimura, M. Fujii, S. Hayashi, D. Kovalev, and F. Koch, Phys. Rev. B, **62**, 12625 (2000).

[73] M. Fujii, K. Toshikiyo, Y. Takase, Y. Yamaguchi, and S. Hayashi, J. Appl. Phys., **94**, 1990 (2003).

[74] N. Lalic, and J. Linnros, J. Luminesc., **80**, 263 (1999).

[75] Nae-Man Park, Tae-Soo Kim, and Seong-Ju Park, Appl. Phys. Lett., **78**, 78 (2001).

[76] R. J. Walters, G. I. Bourianoff, and H. A. Atwater, Nature materials, **4**, 143 (2005).

[77] E. Snoeks, P.G. Kik, and A. Polman, Optical Materials, **5**, 159 (1996).

[78] C. Strohhofer and A. Polman, J. Appl. Phys., **90**, 4314 (2001).

[79] B. Simondi-Teisseire, B. Viana, D. Vivien, A. M. Lejus, Optical Materials, **6**, 267 (1996).

[80] H. Ennen, J. Schneider, G. Pomrenke, and A. Axmann, Appl. Phys. Lett., **49**, 943 (1983).

[81] F. Priolo, G. Franzo, S. Coffa, A. Polman, S. Libertino, R. Barklie, and d. Carey, J. Appl. Phys. **78**, 3867 (1995).

[82] F. Priolo, G. Franzo, S. Coffa, and A. Carnera, Phys. Rev. B, **57** 4443 (1998).

[83] A. J. Kenyon, P. F. Trwoga, M. Federighi, and C. W. Pitt, J. Phys.: Condens. Matter **6**, L319 (1994).

[84] M. Fujii, M. Yoshida, Y. Kanzawa, S. Hayashi, and K. Yamamoto, Appl. Phys. Lett. **71**, 1198 (1997).

[85] M. Fujii, M. Yoshida, S. Hayashi, and K. Yamamoto, J. Appl. Phys. **84**, 4525 (1998).

[86] G. Franzò , V. Vinciguerra, and F. Priolo, Appl. Phys. A: Mater. Sci. Process. **69**, 3 (1999).

[87] C. E. Chryssou, A. J. Kenyon, T. S. Iwayama, C. W. Pitt, and D. E. Hole, Appl. Phys. Lett. **75**, 2011 (1999).

[88] A. J. Kenyon, C. E. Chryssou, and C. W. Pitt, Appl. Phys. Lett., **76**, 688 (2000).

[89] P. G. Kik, and A. Polman, J. Appl. Phys. **91**, 534 (2002).

[90] S. Lettieri, and P. Maddalena, J. Appl. Physics, **91**, 5564 (2002).

[91] Y. Kanemitsu, S. Okamoto, and A. Mito, Phys. Rev. B, **52**, 10752 (1995).

[92] G. V. Prakash, M. Cazzanelli, Z. Gaburro, L. Pavesi, F. Iacona, G. Franzo, and F. Priolo. J. Appl. Phys. **91**, 4607 (2002).

[93] S. Hemandez, P. Pellegrino, A. Martinez, Y. lebour, B. Garrido, R. Spano, M. Cazzanelli, N. Daldosso, L. Pavesi, E. Jordana, and J. M. Fedeli, J. Appl. Phys., **103** (2008), 064309.

[94] E. Borsella, M. Falconieri, S. Botti, S. Martelli, F. Bignoli, L. Costa, S. Grandi, Luigi Sangaletti, B. Allieri, L. Depero, Mater.Sci.Eng., **79**, 55 (2001).

[95] S. Vijayalakshmi, H. Grebel, G. Yaglioglu, R. Pino, R. Dorsinville, C. W. White, J. Appl. Physics, **88** (2000), 6418.

Chapter 2

Coexistence of two different energy transfer processes from Si nanocrystals to Er ions in SiO_2

In this chapter, the mechanism of energy transfer from silicon nanocrystals (Si-ncs) to Er ions (Er^{3+}) is studied by analyzing delayed infrared luminescence from Er^{3+} after short-pulse photo-excitation of Si-ncs photo-sensitiezer. It is shown that two different energy transfer mechanisms, i.e., fast and slow, exist in SiO_2 films containing Si-ncs and Er^{3+} (Er:Si-ncs:SiO_2), and that the ratio of slow to fast processes depends on size of Si-ncs and Er concentration. A simple model assuming that the ratio is determined by the average distance between Si-ncs and Er^{3+} can explain the observed Si-ncs and Er concentration dependences.

2.1 Introduction

Since photo-sensitization of Er^{3+} by Si-ncs was first reported in 1994 [1], great efforts have been devoted to understanding the mechanism of the energy transfer [2–8]. In these previous studies, the coupling between Si-ncs and Er^{3+} was assumed to be very strong. However, very recently, this assumption was found not to be always applicable. In our recent work on Er:Si-ncs:SiO_2 [9], We demonstrated that, after excitation of Si-ncs by a pulse laser with a 5 nsec pulse width, the photoluminescence (PL) intensity of Er^{3+} rises very fast up to about 70% of the maximum intensity, and then starts to rise slowly until reaching the maximum. The observed delay time was distributed from several μsec to several hundredths of a μsec, depending on the sample preparation conditions. The observation of the long PL delay suggests that, in addition to the strong coupling that is

usually considered, a weak coupling process exists, although it might play a minor part in the whole energy transfer process.

In this chapter, we study the time development of Er^{3+} PL intensity after pulsed excitation of Si-ncs hosts in more detail. The author will demonstrate that the ratio of the strong and the weak coupling depends strongly on the size of Si-ncs and Er concentration, and will establish a model which can quantitatively explain the observed size and Er concentration dependences.

2.2 Experimental details

Er:Si-ncs:SiO_2 were prepared by a co-sputtering method. Si, SiO_2 and Er_2O_3 were simultaneously sputter-deposited in argon (Ar) gas, and the deposited films (about 1 μm in thickness) were annealed in a nitrogen (N_2) gas (99.999%) atmosphere for 30 min at temperatures between 1100 and 1250°C. Si-ncs were grown in films of the mixture of SiO_2 and Er_2O_3 during the annealing. In this method, the size of Si-ncs can be controlled by changing the concentration of Si in the films or changing the annealing temperature. The average size of Si-ncs was estimated by cross-sectional transmission electron microscopic (TEM) observations. In this work, the average size of Si-ncs (d_{Si}) was changed from 2.7 to 5.5 nm. PL spectra were measured using a single grating monochromator and a near-infrared photomultiplier with an InP/InGaAs photocathode. The excitation source for taking the spectra was the 457.9 nm line of an Ar-ion laser. In this wavelength, Er^{3+} is not directly excited. For all the spectra, the spectral response of the detection system was corrected by the reference spectrum of a standard tungsten lamp. For the time response measurements, a 532.0 nm line of a Nd:YAG laser was used as the excitation source. The pulse width was 5 nsec and the repetition frequency was 20 Hz. A multi-channel scalar was used in obtaining the decay curves. The overall time resolution of the system was better than 100 nsec.

2.3 Results and discussions

A typical room temperature PL spectrum of Er:Si-ncs:SiO_2 is shown in Fig. 2.1. Strong emission can be observed at around 1.3 eV and 0.81 eV. The 1.3 eV peak is assigned to the recombination of excitons confined in Si-ncs, and the 0.81 eV one to the intra-4f shell transitions of Er^{3+} [10].

The inset of Fig. 2.1 shows PL time transient of Er^{3+} at 0.81 eV after short-pulse photo-excitation with pulse width of 5nsec. We can see that the PL intensity of Er^{3+} rises fast until reaching about 70% of the maximum intensity, and then starts to rise slowly. This delayed time corresponds to the energy transfer time.

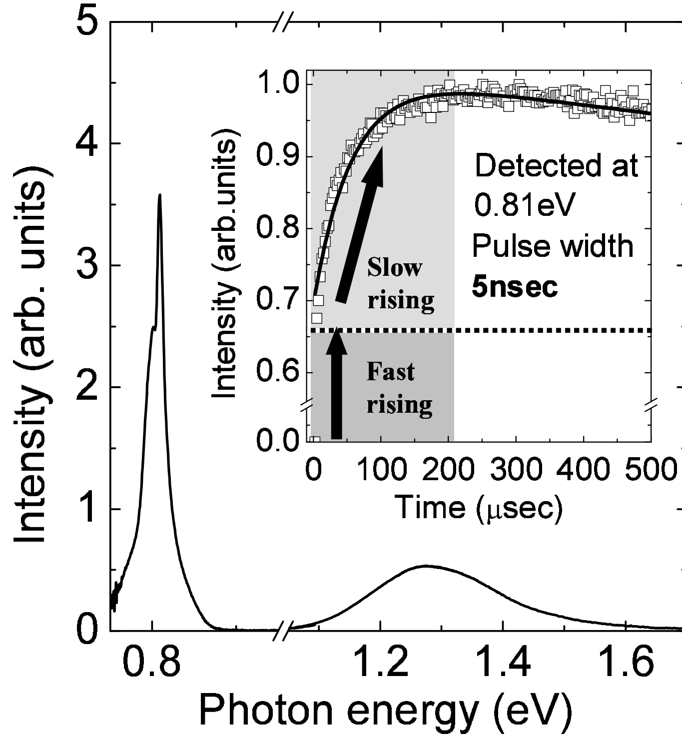

Figure 2.1: PL spectrum of SiO_2 thin film containing Er ions and Si-nc's. In the inset, PL time transient at 0.81 eV just after 5nsec pulsed excitation is shown. The open squares are experimental results, and the solid curve is a result of model fitting.

In order to discuss this in more detail, we quantitatively analyze the observed data. In the present Er and Si-ncs concentration range, we can assume that one nanocrystal interacts with one Er^{3+}. Under this assumption, in the simplest model, Er^{3+} PL intensity is expressed as,

$$I(t) \propto exp(-w_{Er}t) - exp[-(w_{Tr} + w_{Si})t], \tag{2.1}$$

where w_{Si}, w_{Er} and w_{Tr} are the recombination rates of excitons in Si-ncs and Er^{3+}, and the energy transfer rate, respectively. In this equation, both the rising and decaying parts of the curves are expressed with a single exponential function. However, as can be seen in the inset of Fig. 2.1, the intensity rises very fast until reaching about 70% of the maximum intensity and then starts to rise slowly. This behavior is apparently different from Eq. (1).

To reproduce the observed rising curves, we have to consider at least two different energy transfer processes occurring simultaneously; one process is faster than our time resolution (100$nsec$), and the other is slower ($\sim$ 10μsec) and depends strongly on the samples. We define the number of Er^{3+} which interact very strongly with Si-ncs and

contribute to the fast process as N^f_{Er}, and the number of Er^{3+} which interact weakly and contribute to the slow process as N^s_{Er}. The energy transfer rate of each process is w^f_{Tr} and w^s_{Tr}, respectively. Under the assumption that one nanocrystal interacts with one Er^{3+}, N^f_{Er} is equal to the number of Si-ncs interacting strongly with Er^{3+} (N^f_{Si}), and N^s_{Er} is equal to those weakly interacting with Er^{3+} (N^s_{Si}). After pulsed excitation, the number of excited Si-ncs that can transfer energy to Er^{3+} is,

$$N_{Si}(t) = N^f_{Si_0} exp[-(w^f_{Tr} + w_{Si})t] + N^s_{Si_0} exp[-(w^s_{Tr} + w_{Si})t], \tag{2.2}$$

where w_{Si} is the recombination rate of excitons in Si-ncs, and $N^f_{Si_0}$ and $N^s_{Si_0}$ denote the number of Si-ncs excited at t=0. If we ignore direct excitation of Er^{3+}, the excitation rate of Er^{3+} can be,

$$G(t) = w^f_{Tr} N^f_{Si_0} exp[-(w^f_{Tr} + w_{Si})t] + w^s_{Tr} N^s_{Si_0} exp[-(w^s_{Tr} + w_{Si})t], \tag{2.3}$$

and the number of Er^{3+} ions in the excited state is,

$$N_{Er}(t) = \frac{w^f_{Tr} N^f_{Si_0}}{w^f_{Tr} + w_{Si} - w_{Er}} \{exp(-w_{Er}t) - exp[-(w^f_{Tr} + w_{Si})t]\} + \frac{w^s_{Tr} N^s_{Si_0}}{w^s_{Tr} + w_{Si} - w_{Er}} \{exp(-w_{Er}t) - exp[-(w^s_{Tr} + w_{Si})t]\}. \tag{2.4}$$

As can be seen in the inset of Fig. 2.1, the fast process is faster than our time resolution, and is also faster than the lifetimes of Si-ncs PL (100 μsec $\sim$ 1 msec) and Er^{3+} PL ($\sim$5 msec). Therefore, Eq. (4) can be approximated as,

$$N_{Er}(t) = N^s_{Si_0} \{ (\frac{N^f_{Si_0}}{N^s_{Si_0}} + \frac{w^s_{Tr}}{w^s_{Tr} + w_{Si} - w_{Er}}) exp(-w_{Er}t) - \frac{w^s_{Tr}}{w^s_{Tr} + w_{Si} - w_{Er}} exp[-(w^s_{Tr} + w_{Si})t] \}. \tag{2.5}$$

Equation (5) multiplied by w_{Er} results in the PL intneisty. Since the excitation rate of Si-ncs does not depend on whether the energy transfer is fast or slow, $N^f_{Si_0}/N^s_{Si_0}$=N^f_{Si}/N^s_{Si}, and from the assumption that one nanocrystal interacts with one Er^{3+}, N^f_{Si}/N^s_{Si}=N^f_{Er}/N^s_{Er}. Therefore, PL intensity will be,

$$I(t) \propto (\frac{N^f_{Er}}{N^s_{Er}} + \frac{w^s_{Tr}}{w^s_{Tr} + w_{Si} - w_{Er}}) exp(-w_{Er}t) - \frac{w^s_{Tr}}{w^s_{Tr} + w_{Si} - w_{Er}} exp[-(w^s_{Tr} + w_{Si})t]. \tag{2.6}$$

In Eq. (6), N^f_{Er}/N^s_{Er} and w^s_{Tr} are unknown parameters and w_{Er} and w_{Si} can be obtained experimentally from the decay curves of Er^{3+} and Si-ncs PL. The decay time of Si-ncs PL was obtained by fitting the tail part of the decay curves with a single exponential

function. By using N_{Er}^{f}/N_{Er}^{s} and w_{Tr}^{s} as fitting parameters, we fitted the experimental curve and extrated the values. The solid curve in the inset of Fig. 2.1 is the result of the fitting. The model can reproduce the observed data with very good accuracy.

In the above model, the energy transfer time includes pure energy transfer time and the time necessary for excited Er^{3+} to relax to the first excited state ($\sim$2.5μsec) [12], if it is excited to higher excited states. The transfer time of the fast process, which is shorter than our time resolution, is much shorter than the relaxation time. This suggests that the fast energy transfer is made only to the first excited state of Er^{3+} ($^4I_{13/2}$), independent of the size of the nanocrystals. The fact that the energy transfer is made to the first excited state despite the enlargement of the band gap of Si-ncs supports that the fast energy transfer process is bulk-Si:Er-like, i.e., a trap-mediated energy transfer. In bulk-Si:Er systems, energy transfer is considered to be mediated by Er-related trap levels at about 150 meV below the conduction band of Si-ncs; excitons are trapped at that level and the recombination energy of excitons is transferred to Er^{3+} by an Auger-like process [13, 14].

On the other hand, considering the very small energy transfer rate of the slow process, Er-related centers are not expected to be involved and excitons may interact directly with Er^{3+} in the slow process. If excitons in Si-ncs directly interact with Er^{3+}, energy transfer should be made mainly to higher excited states of Er^{3+} because the Si-ncs PL peak energy in the present samples is always above 1.26 eV. The evidence that Er^{3+} is excited to higher excited states is obtained in the PL spectra of Si-ncs, which are partially quenched due to the energy transfer to Er^{3+} [9]; Since the energy levels of the Er^{3+} $4f$ shell are discrete, only Si-ncs with specific band-gap energies corresponding to the energies of intra-$4f$ shell transitions of Er^{3+} can transfer energy with high efficiency, resulting in the partial quenching of PL of Si-ncs.

The ratio of slow to fast processes estimated from the fitting is shown in Fig. 2.2 as a function of size of Si-ncs (a) and Er concentration (b). The ratio depends both on the size and Er concentration. The observed dependences are considered to arise from different average distance between Si-ncs and Er ions, because the fast process requires considerably small separation between Er ions and Si-ncs, while the slow one can occur even if the separation is relatively large.

In order to analyze quantitatively, we introduce a simple model in which Er^{3+} are categorized into three groups depending on the location relative to Si-ncs. We consider three spherical fields around a Si-nc in a cubic as shown in the inset of Fig. 2.2(b). Er^{3+} located in the first field (region (I)) which is the closest to Si-nc are excited by the fast process, and those in the second field (region (II)) by the slow process. Er^{3+} located outside the second field (region (III)) do not interact with Si-nc. Here, the volume of the cubic (V_{cubic}) was determined to be the reciprocal of the concentration of Si-ncs, which was estimated from excess Si concentration and average size of Si-ncs. The number of

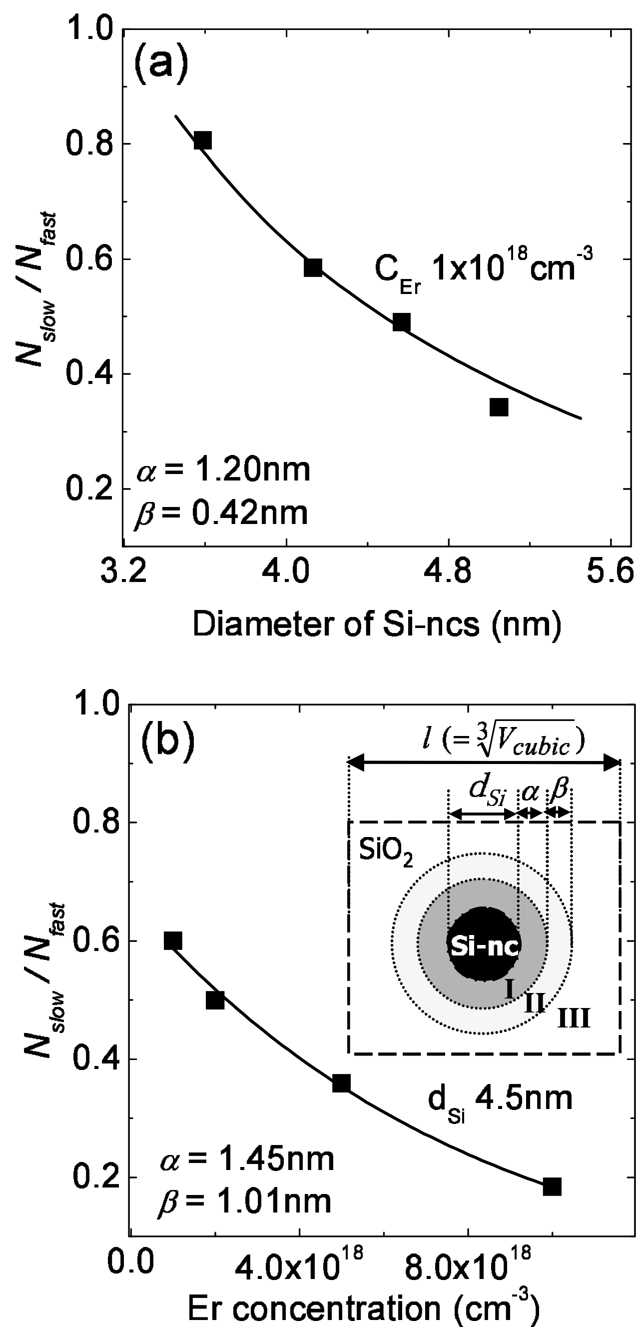

Figure 2.2: The ratio of slow to fast processes as a function of Si-nc's size (a) and Er concentration (b). Filled squares are experimental results, and solid curves are results of model fitting. In the model, three spherical fields around a Si-nc are considered (the inset of (b)).

Er^{3+} in the cubic (N_{Er}) was obtained from Er concentration.

In order to simplify the problem, we make following assumptions. First, Er^{3+} are not inside Si-ncs but on the surface or outside Si-ncs, because the solubility of Er ions in bulk-Si is very low ($10^{14} - 10^{16} cm^{-3}$). Second, one Si-nc can excite at most one Er^{3+} under 5 nsec pulse excitation, because if two excitons are excited in a Si-nc, one of them recombines nonradiatively by Auger interaction between two excitons before transfering its energy to Er^{3+}.

Under these assumptions, the requirement necessary for the fast process is the existence of at least one Er^{3+} in region (I). Assuming that Er^{3+} are uniformly dispersed in SiO_2, the ratio of Si-ncs contributing to the fast process with respect to all Si-ncs (N_{fast}) is given by,

$$N_{fast} = 1 - \left(\frac{V_2 + V_3}{V_1 + V_2 + V_3} \right)^{N_{Er}}, \tag{2.7}$$

where V_1, V_2, and V_3 are the volumes of regions (I), (II), and (III), respectively.

In a similar manner, the ratio of Si-ncs contributing to the slow process can be easily obtained. It should be noted here that if at least one Er^{3+} exists in the region (I), the slow process is suppressed by the fast process. Thus the requirement necessary for the slow process is the existence of at least one Er^{3+} in region (II) and no Er^{3+} in region (I). Therefore, the ratio of Si-ncs cotributing to the slow process (N_{slow}) is given by,

$$N_{slow} = \left(\frac{V_2 + V_3}{V_1 + V_2 + V_3} \right)^{N_{Er}} - \left(\frac{V_3}{V_1 + V_2 + V_3} \right)^{N_{Er}}. \tag{2.8}$$

Thus, the ratio of slow to fast processes (N_{slow}/N_{fast}) can be written

$$\frac{N_{slow}}{N_{fast}} = \frac{(V_2 + V_3)^{N_{Er}} - V_3^{N_{Er}}}{(V_1 + V_2 + V_3)^{N_{Er}} - (V_2 + V_3)^{N_{Er}}}, \tag{2.9}$$

where $V_1 = 4\pi\{(R + \alpha)^3 - R^3\}/3$, $V_2 = 4\pi\{(R + \alpha + \beta)^3 - (R + \alpha)^3\}/3$, and $V_3 = V_{cubic} - 4\pi(R + \alpha + \beta)^3/3$. α and β are the thickness of region (I) and (II), and R is the radius of Si-nc's ($= d_{Si}/2$).

We tried to reproduce the observed data in Fig. 2.2 by fitting them with the equation (2.9) by using α and β as fitting parameters. Results of the fittings are shown by solid curves. Both the size and the Er concentration dependences are well fitted by the model. α and β were estimated to be 1.45nm and 1.01nm from Fig. 2.2 (a), and 1.20nm and 0.42nm from Fig. 2.2 (b). The good reproduction of the observed results indicates that the model is qualitatively correct and the ratio of slow to fast processes is in principle determined by the average distance between Er^{3+} and Si-ncs.

However, α and β estimated from Figs. 2.2 (a) and 2.2 (b) do not coincide perfectly. This disagreement may come from oversimplification of the model. In particular, we don't take into account the effect of neighboring Si-ncs. This effect is crucial in discussing the

size dependence of the ratio in Fig. 2.2 (b), because in this case, the distance between Si-ncs changes depending on the size. Compared to the size dependence, the effect is smaller and the obtained parameters are more reliable for the Er concentration dependence in Fig. 2.2 (a), because the distance is fixed.

2.4 Conclusion

In conclusion, we have succeeded in demonstrating that there are two different energy transfer processes, i.e. slow and fast processes, in Er:Si-ncs:SiO_2. From the estimated energy transfer time, the fast energy process is considered to be bulk-Si:Er-like, i.e., a trap-mediated energy transfer, and the slow energy process is considered to be resonant energy transfer from electron-hole pairs within Si-ncs to second or third excited states of Er^{3+}. The ratio of the two processes was found to depend on the size of Si-ncs and Er concentrations, suggesting that the most dominant factor determining the ratio of slow to fast processes is the average distance between Si-ncs and Er^{3+}. Our simple model succeeded in reproducing qualitatively the observed dependences on the size of Si-ncs and Er concentration.

References

[1] A. J. Kenyon, P. F. Trwoga, M. Federighi, and C. W. Pitt, J. Phys.: Condens. Matter **6**, (1994) L319.

[2] F. Priolo, G. Franzò, D. Pacifici, V. Vinciguerra, F. Iacona, and A. Irrera, J. Appl. Phys. **89**, (2001) 264.

[3] D. Pacifici, G. Franzo, F. Priolo, F. Iacona, and L. D. Negro, Phys. Rev. B **67**, (2003) 245301.

[4] G. Franzò , V. Vinciguerra, and F. Priolo, Appl. Phys. A: Mater. Sci. Process. **69**, (1999) 3.

[5] J. H. Shin, S.-Y. Seo, S. Kim, and S. G. Bishop, Appl. Phys. Lett. **76**, (2000) 1999 .

[6] G. Franzò, D. Pacifici, V. Vinciguerra, F. Priolo, and F. Iacona, Appl. Phys. Lett. **76**, (2000) 2167.

[7] P. G. Kik, M. L. Brongersma, and A. Polman, Appl. Phys. Lett. **76**, (2000) 2325.

[8] M. Fujii, K. Imakita, K. Watanabe, and S. Hayashi, J. Appl. Phys. **95**, (2004) 272.

[9] K. Watanabe, M. Fujii and S. Hayashi, J. Appl. Phys. **90**, (2001) 4761.

[10] M. Fujii, M. Yoshida, Y. Kanzawa, S. Hayashi, and K. Yamamoto, Appl. Phys. Lett. **71**, 1198 (1997).

[11] M. Wojdak, M. Klik, M. Forcales, O. N. Gusev, and T. Gregorkiewicz, Phys. Rev. B **69**, (2004) 233315.

[12] The relaxation time can be estimated from PL lifetime at 1.26 eV due to the $^4I_{11/2}$ to $^4I_{15/2}$ transition. The observed lifetime is about 2.5 μsec at room temperature [**?**]. This time is not pure radiative recombination time but mainly reflects the relaxation of Er^{3+} to the first excited state, indicating that relaxation from higher excited states to the first excited state takes at least 2.5 μsec.

[13] A. Polman, J. Appl. Phys. **82**, 1 (1997).

[14] M. Forcales, T. Gregorkiewicz, M. S. Bresler, O. B. Gusev A. F., I. V. Bradley, and J-P. R. Wells, Phys. Rev. B **67**, 085303 (2003)

Chapter 3

Spectrally resolved energy transfer from excitons in Si nanocrystals to Er ions

In this chapter, energy transfer from Si nanocrystals (Si-ncs) to Er^{3+} is studied spectroscopically. At low temperatures, inhomogeneously broadened PL bands of Si-ncs were partially quenched and some dips were observed. A comparison of the quenched spectra with a photoluminescence excitation spectrum revealed that the dips are due to resonant energy transfer from excitons in Si-ncs to Er^{3+}. For the energy transfer to the ${}^4I_{11/2}$ state of Er^{3+}, two dips, one very clear and the other indistinctive, were observed, while to the ${}^4I_{9/2}$ state two dips with comparable depth were observed. Modification of the band structure of Si-ncs by the quantum size effects is responsible for the different dip structures depending on to which states the energy transfer is made.

3.1 Introduction

Si-ncs are promising materials as a photosensitizer for substances with small oscillator strength such as molecular oxygen (MO) [1–3] and rare earth (RE) ions [4–10]. By placing Si-ncs in close proximity to these substances, their optical excitation cross section is strongly enhanced due to efficient energy transfer from Si-ncs.

The mechanism of energy transfer from Si-ncs to MO has been studied for porous Si, which consists of networks of Si-ncs. Porous Si in vacuum shows an inhomogeneously-broadened featureless photoluminescence (PL) band even at liquid He temperature due to size- and shape-distributions of Si-ncs. By adsorbing MO, the broad PL band is partially

quenched, and periodic dips with the period of 63 meV appear in the inhomogeneously broadened PL band. The dip is the deepest at 1.63 eV that coincides with the energy separation between the second excited $^1\Sigma$ and ground $^3\Sigma$ state of MO ($^3\Sigma$-$^1\Sigma$), indicating that Si-ncs with the bandgap energy of 1.63 eV transfer their excitation energy resonantly to MO. Si-ncs having other bandgap energies have to emit phonons to satisfy the energy conservation rule during the energy transfer process. This results in periodic features in the PL spectra, the period of which corresponds to the energy of maximum density of phonon states of bulk-Si (63 meV). Magneto-optical spectroscopy reveals that the mechanism of the energy transfer is a triplet-triplet annihilation type electron exchange process [2].

Compared to MO, the mechanism of energy transfer to RE ions was less elucidated. Among several RE ions being reported to be sensitized by Si-ncs, Er^{3+} have most intensively been studied because of its possible application in optical telecommunication fields [11–14]. In our previous work, we studied the mechanism of energy transfer by analyzing time transient of PL from Er after pulsed excitation of Si-ncs sensitizer [15, 16]. The analysis revealed that two energy transfer processes, i.e., fast and slow processes work simultaneously. The energy transfer time of the fast process is less than 100 nsec, while that of the slow one is several tenth of μsec. The contribution of the fast process among the total energy transfer process increases, e.g., from 55 % to 77 % in the previous samples [16], with increasing the size of Si-ncs, suggesting that the fast process is essentially the same as that reported for Er doped bulk Si crystals., i.e., excited excitons are trapped to Er-related trap centers and the recombination energy of excitons are transferred to Er^{3+} by an Auger like process [17–19]. On the other hand, the slow energy transfer process is considered to be due to the Förster [20] type Coulombic interaction between excitons in Si-ncs and Er^{3+} staying apart from Si-ncs, because the energy transfer rate showed strong dependence on radiative recombination rate of excitons [16]. The direct interaction between excitons and Er^{3+} should manifest itself as dips in inhomogeneously broadened PL bands of Si-ncs as has been observed in the case of exciton-MO interactions. In fact, we observed small features in PL bands of Si-ncs in SiO_2 films containing Er^{3+} and Si-ncs [15]. Similar features were also reported for Er doped Si-ncs/SiO_2 superlattices [21]. However, the observed features were indistinctive and some of them could be recognized only after taking derivatives. The obscureness of the features prevents detailed analysis of the energy transfer mechanism and the meaning of the features is still controversial.

One of the possible reasons for the obscureness of the features is that the crystallinity of Si-ncs is not perfect, and PL spectra are determined not only by size distribution but also by the energy of defect states. If PL arises mainly from defect states, even when Si-ncs with a particular size transfer energy resonantly to Er^{3+}, PL spectra will be quenched totally and dips will be very shallow and ill-defined. Therefore, improving

the crystallinity of Si-ncs is indispensable to observe distinct features and to discuss the mechanism of energy transfer.

In this work, we have succeeded in preparing Si-ncs which show pronounced spectral dips by carefully controlling sample preparation conditions. PL spectra of these samples are measured as a function of temperature and excitation power.

3.2 Experimental details

Er and Si-ncs co-doped SiO_2 (Er:Si-nc:SiO_2) were prepared by a co-sputtering method. Si, SiO_2 and Er_2O_3 were simultaneously sputter-deposited in argon (Ar) gas, and the deposited films (about 2 μm in thickness) were annealed in a nitrogen (N_2) gas (99.999%) atmosphere for 30 minutes at temperatures above 1200 ^{o}C. Si-ncs were grown in films of the mixture of SiO_2 and Er_2O_3 during the annealing. In this method, the size of Si-ncs can be controlled by changing the concentration of excess Si in films or changing the annealing temperature. Therefore, to realize a particular size distribution, different combinations of annealing temperature and Si concentration are possible. In the present work, we choose higher annealing temperature (above 1200°C) and lower Si concentration than those used in previous work [6, 7].

This preparation condition results in higher crystallinity of Si-ncs. The annealing temperature dependence of the crystallinity has been demonstrated by Iacona et al. by energy-filtered transmission electron microscopy [22]. They showed that in low temperature annealed samples, e.g., ∼1150 ^{o}C, substantial amounts of amorphous clusters remain, and the fraction of amorphous clusters decreases with increasing annealing temperature. In conventional PL spectroscopy excited by blue light, the difference in crystallinity does not appear clearly. However, the difference can be seen when the energy of the exciting laser light is chosen to fall inside a low energy part of the spectral band. Under this resonant excitation condition, if the crystallinity is perfect, PL spectra of Si-ncs show clear features corresponding to the emission and absorption of momentum conserving phonons during the creation and recombination of excitons [24]. If defects are introduced in or on the surface of nanocrystals, the features become ill-defined [23]. In the present high-temperature annealing condition, the PL features are more pronounced than those of the samples annealed at lower temperatures, implying that the number of defective nanocrystals are reduced and majority of excitons recombine radiatively without the participation of surface or defect-related recombination centers.

We have prepared samples with two different size distributions with the average sizes of about 3.4 and 5.8 nm. These sizes are chosen so that PL peak energies coincide with the excitation energies of the $^4I_{11/2}$ and $^4I_{9/2}$ states of Er^{3+}. Er was doped rather heavily (0.2 at%) to make sure that all Si-ncs interact with Er^{3+}.

PL spectra were measured using a single monochromator equipped with a Si charge-coupled device (detection energy 1.2-2.5 eV) or an InGaAs near-Infrared diode array (detection energy 0.7-1.8 eV). The excitation source for taking the spectra was the 488 nm line of an Ar-ion laser. For all the spectra, the spectral response of the detection system was corrected by the reference spectrum of a standard tungsten lamp. In order to measure the PL excitation (PLE) spectra, an optical parametric oscillator (OPO) pumped by the third harmonic of a Nd:YAG laser and a liquid nitrogen cooled Ge photodiode were used as an excitation source and a detector, respectively. A continuous-flow type He cryostat was used to take temperature dependence of PL spectra.

3.3 Results and discussions

PL spectra of Er:Si-ncs:SiO_2 and Si-ncs doped SiO_2 (Si-ncs:SiO_2) at room temperature are shown in Fig. 3.1. The average sizes of Si-ncs are 5.8 and 3.4 nm for Figs. 1(a) and 3.1(b), respectively. A sharp peak at 0.81 eV corresponds to the intra-4f shell transition ($^4I_{13/2}$-$^4I_{15/2}$) of Er^{3+} (Er PL), while the broad one arises from the recombination of excitons confined in Si-ncs (Si-ncs PL), the intensity of which is decreased by Er doping. The quenching of the exciton PL by Er doping is accompanied by the shortening of lifetime as can be seen in the insets Fig. 3.1. This result contradicts with earlier reports that the lifetime of Si-nc PL does not change by Er doping [12]. The shortening of the lifetime is a direct evidence that "slow energy transfer process", which is mentioned in the introduction, competes with the radiative recombination process of exciton.

In Figs. 3.2(a) and 3.2(b), PL spectra of Er:Si-ncs:SiO_2 are shown as a function of temperature. In order to compare the spectral shape, all the spectra are normalized at maximum intensity. At the bottom of these figures, PL spectra of Si-ncs:SiO_2 at 5K are shown. Without Er doping, the spectra are broad and featureless. In contrast, small features start to appear on the spectra of Er:Si-ncs:SiO_2 below 80 K, and clear dips can be seen at 5 K. It is interesting to note that only one dip (at around 1.22 eV) is observed in Fig. 3.2(a), while two dips with nearly identical depth (at around 1.49 eV and 1.55 eV) are observed in Fig. 3.2(b). A small peak at 1.27 eV at low temperatures in Fig. 3.2(b) is the emission of Er^{3+} from the second excited state ($^4I_{11/2}\rightarrow^4I_{15/2}$).

In order to investigate the origin of these dips, PLE spectra of Er PL at 0.81 eV are measured for Er doped SiO_2 (Er:SiO_2) (Fig. 3.2). We can see two peaks corresponding to the $^4I_{15/2}\rightarrow^4I_{9/2}$ and $^4I_{15/2}\rightarrow^4I_{11/2}$ transitions of Er^{3+}. The energy positions of the $^4I_{11/2}$ and $^4I_{9/2}$ states with respect to the ground $^4I_{15/2}$ state are shown with the vertical dashed lines and the labels at the top of the figures. We can see that the positions of PLE peaks roughly coincide with those of dips. This coincidence suggests that the dips are due to energy transfer from excitons in Si-ncs to Er ions. It should be stressed here that the dips

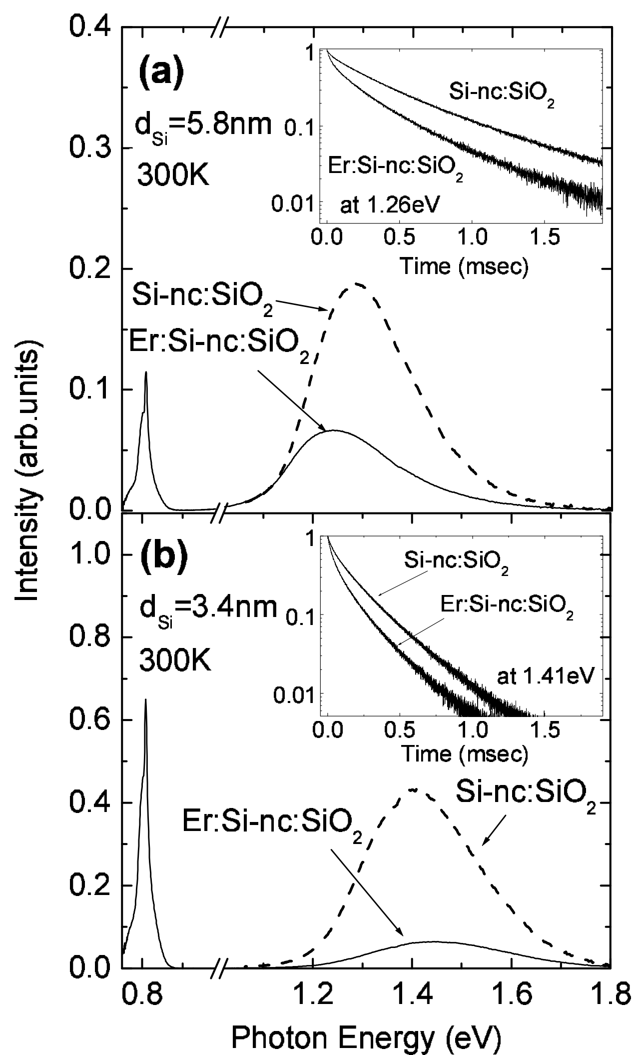

Figure 3.1: PL spectra of Er:Si-nc:SiO_2 and Si-nc:SiO_2 at room temperature. Average sizes of Si-ncs are (a) 5.8 and (b) 3.4 nm. A sharp peak at 0.81 eV is due to the intra-4f shell transition ($^4I_{13/2}\rightarrow{}^4I_{15/2}$) of Er^{3+}, and the broad one to the recombination of excitons confined in Si-ncs. In the insets, decay curves of PL from Si-ncs with and without Er doping are shown.

are caused by non-radiative energy transfer, i.e., the exchange of near-field light, but not by the re-absorption of PL from Si-ncs by Er^{3+}. The absorption cross-section of Er^{3+} is very small, and in the present samples, absorption due to the ${}^4I_{15/2} \rightarrow {}^4I_{9/2}$ and ${}^4I_{15/2} \rightarrow {}^4I_{11/2}$ transitions is not detectable by conventional absorption spectroscopy.

It is interesting to note that in Fig. 3.2(a), the spectral dip does not coincide perfectly with the ${}^4I_{11/2}$ state. It exists at about 57 meV below the ${}^4I_{11/2}$ state. On the other hand, in Fig. 3.2(b), the higher-energy dip coincides perfectly with the ${}^4I_{9/2}$ state, while the lower-energy one again stays at 57 meV below the ${}^4I_{9/2}$ state. The vertical dotted lines are drawn 57 meV below the ${}^4I_{9/2}$ and ${}^4I_{11/2}$ states. The reason that dips appear at 57 meV below the ${}^4I_{11/2}$ and ${}^4I_{9/2}$ states can be explained by considering the fact that Si-ncs inherit the indirect bandgap nature of bulk Si crystals. In bulk Si, the conduction band bottom is located in the vicinity of the X points of the Brillouin zone (Δ minima), and thus emission or absorption of momentum-conserving phonons are required for the optical transition. Usually, TO phonon-assisted transition is the most dominant and PL maximum appears at 57 meV (=TO phonon energy at Δ minima) below the bandgap. Similarly in Si-ncs, TO phonon-assisted transition is reported to be the dominant recombination path in the present size range [24].

In Fig. 3.3, the energy diagram of Er^{3+} and Si-ncs are depicted. Si-ncs with the bandgap energy of 1.28 eV transfer energy resonantly to Er^{3+}. Since, without Er doping, these Si-ncs luminesce at 1.22 eV by emitting one TO(Δ) phonon, PL quenching appears at around 1.22 eV. Similarly, resonant energy transfer from Si-ncs having the bandgap energy of 1.55 eV to the ${}^4I_{9/2}$ state results in the quenching at 1.49 eV.

If Si-ncs are purely indirect bandgap semiconductors, dips should appear always at 57 meV below excited levels of Er^{3+}. In fact, in Fig. 3.2(a), we can see only one dip at 57 meV below the ${}^4I_{11/2}$ state. This means that Si-ncs having the bandgap energy in this region hold the indirect-bandgap nature strongly. On the other hand, two dips with nearly identical depth can be seen in Fig. 3.2(b). The observation of the dip exactly at the energy of the ${}^4I_{9/2}$ state implies that probability of a quasi-direct nonphonon optical transition is not negligibly small and it can compete with the TO(Δ) phonon-assisted transition.

The transition from indirect bandgap to quasi-direct one is a result of the quantum size effect. The confinement of excitons in a space comparable or smaller than the Bohr radius of bulk excitons leads to uncertainty of quasimomentum and breakdown of the momentum conservation rule. Although this effect has been well-known and theoretically studied in detail [25], direct observation of the effect is not straightforward because of inhomogeneous broadening of PL bands. In order to lift the inhomogeneous broadening and extract the information of size-selected Si-ncs, spectral narrowing techniques such as resonant PL and hole burning spectroscopy should be employed [24, 26]. The dips observed

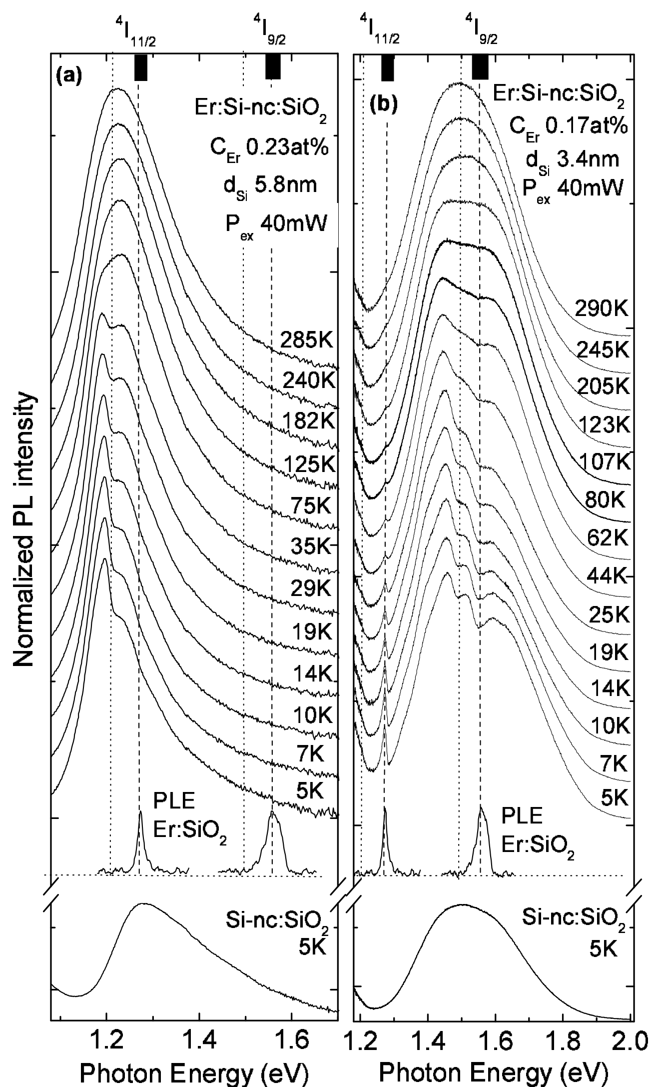

Figure 3.2: Temperature dependence of PL spectra of Er:Si-nc:SiO$_2$ (upper part). The average sizes of Si-ncs are (a) 5.8 and (b) 3.4 nm. PL spectra of Si-nc:SiO$_2$ are shown in the lower part and PLE spectrum of Er:SiO$_2$ is shown in the middle part. Vertical dashed lines are drawn to the energies of $^4I_{15/2} \rightarrow ^4 I_{11/2}$ and $^4I_{15/2} \rightarrow ^4 I_{9/2}$ transitions of 4f shell of Er^{3+}. Vertical dotted lines are drawn 57 meV below these energies.

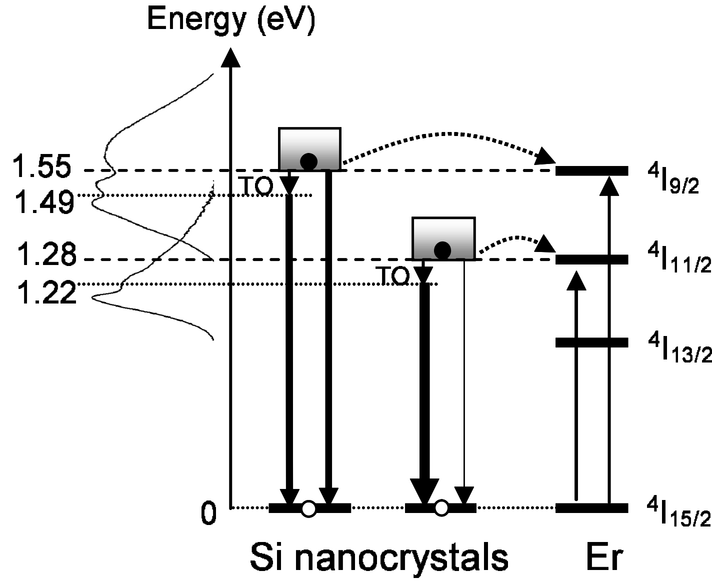

Figure 3.3: Schematic illustration of an energy-level diagram of Si-ncs and Er^{3+}. Si-ncs with the bandgap energies of 1.55 and 1.28 eV can resonantly excite Er^{3+} to the $^4I_{9/2}$ and $^4I_{11/2}$ states, respectively. The luminescence energies of these nc-Si are one TO(Δ) phonon energy below or correspond to $^4I_{9/2}$ or $^4I_{11/2}$ states, resulting in dips in the positions shown in the figure.

in this work can be regarded as holes in hole burning spectroscopy and quenched spectral region provides information on size-selected Si-ncs. Therefore, the present approach, i.e., digging spectral holes by resonant energy transfer to discrete electronic states of an energy acceptor, offers a new tool to extract information of size-selected semiconductor nanocrystals in inhomogeneously broadened PL bands.

The dips in inhomogeneously broadened PL band appear most clearly when PL maximum exists at the energy of excited states of Er^{3+}. However, it is not easy to tune sample preparation conditions to realize it. Fortunately, fine tuning of the PL maximum is possible by controlling excitation power. PL lifetime of Si-ncs at low temperatures is in the msec range, and thus the condition of the formation of two excitons in a nanocrystal can easily be achieved at rather low excitation power. In a Si-nc having two excitons simultaneously, Auger interaction between them is so efficient that one of them recombines nonradiatively by giving kinetic energy to an electron or a hole of the other exciton, resulting in saturation of PL intensity [27]. This effect is more significant for larger Si-ncs because of longer exciton lifetime. Therefore, at high excitation power, a lower-energy side of PL bands saturates, resulting in a high-energy shift of the band.

In the lower part of Fig. 3.4, PL spectra of Si-nc:SiO_2 excited by different powers are

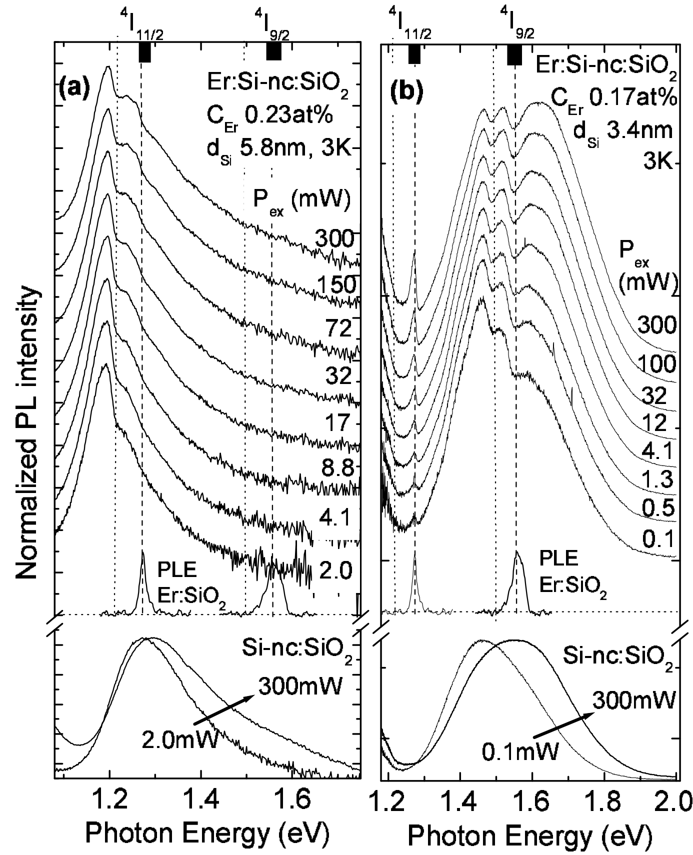

Figure 3.4: Excitation power dependence of PL spectra of Er:Si-nc:SiO$_2$ (upper part).The average sizes of Si-ncs are (a) 5.8 and (b) 3.4 nm. PL spectra of Si-nc:SiO$_2$ excited by two different powers are shown in the lower part and PLE spectrum of Er:SiO$_2$ is shown in the middle part. Vertical dashed lines are drawn to the energies of $^4I_{15/2} \rightarrow ^4 I_{11/2}$ and $^4I_{15/2} \rightarrow ^4 I_{9/2}$ transitions of 4f shell of Er^{3+}. Vertical dotted lines are drawn 57 meV below these energies.

compared. The shape of PL features changes depending on excitation power. We can see that the dips are more pronounced with increasing excitation power. This is because PL peak energy of Si-ncs approaches the excited states of Er^{3+} at higher excitation power. It is worth noting that, in Fig. 3.4(a), a very weak dip appears at the position of the $^4I_{11/2}$ state when the PL band shifts to higher energy and the slope of the envelope function at the position becomes smaller by high power excitation. This suggests that the band structure of Si-ncs with the band gap energy of 1.26 eV is not purely indirect but quasi-direct transition is slightly allowed.

3.4 Conclusion

We have shown that inhomogeneously broadened PL bands of Si-ncs are partially quenched due to resonant energy transfer to discrete electronic states of Er^{3+}. The observation of clear dips is the evidence that there is direct interaction between excitons in Si-ncs and Er^{3+}. The analysis of the dips gives us valuable information for electronic structures of size-selected Si nanocrystals. Si nanocrystals with the bandgap energy of around 1.28 eV strongly hold indirect bandgap nature of bulk Si crystals, while quasi-direct non-phonon optical transition becomes possible in Si-ncs of 1.55 eV bandgap.

References

[1] D. Kovalev, E. Gross, N. Künzner, F. Koch, V. Yu. Timoshenko, and M. Fujii, Phys. Rev. Lett. **89**, 137401 (2002).

[2] E. Gross, D. Kovalev, N. Künzner, J. Diener, F. Koch, V. Yu. Timoshenko, and M. Fujii, Phys. Rev. B **68**, 115405 (2003).

[3] M. Fujii, S. Minobe, M. Usui, S. Hayashi, E. Gross, J. Diener, and D. Kovalev, Phys. Rev. B, **70**, 085311 (2004).

[4] C. E. Chryssou, A. J. Kenyon, T. S. Iwayama, C. W. Pitt, and D. E. Hole, Appl. Phys. Lett. **75**, 2011 (1999).

[5] A. J. Kenyon, P. F. Trwoga, M. Federighi, and C. W. Pitt, J. Phys.: Condens. Matter **6**, L319 (1994).

[6] M. Fujii, M. Yoshida, Y. Kanzawa, S. Hayashi, and K. Yamamoto, Appl. Phys. Lett. **71**, 1198 (1997).

[7] M. Fujii, M. Yoshida, S. Hayashi, and K. Yamamoto, J. Appl. Phys. **84**, 4525 (1998).

[8] G. Franzò, V. Vinciguerra, and F. Priolo, Appl. Phys. A: Mater. Sci. Process. **69**, 3 (1999).

[9] J. H. Shin, S.-Y. Seo, S. Kim, and S. G. Bishop, Appl. Phys. Lett. **76**, 1999 (2000).

[10] K. Watanabe, H. Tamaoka, M. Fujii, K. Moriwaki, and S. Hayashi, Physica E **13**, 1038 (2002).

[11] D. Pacifici, G. Franzo, F. Priolo, F. Iacona, and L. DalNegro, Phys. Rev. B **67**, 245301 (2003).

[12] P. G. Kik, and A. Polman, J. Appl. Phys. **88**, 1992 (2000).

[13] F. Priolo, G. Franzò, D. Pacifici, V. Vinciguerra, F. Iacona, and A. Irrera, J. Appl. Phys. **89**, 264 (2001).

[14] A. J. Kenyon, C. E. Chryssou, C. W. Pitt, T. Shimizu-Iwayama, D. E. Hole, N. Sharma, and C. J. Humphreys, J. Appl. Phys. **91**, 367 (2002).

[15] K. Watanabe, M. Fujii, and S. Hayashi, J. Appl. Phys. **90**, 4761 (2001).

[16] M. Fujii, K. Imakita, K. Watanabe, and S. Hayashi, J. Appl. Phys. **95**, 272 (2004).

[17] M. S. Bresler, O. B. Gusev, B. P. Zakharchenya, and I. N. Yassievich, Phys. Solid State **38**, 813 (1996).

[18] M. Forcales, T. Gregorkiewicz, M. S. Bresler, O. B. Gusev, I. V. Bradley, and J-P. R. Wells, Phys. Rev. B. **67**, 085303 (2003).

[19] M. Forcales, T. Gregorkiewicz, and M. S. Bresler, Phys. Rev. B. **68**, 035213 (2003).

[20] T. Förster, Ann. Phys. (N.Y) **2**, 55 (1948).

[21] V. Yu. Timoshenko, M. G. Lisachenko, O. A. Shalygina, B. V. Kamenev, D. M. Zhigunov, S. A. Teterukov, P. K. Kashkarov, J. Heitmann, M. Schmidt, and M. Zacharias J. Appl. Phys. **96**, 2254 (2004).

[22] F. Iacona, C. Bongiorno, C. Spinella, S. Boninelli and F. Priolo, J. Appl. Phys. **95**, 3723 (2004).

[23] M. Fujii, D. Kovalev, J. Diener, F. Koch, S. Takeoka and S. Hayashi, J. Appl. Phys. **88**, 5772 (2000).

[24] D. Kovalev, H. Heckler, M. Ben-Chorin, G. Polisski, M. Schwartzkopff, and F. Koch Phys. Rev. Lett. **81**, 2803 (1998).

[25] M. S. Hybertsen, Phys. Rev. Lett. **72**, 1514 (1994).

[26] D. Kovalev, H. Heckler, B. Averboukh, M. Ben-Chorin, M. Schwartzkopff, and F. Koch, Phys. Rev. B **57**, 3741 (1998).

[27] M. Wojdak, M. Klik, M. Forcales, O. B. Gusev, T. Gregorkiewicz, D. Pacifici, G. Franzò, F. Priolo, and F. Iacona, Phys. Rev. B **69**, 233315 (2004).

Chapter 4

Interaction between Er ions and shallow impurities in Si nanocrystals

In this chapter, the interaction between Er^{3+} and shallow impurities in Si nanocrystals (Si-ncs) is studied for SiO_2 films containing Er and Si-ncs (Er:Si-ncs:SiO_2). The luminescence property of Er^{3+} is strongly modified by shallow impurities in Si-ncs. The formation of excess carriers in Si-ncs by P or B doping results in the quenching of infrared photoluminescence (PL) of Er^{3+} and the shortening of the lifetime. When P and B are doped simultaneously and carriers are compensated, the intensity and the lifetime are recovered. It is shown that the mechanism of the interaction is Auger de-excitation of excited Er^{3+} with the interaction of electrons or holes in Si-ncs. The estimated Auger coefficient is found to be two orders of magnitude smaller than that of Er doped bulk Si at low temperatures where carriers are bound to donor or acceptor ions, and four orders of magnitude smaller than that at room temperature. This small Auger coefficient makes Si-ncs immune from the impurity Auger de-excitation process compared to Er doped bulk Si and is considered to be responsible for temperature independent efficient PL of Er:Si-ncs:SiO_2 systems.

4.1 Introduction

Si nanocrystals (Si-ncs) act as an efficient photosensitizer for Er ions (Er^{3+}) [1–4]. The excitation cross-section of Er^{3+} in SiO_2 (Er:SiO_2) is enhanced by more than four orders of magnitude if Si-ncs are simultaneously doped (Er:Si-ncs:SiO_2) [5–8]. The enhanced excitation cross-section is due to indirect excitation of Er^{3+} by the energy transfer from

Si-ncs. Since the absorption band of Si-ncs covers the whole visible range, Er^{3+} can be excited by white light. The luminescence from Er^{3+} in this system exhibits almost no temperature quenching. Due to these remarkable features this system is considered to be a key component to realize planar waveguide type compact optical amplifier operating at 1.54 μm [9].

Detailed experimental and theoretical studies have been carried out to elucidate the mechanism of energy exchange between Si-ncs and Er^{3+} [5–8, 10, 11]. In previous papers [10, 11], we studied the photoluminescence (PL) transient of Er^{3+} after pulsed excitation of Si-ncs hosts and found that the intensity continues to rise after finishing excitation. The rising part contains valuable information about the energy exchange mechanism. The analysis of the rising part revealed that there are two different energy transfer processes occurring simultaneously, i.e., fast and slow processes, and the ratio of the fast to slow processes changes depending on the size of Si-ncs and Er concentration. From the size dependence of the energy transfer time, the fast process was assigned to be a trap-mediated process; an excited electron is trapped to Er^{3+} related center in the bandgap, the recombination energy of an bound exciton is transferred to Er^{3+} by Auger-like process, and Er^{3+} is excited to the first excited state [11]. This process is essentially the same as that in Er doped bulk Si crystals (Er:bulk-Si) [12–14]. On the other hand, the slow process is a characteristic one occurring only in nanocrystalline systems. This is probably the Förster [15] type Coulombic interaction between free-excitons in Si-ncs and Er^{3+}. Although the ratio of slow to fast processes increased with decreasing the size of Si-ncs, the fast process

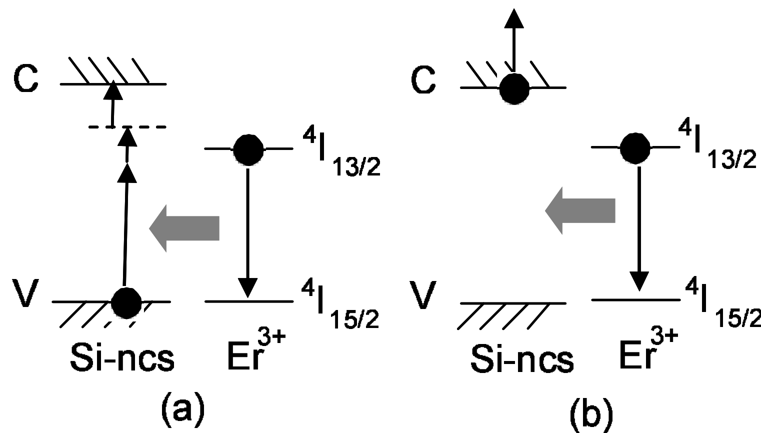

Figure 4.1: Schematic representations of two possible nonradiative de-excitation processes for Er^{3+} in bulk Si: (a) energy back transfer, and (b) Auger de-excitation with free electrons.

was always the dominant energy transfer process in all the samples studied.

This conclusion seems to contradict the fact that luminescence properties of Er:Si-ncs:SiO_2 are much different from those of Er:bulk-Si. Especially, the degree of temperature quenching of PL is much different; PL from Er:Si-ncs:SiO_2 is almost insensitive to temperature, while that from Er:bulk-Si shows very strong temperature quenching. As the origin of the strong temperature quenching of Er:bulk-Si, two major de-excitation processes are considered [16, 17]. The first one is an energy back-transfer process [Fig. 4.1(a)]. Since the lifetime of excited state of Er^{3+} is very long, the reverse energy transfer process can compete with spontaneous emission; excited Er^{3+} relaxes by exciting an electron to the trap level in the bandgap of host Si. If the electron is thermally activated to the conduction band, luminescence from Er^{3+} is lost. This process becomes more significant at higher temperatures, resulting in very strong temperature quenching. The other de-excitation process is Auger de-excitation of excited Er^{3+} with energy transfer to free carriers in host Si [Fig. 4.1(b)]. The Auger coefficient of this process is determined to be $C_A = 5\times10^{-13}cm^3s^{-1}$ for both free electrons and free holes [16, 18]. When free carriers are frozen and the donor and acceptor levels are occupied at low temperatures, the interaction is made between Er^{3+} and electrons (or holes) bound to shallow donors (acceptors). The efficiency of this process is two orders of magnitude smaller than that of the Auger de-excitation with free carriers [16, 18]. Therefore, the efficiency of the Auger de-excitation is also strongly enhanced at higher temperatures.

The fact that Er:Si-ncs:SiO_2 shows very small temperature quenching suggests that these de-excitation processes are inefficient. The asymmetry between efficient excitation and inefficient de-excitation is thus the origin of the characteristic luminescence properties. The reason for the small de-excitation efficiency can qualitatively be explained as follows. The de-excitation by back-transfer is completed by two consecutive processes, i.e., the excitation of an electron to an Er-related level and the thermalization of the electron to the conduction band [see Fig. 4.1(a)]. Er-related-defect level is considered to be not strongly affected by the size of Si-ncs because a localized state is usually not strongly modified by quantum size effects [19–21]. On the other hand, the conduction band edge goes up with decreasing the size. As a result, the energy necessary to release an electron from the level becomes larger, making the thermalization of an electron inefficient even at room temperature. The other de-excitation process, i.e., the Auger de-excitation shown in Fig. 4.1(b), is possible only when free or bound carriers exist in host materials. This process is thus expected to be prohibited if shallow impurities do not exist in Si-ncs. In Er:Si-ncs:SiO_2 systems studied so far, shallow impurities are not intentionally doped, resulting in the absence of the de-excitation process. However, if doped Si-ncs are used as a photosensitizer, it is highly plausible that excited Er^{3+} has interaction with shallow impurities. A detailed study on the interaction provides additional information on the

mechanism of energy exchange and is crucial in fully understanding the differences and similarities between Er:bulk-Si and Er:Si-ncs:SiO_2 systems. The study also provides vital information on the interaction between excited Er^{3+} and photogenerated carriers in Si-ncs. The knowledge on the interaction is indispensable to discuss whether or not multiple Er^{3+} can be excited by a single nanocrystal.

In this chapter, we have studied the interaction between excited Er^{3+} and shallow impurities in Si-ncs by controlling P and/or B concentration in Si-ncs systematically. We will demonstrate that PL properties of Er^{3+} are strongly modified by shallow impurities in Si-ncs and discuss the mechanism of the interaction.

4.2 Experimental details

Films containing Er and shallow-impurity-doped Si-ncs were prepared by a cosputtering method [22–24]. Si, Er_2O_3, SiO_2, borosilicate glass (BSG) and/or phosphosilicate glass (PSG) were simultaneously sputter-deposited in Ar gas on a quartz or a Si substrate. The thickness of films was about 1μm. P (B) concentration in films was controlled by changing the areal ratio of P_2O_5 (B_2O_3) in sputtering targets. The average concentration of P_2O_5 in a whole film was determined by an electron probe microanalysis, and that of B_2O_3 by the intensity ratio of Si-O and B-O vibration signals in infrared (IR) absorption spectroscopy [24, 25]. Er concentration was fixed to be about 0.02 at.%.

After the deposition, films were annealed in N_2 gas (99.999%) atmosphere for 30 min at 1150 °C. By annealing, Si-ncs were grown in films of the mixture of SiO_2, Er_2O_3, B_2O_3 and/or P_2O_5. During the growth of Si-ncs, P and/or B were incorporated and activated in Si-ncs. Growth of single-crystalline Si-ncs in glass matrices was confirmed by transmission electron microscopic observations [24, 26]. The average size of Si-ncs in pure SiO_2 was about 4 nm in diameter. At low P and B concentration, the size of Si-ncs was almost independent of impurity concentration, while at high concentration (e.g., >1 mol%), the average size became slightly larger than that of Si-ncs in pure SiO_2 with the same Si concentration. This is because glass matrices are softened by P and B doping, resulting in longer diffusion length of Si atoms during annealing, which makes particles slightly larger [24].

The evidences that P and/or B are doped into substitutional sites of Si-ncs and are electrically active have been obtained from IR absorption spectroscopy [22] and electron spin resonance (ESR) spectroscopy [23]. In IR absorption spectra, when P (B) was doped, broad absorption due to free-carrier (or confined-carrier) absorption, i.e., intra-conduction (valence) band transitions of electrons (holes), was observed, and it became stronger with increasing impurity concentration [22]. On the other hand, the absorption became very weak if nearly the same amount of P and B was doped simultaneously, meaning that

carriers were compensated. In ESR spectra, a broad signal which can be assigned to free carriers was observed by P doping, and at low temperatures, hyper-fine splitting of the signal due to the interaction of electron spin with the P nuclear spin was observed [23]. The observed hyper-fine splitting was much larger than that of a P donor in bulk Si, being the direct evidence that P donor wavefunction was squeezed by quantum confinement effects.

Although the existence of electrically active shallow impurities in Si-ncs can be evidenced by IR absorption and ESR studies, the number of active dopants or excess carriers in each nanocrystal cannot simply be estimated even if the average P or B concentration in a whole film is known, because solubility of dopants is different between Si-ncs and SiO_2, and they may precipitate at interface regions. However, considering the small size of nanocrystals the number of carriers should be very small even when impurity concentration is very high, e.g., impurity concentration of 1×10^{20} cm^{-3} corresponds to in average 3.2 impurities per a nanocrystal 4 nm in diameter.

PL spectra were measured by using a single grating monochromator and an InGaAs near-Infrared diode array. The spectral response of the detection system was calibrated with the aid of a reference spectrum of a standard tungsten lamp. For the time transient measurements, a 510 nm line of an optical parametric oscillator (OPO) pumped by the third harmonic of a Nd:YAG laser was used as an excitation source (pulse energy 0.5 mJ/cm^2, pulse width 5 nsec, and repetition frequency 20 Hz). In this wavelength, Er^{3+} is not directly excited. This means that only Er^{3+} having interaction with Si-ncs can be excited by the energy transfer, and that not interacting with Si-ncs is not excited. Emitted light was detected by a near infrared photomultiplier (5509-72, Hamamatsu) and decay curves were recorded by a multichannel scaler. All measurements were carried out at room temperature.

As references, we studied PL properties of Er doped PSG (Er:PSG) and Er doped BSG (Er:BSG) prepared by the same procedure as that used for the other samples. Er^{3+} in these samples cannot be excited by 510 nm light. We therefore employed 521 nm light to excite Er^{3+} for the samples not containing Si-ncs.

4.3 Results and discussions

4.3.1 P or B doping

Figure 4.2(a) shows PL spectra of Si-ncs and Er doped PSG (Er:Si-ncs:PSG) with different P concentration. Peaks are observed at around 1.4 eV and 0.81 eV. The 1.4 eV peak is assigned to the recombination of excitons confined in Si-ncs, and the 0.81 eV one to the intra-4*f* shell transition of Er^{3+} (Er-PL). In Fig. 4.2(b), PL intensities of Si-ncs and Er^{3+} are plotted as a function of P concentration. The PL intensity of Si-ncs first

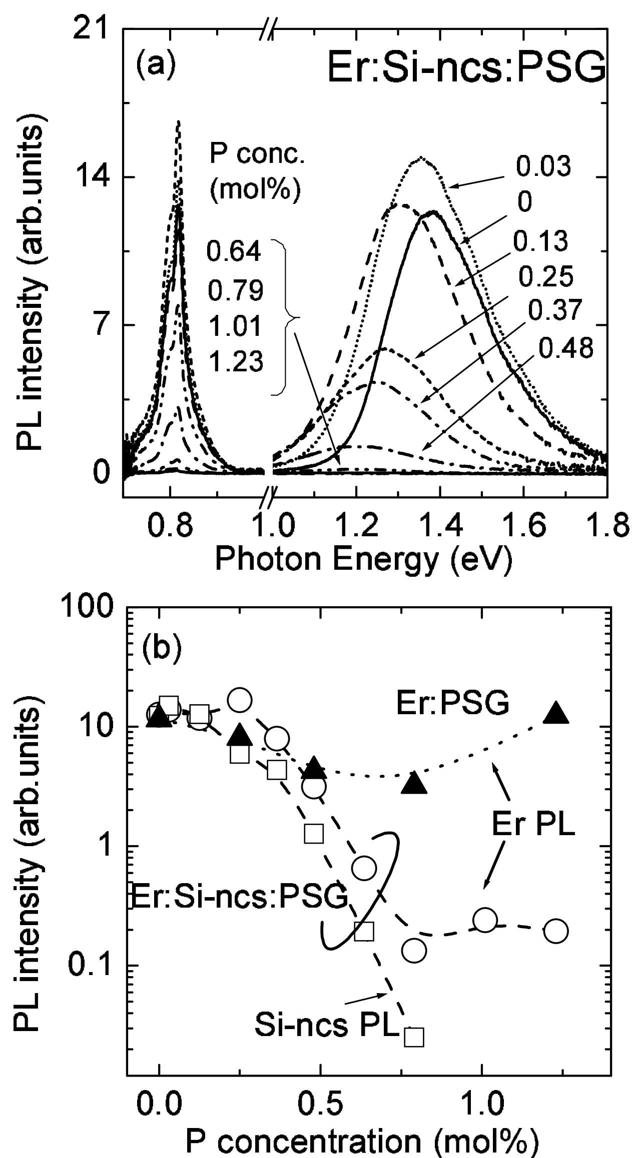

Figure 4.2: (a) PL spectra of Er:Si-ncs:PSG with different P concentration. A broad band centered at around 1.4 eV is due to recombination of excitons in Si-ncs and a sharp one at 0.81 eV arises from intra-4f shell transition of Er^{3+}. (b) P concentration dependence of PL peak intensities of Er^{3+} and Si-ncs in Er:Si-ncs:PSG, and that of Er^{3+} in Er:PSG.

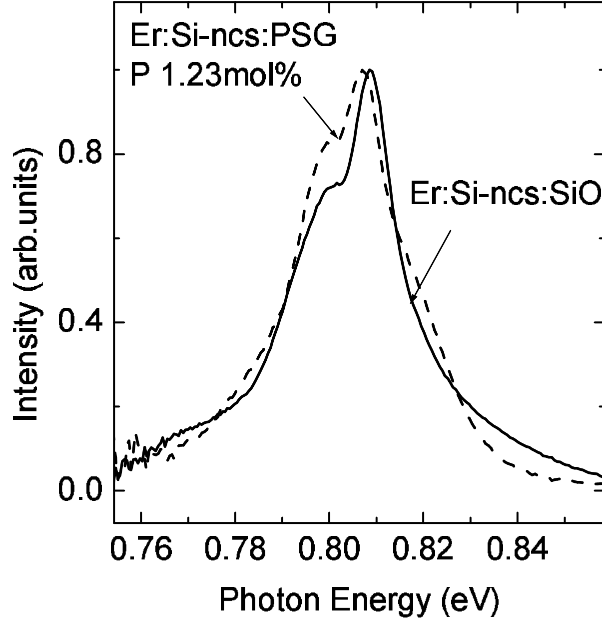

Figure 4.3: PL spectra of Er^{3+} in Er:Si-ncs:SiO_2 (solid curve) and in Er:Si-ncs:PSG (P concentration of 1.23mol%) (dashed curve).

increases slightly with increasing P concentration and then decreases monotonously. In the present Er concentration, Si-ncs not interacting with Er^{3+} remain in a film, and the PL arises mainly from these Si-ncs, because strong interaction with Er^{3+} efficiently quenches the PL. Therefore, the observed P concentration dependence can be explained by the same model proposed for Si-ncs in PSG without Er^{3+} doping (Si-ncs:PSG) [22, 23]. Low concentration doping results in inactivation of dangling-bond defects at Si-SiO_2 interfaces, while heavy doping results in the formation of excess electrons in Si-ncs, which quenches exciton luminescence by an impurity Auger process.

Below the P concentration of 0.79 mol%, the intensity of Er-PL shows similar behavior to that of Si-ncs, while above 0.79 mol%, the intensity is slightly recovered. It should be stressed here that the observed strong P concentration dependence of the intensity below the P concentration of 0.79 mol% does not come from a modified local environment of Er^{3+} by P doping. This can be proved by studying P concentration dependence of PL from Er:PSG. Without Si-ncs, the variation of the intensity by P doping is much smaller. Furthermore, below the P concentration of 0.79 mol%, spectral shape of Er-PL is independent of P concentration. The observed strong quenching is thus due to the interaction between Er^{3+} and P in Si-ncs.

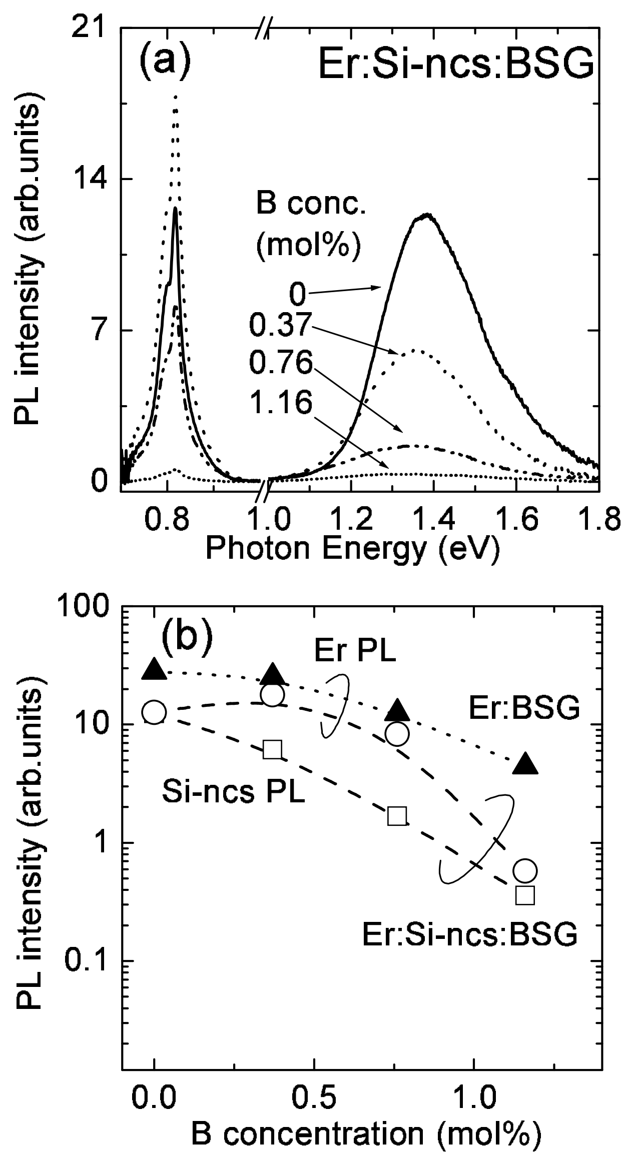

Figure 4.4: (a) PL spectra of Er:Si-ncs:BSG samples with different B concentration. (b) B concentration dependence of PL peak intensities of Er^{3+} and Si-ncs in Er:Si-ncs:BSG, and that of Er^{3+} in Er:BSG.

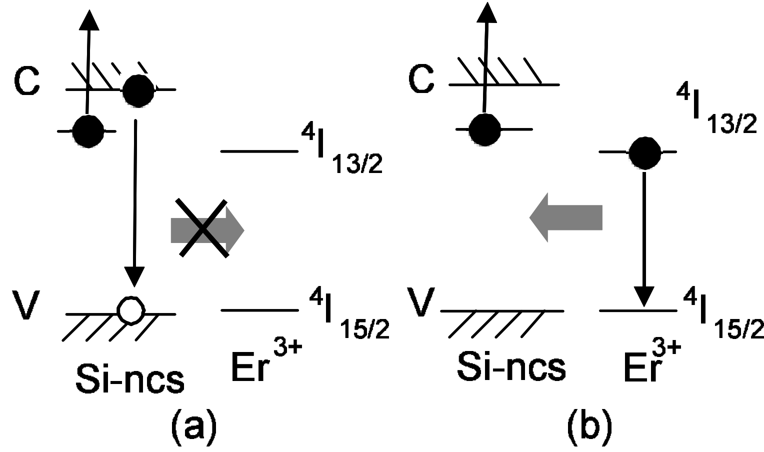

Figure 4.5: Schematic representations of two possible mechanisms for the quenching of PL from Er^{3+}: (a) Auger recombination of an exciton within Si-ncs with the interaction of an excess electron bound to a P donor, and (b) Auger de-excitation of excited Er^{3+} with the interaction of an electron in Si-ncs.

Above the P concentration of 0.79 mol%, P concentration dependence of PL from Er^{3+} deviates from that from Si-ncs, suggesting that the local environment of Er^{3+} is changed from that of low P concentration samples. In fact, above 0.79 mol%, the spectral shape of Er^{3+} is modified significantly as can be seen in Fig. 4.3. Although the effect of the local environment of Er^{3+} is interesting to study in detail, we will restrict our attention to the P concentration range of smaller than 0.79 mol%, because the purpose of this work is to study the interaction between Er^{3+} and shallow impurities, and the change of the local environment makes the analysis of data more complicated.

Figure 4.4(a) shows PL spectra of Si-ncs and Er^{3+} doped BSG (Er:Si-ncs:BSG) with various B concentration. In contrast to the case of P doping, the change of spectral shape of Er-PL is not seen even at the highest B concentration. The PL intensities of Si-ncs and Er^{3+} are plotted in Fig. 4.4(b) as a function of B concentration together with that of Er^{3+} in Er:BSG. We can see that the effect of B doping on the PL properties of Si-ncs and Er^{3+} are qualitatively the same as that of P doping. This suggests that the mechanism of PL quenching by doping is within the first approximation independent of the polarity of doped carriers. In the following, we will discuss the mechanism mainly for P doped samples. The same discussion can be applied to B doped samples.

If excess carriers are supplied to Si-ncs, two quenching paths become active. The first one is Auger interaction within Si-ncs; an exciton recombines nonradiatively by giving kinetic energy to an excess carrier [Fig. 4.5(a)]. If the rate of this process is comparable to or larger than that of energy transfer to Er^{3+}, the energy transfer efficiency is suppressed. Therefore, PL efficiency of Er^{3+} interacting with doped Si-ncs is smaller than

that interacting with pure Si-ncs. With increasing impurity concentration, the number of doped Si-ncs increases, resulting in the quenching of Er-PL. This process does not affect the lifetime of the PL. The other mechanism of PL quenching is Auger de-excitation of excited Er^{3+} by giving energy to an excess carrier in Si-ncs [Fig. 4.5(b)]. In this case, PL quenching is accompanied by the shortening of the lifetime. Therefore, these two processes can be distinguished by studying PL lifetime as a function of P(B) concentration.

Figures 4.6(a) and 4.6(b) show PL time transients of Er^{3+} for Er:Si-ncs:PSG and Er:Si-ncs:BSG respectively. Without P (B) doping, the decay curve is nearly a single-exponential function with the lifetime of about 3.8 msec. By P (B) doping, the lifetime becomes shorter, and the decay curve deviates from a single-exponential function. The shortest lifetime observed is about 480 μsec for Er:Si-ncs:PSG with the P concentration of 0.79 mol%. In Fig. 4.7, the lifetime is plotted as a function of P (B) concentration together with the data obtained for Er:PSG and Er:BSG. The lifetime of Er-PL for Er:PSG and Er:BSG does not depend strongly on P and B concentrations. The observed shortening of lifetime in Er:Si-ncs:PSG(BSG) is thus due to the interaction of excited Er^{3+} with shallow impurities in Si-ncs.

As discussed in the introduction, the cross-section of impurity Auger interaction in Er:bulk-Si is two orders of magnitude different depending on whether carriers are free or bound. In Si-ncs, donors or accepters are considered to be not ionized even at room temperature because of the enhanced ionization energy by quantum size effects [19–21]. Therefore, Er^{3+} interacts with bound carriers in Si-ncs, and thus the situation is similar to Er:bulk-Si at low temperatures. Unfortunately, theory of Auger de-excitation of impurities with bound carriers does not lead to a simple final formula, and thus a phenomenological treatment has been applied to quantitatively analyze the phenomena in Er:bulk-Si [16]. In the treatment, the effective Auger coefficient (C_A) is estimated from the relation, $1/\tau = 1/\tau_0 + C_A N_A$, where τ and τ_0 are the lifetime of Er^{3+} for the samples with and without impurity doping, and N_A the excess carrier concentration [16]. In the present samples, N_A can not simply be estimated from average P or B concentration, because P or B are not expected to be uniformly distributed. However, rough estimation is possible. For example, for the Er:Si-ncs:PSG sample with P concentration of 0.79 mol%, PL intensity of Si-ncs is nearly completely quenched. This suggests that almost all Si-ncs have at least one electrically active P atom. One P in a nanocrystal with 4 nm in diameter corresponds to the P concentration of $3{\times}10^{19} cm^{-3}$. Thus N_A should be lager than $3{\times}10^{19} cm^{-3}$. This estimation gives us the maximum possible value of C_A of $6.1 \times 10^{-17} cm^3 s^{-1}$. This value is two orders of magnitude smaller than that reported for Er^{3+} doped bulk Si for bound carriers [16]. Similar value is obtained for Er:Si-ncs:BSG samples.

It is now clear that the shortening of PL lifetime by the impurity Auger process is the cause of observed quenching of Er-PL. However, the quenching cannot be fully explained

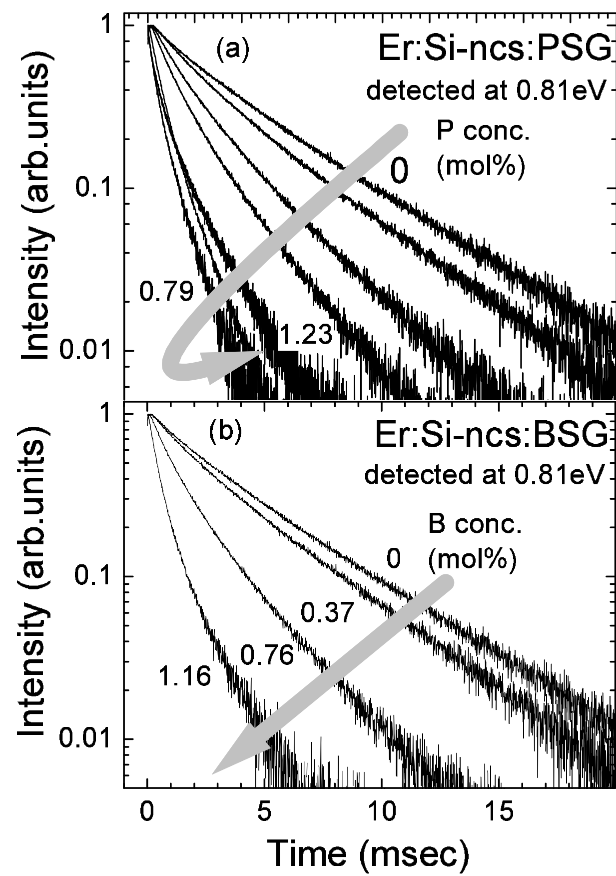

Figure 4.6: PL time transient of Er^{3+} for (a) Er:Si-ncs:PSG and (b) Er:Si-ncs:BSG.

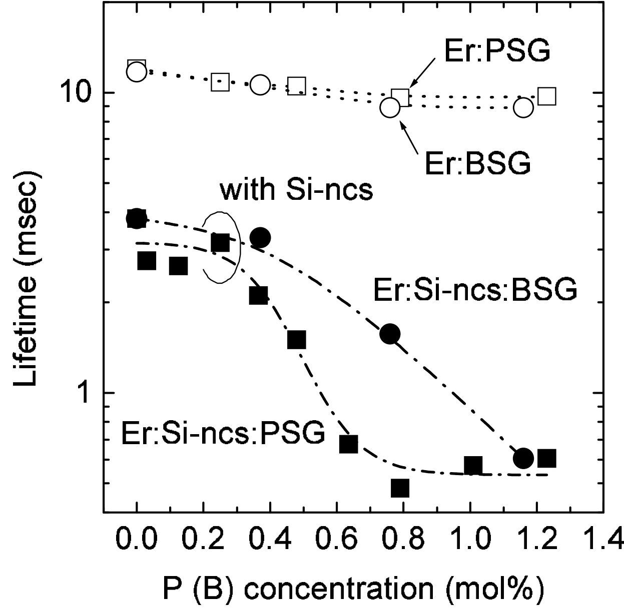

Figure 4.7: PL lifetime of Er^{3+} as a function of P(B) concentration for Er:Si-ncs:PSG, Er:nc-S:BSG, Er:PSG, and Er:BSG.

by the mechanism. In the case of P doping the intensity of Er-PL is decreased by two orders of magnitude, while the lifetime is shortened by one order of magnitude. This difference suggests that impurity Auger within Si-ncs [Fig. 4.5(a)] competes with energy transfer to Er^{3+}, and is also responsible for the quenching. As mentioned in the introduction, there are two energy transfer processes, i.e., fast and slow processes. Among them, the slow process, the time scale of which is μsec range, is more strongly affected. In fact, the slow rising part of Er-PL after pulsed excitation disappears by P or B doping.

4.3.2 P and B doping

PL properties of simultaneously P and B doped samples (Er:Si-ncs:BPSG) give us additional information on the interaction between Er^{3+} and shallow impurities. Figure 4.8 compares the PL spectra of Er^{3+} in Er:Si-ncs:SiO_2, Er:Si-ncs:BSG and Er:Si-ncs:BPSG. B concentration in Er:Si-ncs:BSG and Er:Si-ncs:BPSG is the same (1.16 mol%). We can see that quenching of Er-PL by B doping is recovered by adding P to nearly the same intensity as that of Er:Si-ncs:SiO_2. The recovery of the PL intensity is accompanied by the appearance of a broad peak below the bandgap of bulk Si. The low energy peak has

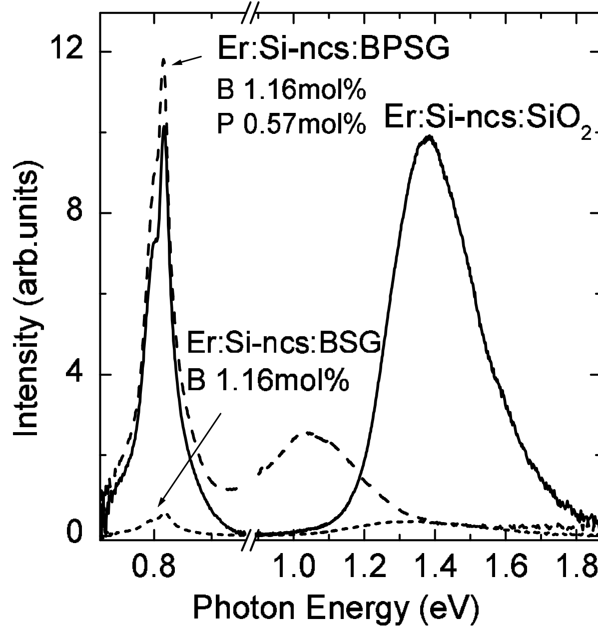

Figure 4.8: (a)PL spectra of Er:Si-ncs:SiO_2 (solid curve), Er:Si-ncs:BSG (dotted curve) and Er:Si-ncs:BPSG (dashed curve). B concentration in Er:Si-ncs:BSG and Er:Si-ncs:BPSG is the same.

been observed for B and P doped Si-ncs without Er doping, and assigned to the optical transition between impurity states formed in the bandgap of Si-ncs by B and P doping [24, 27]. The intensity of the impurity-related PL of Er:Si-ncs:BPSG is much larger than that of Er:Si-ncs:BSG due to the compensation of excess carriers in Si-ncs.

The recovery of Er-PL by P doping can also be explained by carrier compensation. By compensation, both Auger recombination processes shown in Figs. 4.5(a) and 4.5(b), i.e., within Si-ncs and between excited Er^{3+} and carriers in Si-ncs, respectively, are suppressed. The suppression of the second de-excitation process should manifest itself as recovering of the lifetime of PL. Figures 4.9(a) and 4.9(b) show time transient of Er-PL in Er:Si-ncs:BPSG. B concentration is fixed to 1.16 mol%, and P concentration is changed from 0 to 1.22 mol% [from 0 to 0.57 mol% in Fig. 4.9(a), and from 0.57 to 1.22 mol% in Fig. 4.9(b)]. The lifetime estimated from Fig. 4.9 is plotted in Fig. 4.10 as a function of P concentration together with the PL intensities of Si-ncs and Er^{3+}. In Fig. 4.9(a) and Fig. 4.10, we can see that the lifetime of Er-PL, which is shortened by B doping, is drastically recovered by adding P. The longest lifetime observed is about 3 msec. This value is very close to that of Er:n-Si:SiO_2 (3.8 msec), meaning that carriers in Si-ncs are

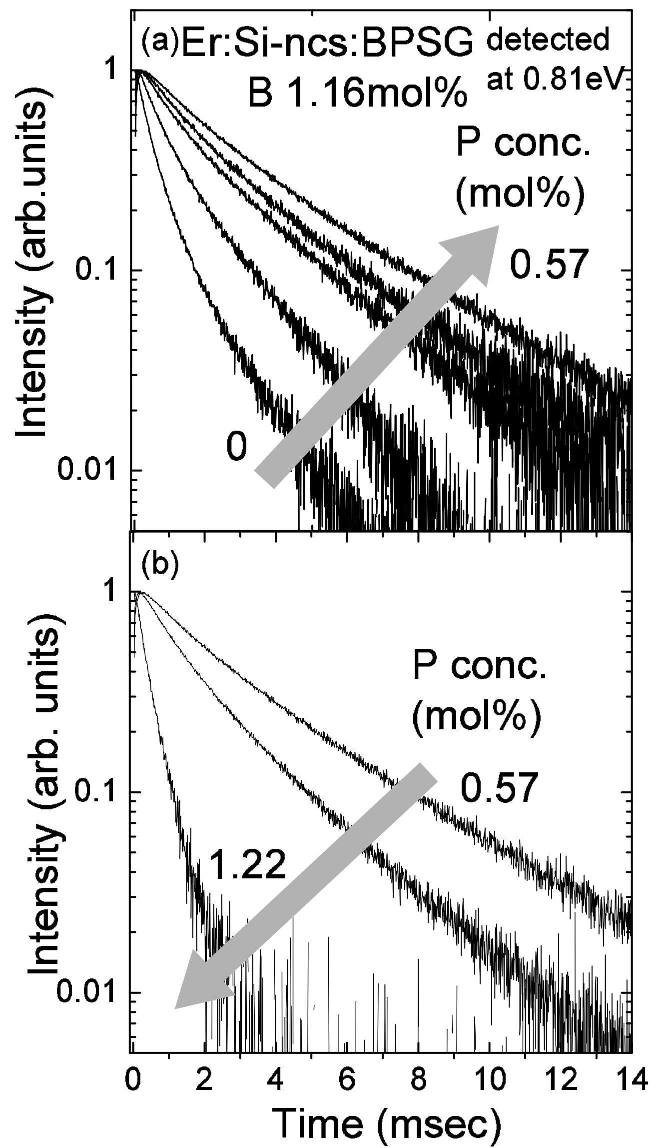

Figure 4.9: PL time transient of Er^{3+} in Er:Si-ncs:BPSG. B concentration is fixed to 1.16mol%, and P concentration is changed (a) from 0 to 0.57 mol% and (b) from 0.57 to 1.22 mol%.

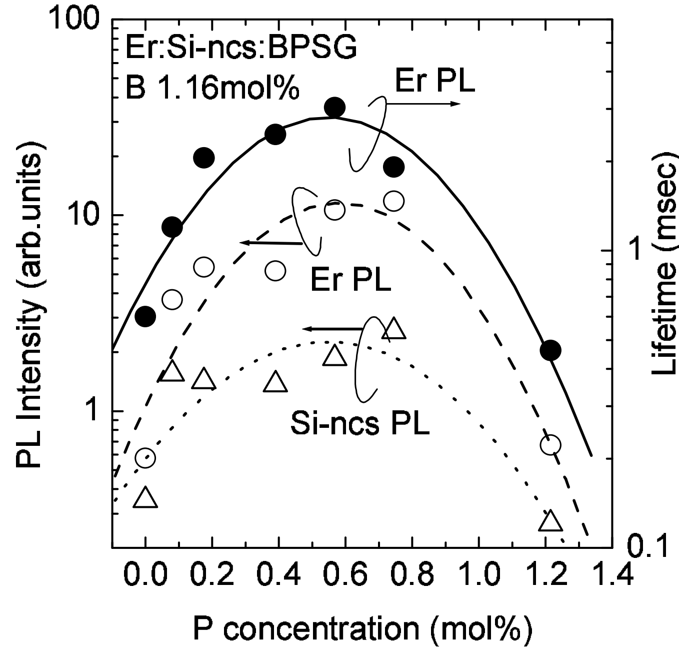

Figure 4.10: The intensities of Si-ncs (△) and Er (◯) PL, and the lifetime of Er PL (•) as a function of P concentration for Er:Si-ncs:BPSG. B concentration is fixed to 1.16 mol%.

almost perfectly compensated and Auger de-excitation does not work. In fact, the PL intensities of both Si-ncs and Er^{3+} are the maximum at this P concentration.

After passing through the longest lifetime point, further increase of P concentration results in shortening of lifetime, which is accompanied by the quenching of PL from Si-ncs and Er^{3+} (Fig. 4.9(b) and Fig. 4.10). Formation of excess electrons by further P doping realizes the same situation as that of Er:Si-ncs:PSG.

In Fig. 4.10, the longest PL lifetime is obtained when B and P concentration in a whole film is 1.16 mol% and 0.54 mol%, respectively, indicating that carriers in Si-ncs are perfectly compensated in this concentration. This result contradicts our previous results on PL from P and B co-doped Si-ncs [27]. In that case, PL from Si-ncs was the strongest when B and P concentration in a whole film was nearly the same. Two mechanisms are considered as the origin of the discrepancy. The first one is that the distribution of B and P in a film is modified by Er doping, i.e., suppression of B doping in Si-ncs or enhancement of P doping, resulting in carrier compensation in Si-ncs when P concentration in a whole film is nearly the half of B concentration. The second possible model is that doped Er^{3+} acts as a donor and thus smaller amount of P is necessary for compensation. Donor

behavior of Er^{3+} is well known in Er:bulk-Si and compensation of the donor by B doping is demonstrated [16]. At present, we have no direct evidence to decide which mechanism is working.

4.4 Conclusion

We have studied the interaction between shallow impurities in Si-ncs and Er^{3+}. It was shown that shallow impurity doping drastically decreases the efficiency of Er-PL. Two different Auger processes are responsible for the quenching. Auger recombination of photoexcited excitons with the interaction of electrons or holes supplied by impurity doping competes with energy transfer to Er^{3+} and degrades energy transfer efficiency. Even if excitation of Er^{3+} by the energy transfer is successfully completed, radiative relaxation of Er^{3+} has to compete with Auger de-excitation with the interaction of electrons or holes in Si-ncs, resulting in shortening of lifetime and degradation of the quantum efficiency. These effects are very similar to that observed for Er:bulk-Si, thus supporting our previous conclusion that the mechanism of the interaction between Si-ncs and Er^{3+} is qualitatively the same as that of Er:bulk-Si [11]. However, there are some quantitative differences. The estimated Auger coefficient is found to be two orders of magnitude smaller than that of Er:bulk-Si at low temperatures where carriers are bound to donor or acceptor ions, and four orders of magnitude smaller than that at room temperature. This small Auger coefficient makes Si-ncs immune from the impurity Auger de-excitation process compared to Er:bulk-Si and is considered to be one of the origins of temperature independent efficient PL of Er:Si-ncs:SiO_2 systems.

We also studied the effects of carrier compensation on PL from Er^{3+} and demonstrated that perfectly compensated Si-ncs does not degrade PL from Er^{3+}, although PL properties of Si-ncs themselves are strongly modified. The recovery of luminescence properties by compensation is another evidence of the interaction between excited Er^{3+} and shallow impurities in Si-ncs.

It is very plausible that Auger de-excitation of Er^{3+} with the interaction of carriers in Si-ncs is not limited to the situation that the carriers are supplied by shallow impurity doping. The de-excitation may also be possible in Er:Si-ncs:SiO_2 containing pure Si-ncs if second exciton is photogenerated in a nanocrystal when Er^{3+} is already excited by the energy transfer from the nanocrystal. The Auger interaction of the excited Er^{3+} with the photogenerated carrier may quench Er-PL, if the rate of this process is comparable to or larger than that of the energy transfer rate. If this process really works, excitation of multiple Er^{3+} by a single nanocrystal becomes very inefficient, and one nanocrystal can excite only one Er^{3+} during the lifetime of excited Er^{3+}. This conclusion is consistent with the result obtained by Kik et al. [8].

References

[1] C. E. Chryssou, A. J. Kenyon, T. S. Iwayama, C. W. Pitt, and D. E. Hole, Appl. Phys. Lett. **75**, 2011 (1999).

[2] A. J. Kenyon, P. F. Trwoga, M. Federighi, and C. W. Pitt, J. Phys.: Condens. Matter **6**, L319 (1994).

[3] M. Fujii, M. Yoshida, Y. Kanzawa, S. Hayashi, and K. Yamamoto, Appl. Phys. Lett. **71**, 1198 (1997).

[4] M. Fujii, M. Yoshida, S. Hayashi, and K. Yamamoto, J. Appl. Phys. **84**, 4525 (1998).

[5] D. Pacifici, G. Franzo, F. Priolo, F. Iacona, and L. DalNegro, Phys. Rev. B **67**, 245301 (2003)

[6] F. Priolo, G. Franzò, D. Pacifici, V. Vinciguerra, F. Iacona, and A. Irrera, J. Appl. Phys. **89**, 264 (2001).

[7] A. J. Kenyon, C. E. Chryssou, C. W. Pitt, T. Shimizu-Iwayama, D. E. Hole, N. Sharma, and C. J. Humphreys, J. Appl. Phys. **91**, 367 (2002).

[8] P. G. Kik, and A. Polman, J. Appl. Phys. **88**, 1992 (2000).

[9] J. H. Shin, S.-Y. Seo, S. Kim, and S. G. Bishop, Appl. Phys. Lett. **76**, 1999 (2000).

[10] K. Watanabe, M. Fujii, and S. Hayashi, J. Appl. Phys. **90**, 4761 (2001).

[11] M. Fujii, K. Imakita, K. Watanabe, and S. Hayashi, J. Appl. Phys. **95**, 272 (2004).

[12] M. S. Bresler, O. B. Gusev, B. P. Zakharchenya, and I. N. Yassievich, Phys. Solid State **38**, 813 (1996).

[13] M. Forcales, T. Gregorkiewicz, M. S. Bresler, O. B. Gusev, I. V. Bradley, and J-P. R. Wells, Phys. Rev. B. **67**, 085303-1 (2003).

[14] M. Forcales, T. Gregorkiewicz, and M. S. Bresler, Pys. Rev. B. **68**, 035213-1 (2003).

[15] T. Förster, Ann. Phys. (N.Y) **2**, 55 (1948).

[16] F. Priolo, G. Franzò, S. Coffa, and A. Carnera, Phys. Rev. B **57**, 4443 (1998).

[17] S. Coffa, G. Franzò, F. Priolo, A. Polman, and R. Serna, Phys. Rev. B **49**, 16313 (1994).

[18] A. Suchocki, and J. M. Langer, Phys. Rev. B **39**, 7905 (1989).

[19] C. Delerue, M. Lannoo, G. Allan, E. Martin, I. Mihalcescu, J. C. Vial, R. Romestain, F. Muller, and A. Bsiesy, Phys. Rev. Letts. **75**, 2228 (1995).

[20] C. Delerue, M. Lannoo, G. Allan, and E. Martin, Thin Solid Films **255**, 27 (1995).

[21] G. Allan, C. Delerue, M. Lannoo, and E. Martin, Phys. Rev. B **52**, 11982 (1995).

[22] A. Mimura, M. Fujii, S. Hayashi, D. Kovalev, and F. Koch, Phys. Rev. B **62**, 12625 (2000)

[23] M. Fujii, A. Mimura, S. Hayashi, Y. Yamamoto, and K. Murakami, Phys. Rev. Lett. **89**, 206805-1 (2002)

[24] M. Fujii, K. Toshikiyo, Y. Takase, Y. Yamaguchi, and S. Hayashi, J. Appl. Phys. **94**, 1990 (2003).

[25] A. S. Tenny, J Electrochem. Soc. **118**, 1658 (1971).

[26] S. Takeoka, M. Fujii, and S. Hayashi, Phys. Rev. B **62**, 16820 (2000).

[27] M. Fujii, Y. Yamaguchi, Y. Takase, K. Ninomiya, and S. Hayashi, Appl. Phys. Lett. **85**, 1158 (2004).

Chapter 5

Enhancement of radiative recombination rate of excitons in Si nanocrystals on a Au film

In this chapter, the author demonstrates time-resolved photoluminescence (PL) spectra of Si nanocrystals doped SiO_2 on Au thin films. It is shown that the PL intensity within several tenth of μs after excitation is enhanced by the presence of Au films. The data suggest that the radiative recombination rate of excitons in Si-ncs is enhanced, and the degree of the enhancement depends strongly on the emission photon energy. The enhancement is found to arise from the modification of the local photonic mode density by the presence of Au thin films.

5.1 Introduction

Silicon nanocrystals (Si-ncs) show strong photoluminescence (PL) at room temperature due to the recombination of excitons confined in the zero-dimensional quantum confined system [1–4]. The high-efficiency of the PL arises from two mechanisms. The first one is the restriction of carrier transport in nanometer scale regions, and resultant suppression of non-radiative recombination processes via defects or impurities. The second one is the enhancement of the radiative recombination rate. Because of the confinement of excitons in a space smaller than the exciton Bohr radius of bulk Si crystals, the overlap of electron and hole wavefunctions becomes large in both real and momentum spaces, resulting in the enhancement of the spontaneous emission rate [3, 4]. However, even for Si-ncs as small as a few nanometers in diameter, indirect bandgap nature of bulk Si crystals is strongly inherited, and thus the radiative recombination rate is still not large enough

[3, 4]. Therefore, further improvement of the radiative rate is required to realize Si based light-emitting devices.

The radiative rate of an emitter can be modified by controlling the local photonic environments by placing it in a microcavity or in the vicinity of metal surface [5–10]. The simplest explanation of the phenomena is the interaction of emitter's field with the reflected field; if reflected field interacts with the emitter in phase, the radiative decay rate is enhanced, while out of phase, it is suppressed [11, 12]. As a result, the radiative rate oscillates depending on the distance from the surface. Another explanation of the phenomena is that the local photonic mode density (PMD) is changed in the vicinity of metal surface, and this change results in the modification of the radiative rate, because it is proportional to PMD [13–15]. The modification of radiative rate by controlling the photonic environment has been demonstrated for dye molecules [16, 17], rare-earth ions [5, 7, 10], and semiconductor quantum dots or nanocrystals [18, 19].

The purpose of this chapter is to demonstrate the enhancement of the radiative recombination rate of Si-ncs by Au thin films and also to clarify the effect of PMD on emission properties of indirect bandgap semiconductors. The advantage of Si-ncs to study the effect is that the PL band is very broad due to size and shape distributions, and the lifetime at low temperatures is very slow ($\sim$5 ms) and almost independent of the PL energy, i.e., the size, because at low temperatures almost all excitons stay in spin-forbidden triplet states [2, 20, 21]. The broad PL band allows us to study the emission energy dependence of the effects in one measurement. The author shows that the radiative rate can be enhanced by the presence of Au thin films by time-resolved PL measurements of Si-ncs at low temperatures.

5.2 Experimental details

SiO_2 films containing Si-ncs were prepared by a co-sputtering method. Si and SiO_2 were simultaneously sputter-deposited on SiO_2 substrates, and the deposited films (300 nm in thickness) were annealed in a nitrogen (N_2) gas (99.999 %) atmosphere for 30 minutes at temperatures above 1200 ^{o}C. Si-ncs were grown in the films during the annealing. In this method, the size of Si-ncs can be controlled by the concentration of excess Si in the films or the annealing temperature. We have prepared samples with two different size distributions with the average sizes of about 3.4 and 5.8 nm (samples A and B) by changing excess Si concentration. The refractive indices at 1.5 eV estimated from Bruggeman effective medium theory [22] are 1.47 and 1.55 for samples A and B, respectively. After annealing, Au films (10 μm in thickness) were deposited on a part of sample surface by vacuum evaporation.

PL was excited by 457.9 nm light of an optical parametric oscillator (OPO) pumped by

the third harmonic of a Nd:YAG laser (pulse energy 0.5 mJ/cm^2, pulse width 5 nsec, and repetition frequency 20 Hz) through a transparent fuzed quartz substrate. The incident light was aligned perpendicular to the sample surface and PL was corrected from the same side. Conventional PL spectra were measured by using a single grating monochromator equipped with an InGaAs near-infrared diode array or a Si charge coupled device. The spectral response of the detection system was calibrated with the aid of a reference spectrum of a standard tungsten lamp. For PL decay measurements, a near infrared photomultiplier (5509-72, Hamamatsu) and a multichannel scaler were used. Time resolved PL spectra were constructed by combining PL decay curves measured in the wavelength range between 650 and 1250 nm. All measurements were carried out at 5 K.

5.3 Results

In the insets of Figs. 5.1(a) and 5.1(b), PL spectra of bare and Au-coated samples are compared for samples A and B, respectively. The PL arises from the recombination of excitons in Si-ncs (Si-nc PL) and is inhomogeneously broadened due to size distribution, and resultant bandgap distribution. In order to compare PL intensities of bare and Au-coated samples, the reflection of excitation and emission light at Au surface is taken into account. The reflection coefficient of a Au film is about 0.3 for the excitation wavelength, and is almost 1 for the detection wavelength [23]. Therefore, at maximum, excitation power and detection efficiency of Au-coated samples are 1.3 and 2 times, respectively, larger than those of bare samples. PL intensities of Au-coated samples in the insets of Figs. 5.1(a) and 5.1(b) are thus divided by a factor of 2.6. To confirm the appropriateness of the factor, we studied how much the PL intensity is enhanced when a Au film is deposited on the back-side of the sample. In this situation, there is no direct interaction between Si-ncs and Au, and the enhancement arises only from the reflection of excitation and emission light. The observed enhancement factor was about 2.5, which is very close to the value we employed,. i.e., 2.6. After the correction, we can see that PL intensities are decreased about 40 % and 10 % by Au deposition for samples A and B, respectively. The decrease is due to the excitation of surface plasmons and lossy waves in the Au layer by energy trasnfer from Si-ncs.

PL decay curves of samples A and B are shown in Figs. 5.1(a) and 5.1(b), respectively. The decay curves are normalized at the maximum intensities. The decay curves of the samples without Au coating consist of fast and slow components. The slow component is assigned to radiative recombination of excitons confined in Si-ncs, while the fast one to that trapped at defects at Si/SiO_2 interfaces. The contribution of the fast component is larger at lower detection energy, because the maximum of the defect-related PL is at around 0.8 eV [24, 25]. The lifetime of the exciton PL is very long (several ms) due to the

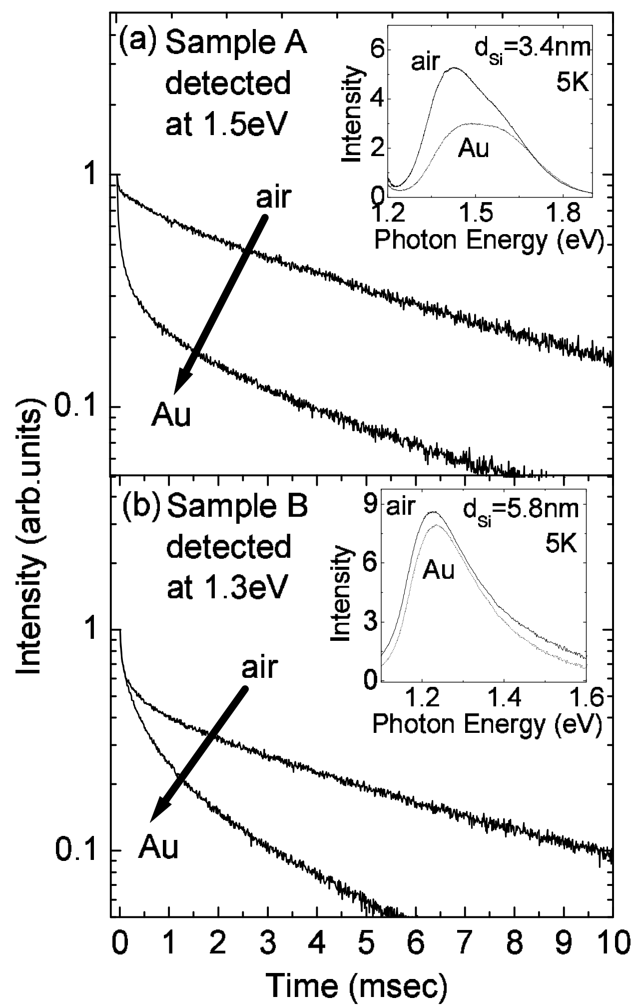

Figure 5.1: PL decay curves of Si nanocrystals (a) 3.4 nm and (b) 5.8 nm in average diameter detected at 1.5 and 1.3 eV, respectively at 5 K. Insets: PL spectra.

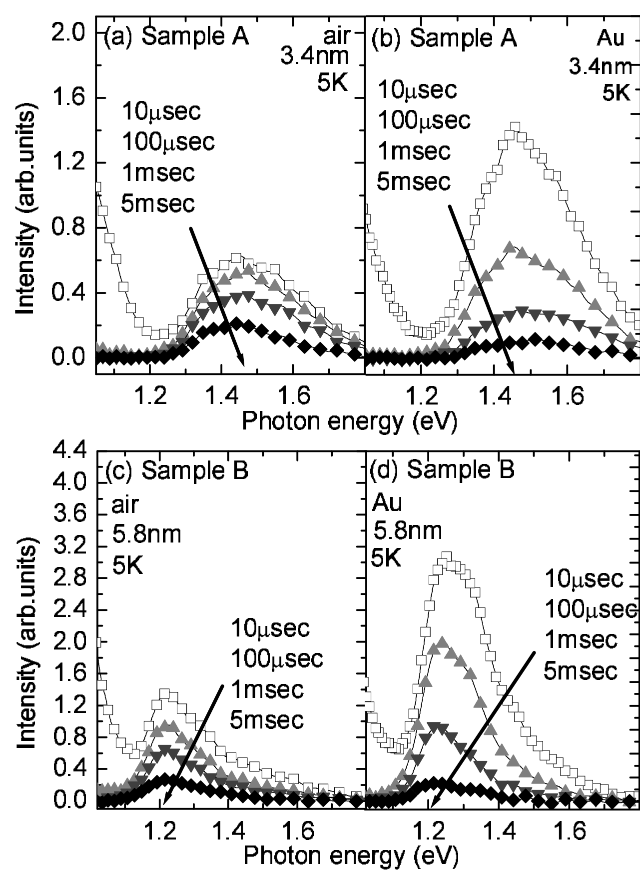

Figure 5.2: Time-resolved PL spectra of Si-ncs at low temperature for sample A [(a) and (b)], and sample B [(c) and (d)]. The spectra of bare samples [(a) and (c)] and samples with Au films [(b) and (d)] are shown.

occupation of excitons in spin-forbidden triplet states.

By depositing Au thin films on top, the decay curves are strongly modified and the lifetimes are shortened by roughly an order of magnitude in the presence of Au thin films. It is worth noting that the change in the lifetime caused by Au coating is much larger than that in the intensity. For example, for sample B, the PL intensity is decreased only about 10 %, while the lifetime is shortened by an order of magnitude. This suggests that radiative decay rates as well as non-radiative ones are modified by the Au layer.

To study the emission energy dependence of the effect, we measured time resolved PL spectra at low temperature. Figures 5.2(a) and 5.2(c) show the results obtained for the samples without Au coating [Fig. 5.2(a): sample A, Fig. 5.2(c): sample B], while Figs. 5.2(b) and 5.2(d) for those with Au layers. The PL intensities of Au-coated samples are divided by 2.6 to correct the reflection of incident and emission light by a Au layer. By comparing Figs 5.2(a) and 5.2(b), we notice that the PL intensity of the Au-coated sample [Fig. 5.2(b)] just after excitation (t = 10 μsec) is much larger than that of the bare sample [Fig. 5.2(a)], although it decays much faster. The very fast decay results in smaller PL intensity of Au-coated samples in time-integrated spectra in Fig. 5.1. The same result can be seen for the samples with the Si-nc size of 5.8nm (sample B) [Fig.

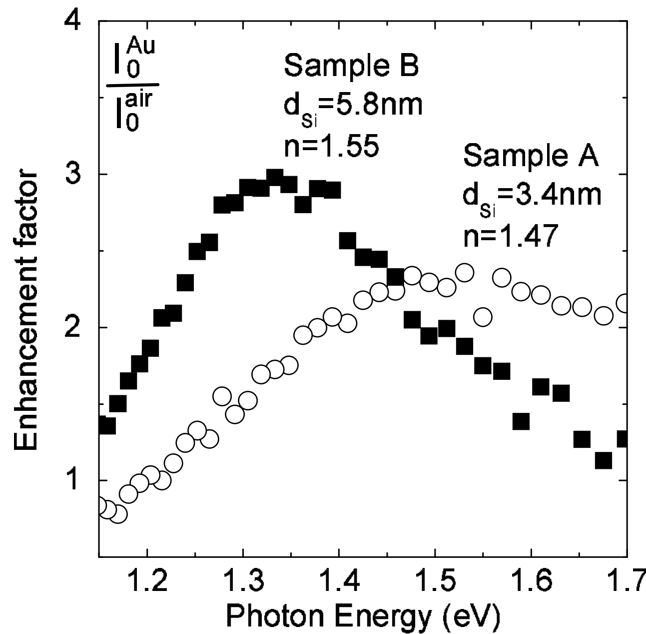

Figure 5.3: The ratio of the PL intensity (enhancement factor) of Au-coated to bare samples at t = 10 μ sec.

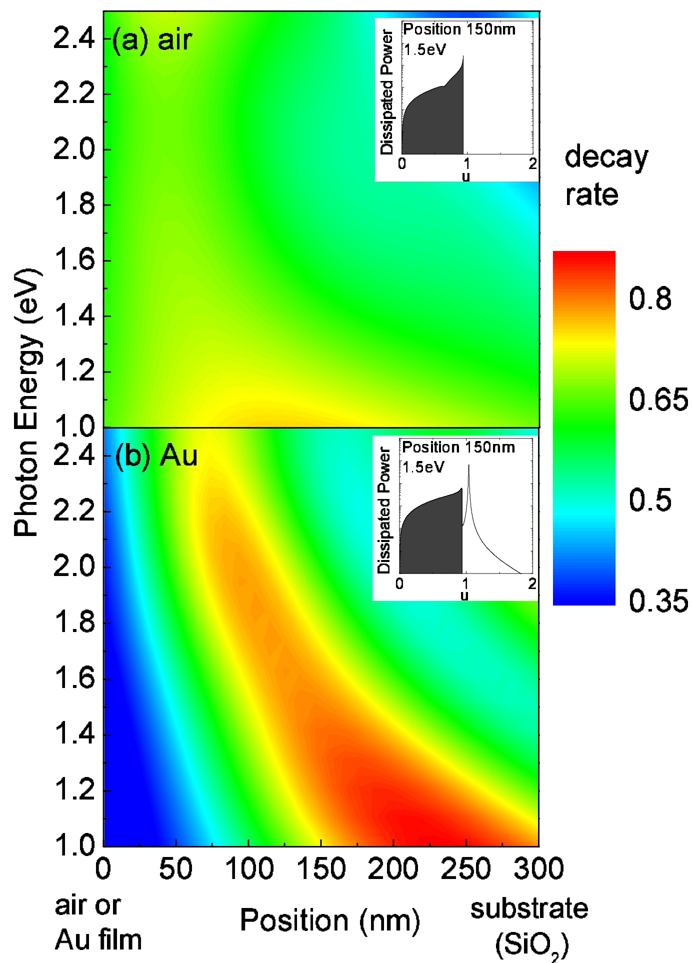

Figure 5.4: Contour plots of calculated radiative decay rates for (a) a bare and (b) a Au-coated samples as a function of photon energy and the position of emitter from air or Au layer. The decay rate is normalized to that in vacuum. The insets show the power dissipation spectra as a function of in-plane wavevector (u).

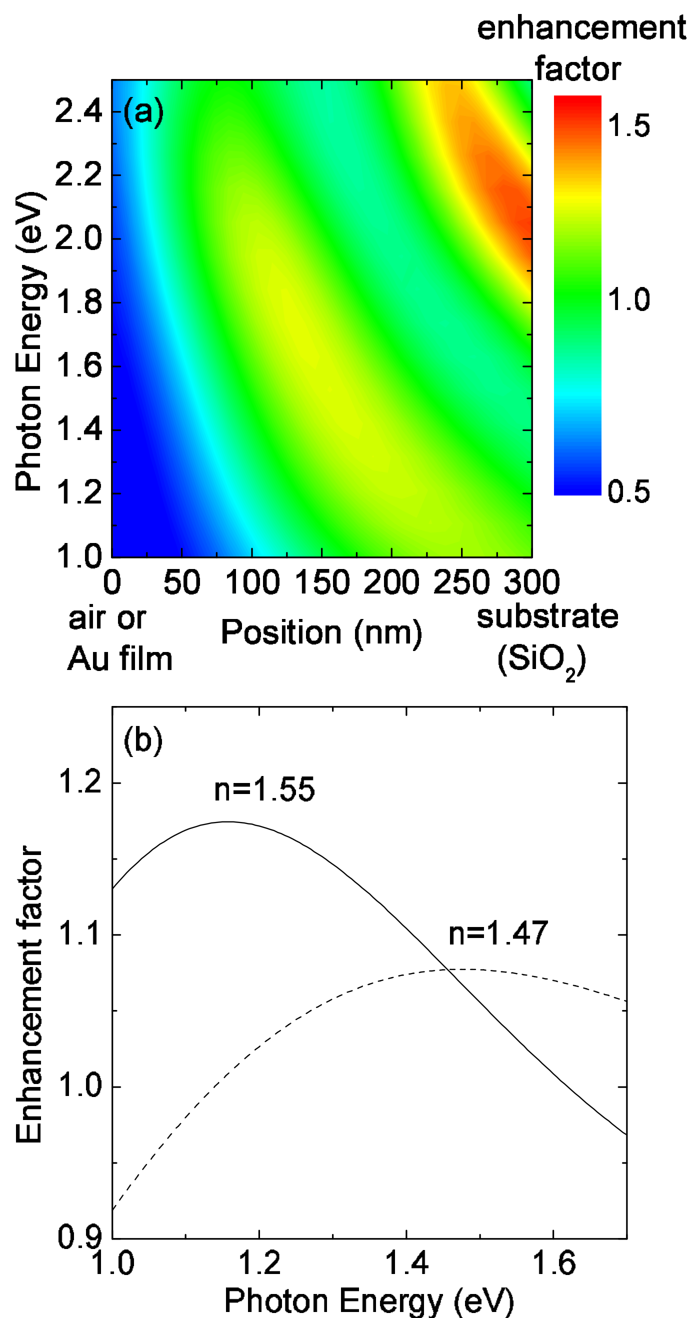

Figure 5.5: (a) The ratio of calculated radiative decay rate (enhancement factor) of the Au-coated to bare samples obtained by dividing Fig. 4(b) by Fig. 4(a). (b) Enhancement factor as a function of photon energy obtained by integrating that of dipoles positioned between 0 and 300 nm from the surface (interface) for the refractive indices of the active layers of 1.55 and 1.47.

5.2(c) and 5.2(d)]. The very fast PL at low energy side is due to defects at Si-ncs/SiO_2 interfaces [24, 25].

The enhancement of the PL intensity at $t = 10$ μsec by Au-coating strongly suggests that the radiative decay rate is enhanced, because if the shortening of the lifetime is caused only by the introduction of new non-radiative recombination processes, PL intensity should be decreased in all time regions. In a simplified model, PL intensity [$I(t)$] after pulse excitation is expressed as $I(t) = W_r N_0 exp(-W_{total} t)$, where W_r and W_{total} are a radiative decay rate and a total decay rete (summation of radiative and nonradiative decay rates), respectively and N_0 the number of excited emitters by pulse excitation. If the time after excitation is much shorter than the lifetime of the emitter, i.e., $W_{total} t \ll 1$, PL intensity is expressed as $I(t) = W_r N_0$. In Fig. 5.2, the effect of reflection at Au surface is corrected, and thus N_0 is considered to be the same, and at $t = 10$ μsec $W_{total} t \ll 1$ is satisfied. Therefore, the observed enhancement of PL intensity at $t = 10$ μsec can be considered to be due to the enhancement of the radiative decay rate.

In order to know the emission energy dependence of the radiative rate enhancement, PL intensities at $t = 10$ μsec of Au-coated samples are divided by those of bare samples (I_0^{Au}/I_0^{air}). The results are shown in Fig. 5.3. We can see strong wavelength dependence of the enfacement factor. For example, for sample B, we see 3 times enhancement at 1.3 eV , while no enhancement at 1.7 eV. The maximum energy of the enhancement factor depends on the samples. In sample A, the maximum appears at around 1.5 eV.

5.4 Discussions

The modification of the radiative and nonradiative decay rates by placing a Au thin film can be calculated by a model developed by Chance et al. [12]. The model considers the emitter to be an oscillating electric dipole, which is damped by its radiation. The power dissipation of the dipole is determined by the imaginary part of the electric field at the position of the dipole, which is given by the summation of the dipolar field and the field reflected at the interfaces. We performed the calculation for three layer structures, i.e., air (or Au) / Si-nc doped SiO_2 / SiO_2. For the calculation, the refractive index of the SiO_2 substrate was set to 1.45, and those of Si-ncs doped SiO_2 to 1.47 and 1.55, which correspond to samples A and B, respectively. In the energy range studied, the dispersion of the refractive indices are small (∼2 %), and thus they are assumed to be constant. The photon energy dependence of the dielectric constant of Au thin film was taken from the literature [23].

Figure 5.4 shows the calculated results for $n = 1.55$. The insets of Figs. 5.4(a) and 5.4(b) show the power dissipation spectra of the bare and Au-coated samples as a function of a in-plane wavevector (u). The photon energy is 1.5 eV and the position of dipole is

the center of the emissive layer, i.e., 150 nm from the surface (or the Au layer). In-plane wavevector is normalized with respect to the far field wavevector. The wavevector larger than 1 corresponds to the evanescent waves of the dipole and not transport energy if there are no absorbing medium in its close proximity. By depositing a Au layer, a very sharp peak appears at around u=1.036 due to the excitation of surface plasmons at the interface between Au thin film and the emissive layer (Si-ncs doped SiO_2). Power dissipation for even larger wavevector range is due to the excitation of intra- and inter-band transitions in the metal. For both samples, u >0.938 results in the total internal reflection at the interface of the emissive layer and the substrate. Therefore, modes with the values of $0<u<0.938$ have propagating far-field components; we shall refer to them as radiative.

Figures 5.4(a) and 5.4(b) compare the calculated radiative decay rates for the bare and Au-coated samples as a function of photon energy (vertical axes) and a position of emitter from the surface (or the Au layer) (horizontal axes). The radiative decay rate can be calculated by integrating the power dissipation spectra for $0<u<0.938$, and is normalized to the rate in vacuum. The calculation is made for the refractive index of 1.55 for the Si-ncs doped SiO_2 layer. We can see that the decay rate is strongly modified by the presence of the Au thin film. Because of the interference of the field produced by the dipole and that reflected by the Au layer the radiative rate oscillates depending on the distance from the interface [Fig 5.4(b)].

By dividing Fig. 5.4(b) by Fig. 5.4(a), the enhancement factor of the radiative rate is obtained as a function of photon energy and the position of a dipole. The result of the division is shown in Fig. 5.5(a). The oscillation of the enhancement factor arises from that of the radiative decay rate of the Au-coated sample. In order to compare the calculated results with experimental results shown in Fig. 5.3, the enhancement factor is averaged over the dipole position from 0 to 300 nm. The results are shown in Fig 5.5(b) for the refractive indices of the Si-ncs doped SiO_2 layers of 1.47 and 1.55. We can see that the enhancement factor depends strongly on the photon energy. The maximum of the enhancement factor shifts to lower energy with increasing the refractive indices. This behavior is very similar to the experimental results shown in Fig. 5.3, suggesting that the observed radiative rate enhancement is due to the interference of the dipole filed with the reflected field. In other words, the PMD near the Au layer is enhanced, resulting in the radiative rate enhancement.

Although the model qualitatively explains the mechanism of the radiative rate enhancement, there are some quantitative disagreements. First, the maximum of the radiative rate enhancement for sample B appears at higher energy compared to that obtained by calculation for n = 1.55. This disagreement seems to arise from the defect-related PL observed at the low-energy side of exciton PL. In the present work, the enhancement factor is estimated from the PL intensity at t = 10 μsec under the assumption that the PL

lifetime is much longer than 10 μsec. The assumption is valid for exciton luminescence, the typical lifetime of which at low temperature is 5 ms. However, the lifetime of the defect-related PL is several μsec, which does not satisfy the assumption. This means that the enhancement factor cannot be estimated properly at low energies, where the intensity of defect-related PL at $t = 10$ μsec is comparable to that of exciton PL. Probably, the enhancement factor in Fig. 5.3 is underestimated at the lower energy side, resulting in the disagreement with the theoretical calculation. Another quantitative disagreement is that the observed enhancement factors are larger than the calculated ones. One of the possible reasons for the disagreement is that the present Au films are not perfectly flat (the root-mean-square roughness of $\sim$ 10 nm). Further studies by systematically changing the degree of roughness is required for quantitative discussion.

5.5 Conclusion

Time-resolved PL spectra of Si-ncs revealed that the radiative recombination rate of excitons in spin-forbidden triplet states can be enhanced by the presence of Au films, and that the degree of enhancement depends strongly on the emission photon energy. We showed that the observed enhancement can qualitatively be explained by that of PMD. The degree of the enhancement of the radiative recombination rate was larger than that predicted by theoretical calculations, suggesting that roughness on the Au layer plays an important role for the enhancement, and by properly controlling the roughness, larger enhancement factor will be obtained.

References

[1] L. T. Canham, Appl. Phys. Lett. **57** (1990) 1046.

[2] S. Takeoka, M. Fujii, and S. Hayashi, Phys. Rev. B **62** (2000) 16820.

[3] C. Delerue, M. Lannoo, G. Allan, and E. Martin, Thin Solid Films **255** (1995) 27.

[4] D. Kovalev, H. Heckler, G. Polisski, and F. Koch, Phys. Stat. Sol(b), **215** (1999) 871.

[5] E. Snoeks, A. Lagendijk, and A. Polman, Phys. Rev. Lett. **74** 2459 (1995).

[6] M. Suzuki, H. Yokoyama, S. D. Brorson, and I. E. Ippen, Appl. Phys. Lett. **58** (1991) 998.

[7] A. M. Vredenberg, N. E. J. Hunt, E. F. Schubert, D. C. Jacobson, J. M. Poate, and G. J. Zydzik, Phys. Rev. Lett. **71** (1993) 517.

[8] R. M. Amos and W. L. Barnes, Phys. Rev. B **55** (1997) 7249.

[9] P. T. Worthing, R. M. Amos, and W. L. Barnes, Phys. Rev. A **59** (1999) 865.

[10] J. Kalkman, L. Kuipers, and A. Polman, Appl. Phys. Lett. **86** (2005) 041113.

[11] G. W. Ford, and W. H. Weber, Phys. Rep. **113** (1985) 195.

[12] P. R. Chance, A. Prock, and R. Silbey, Adv. Chem. Phys. **37** (1978) 1.

[13] K. H. Drexhage, *in Progress in Optics*, edited by E. Wolf (North-Holland, Amsterdam 1974), Vol. 12, p. 153.

[14] W. L. Barnes. J. Mod. Opt. **45** (1998) 661.

[15] K. Joulain, R. Carminati, J. P. Mulet, and J. J. Greffet, Phys. Rev. B **68** (2003) 245405.

[16] J. R. Lakowicz, Y. Shen, S. D'Auria, J. Malicka, J. Fang, Z. Gryczynski, and I. Gryczynski, Analytical Biochemistry **301** (2002) 261.

[17] A. Leitner, M. E. Lippitsch, S. Draxler, M. Riegler, and F. R. Aussenegg, Appl. Phys. B **36** (1985) 105.

[18] X. Brokmann, L. Coolen, M. Dahan, and J. P. Hermier, Phys. Rev. Letts., **93** (2004) 107403.

[19] S. F. Wuister, C. de M. Donegá , and A. Meijerinka, J. Chem. Phys., **121** (2004) 4310.

[20] P. D. J. Calcott, K. J. Nash, L. T. Canham, M. J. Kane, and D. Brumhead, J. Lumin. **57** (1993) 257.

[21] P. D. J. Calcott, K. J. Nash, L. T. Canham, M. J. Kane, and D. Brumhead, J. Phys.: Condens. Matter **5** (1993) L91.

[22] P.A.Snow, E.K.Squire, P.ST.J.Russell, and L.T.Canham, J. Appl. Phys. **86** (1999) 1781.

[23] David W. Lynch, and W. R. Hunter, *Handbook of Optical Constants in Solid*, edited by Edward D. Palik (Academic Press, Inc.).

[24] B. K. Meyer, D. M. Hofmann, W. Stadler, V. Petrova-Koch, F. Koch, Appl. Phys. Lett. **63** (1993) 2120.

[25] B. K. Meyer, D. M. Hofmann, W. Stadler, V. Petrova-Koch, F. Koch, P. Emanuelsson, and P. Omling, J. Lumin. **57** (1993) 137.

[26] K. Okamoto, I Niki, A. Shvartser, Y. Narukawa, T. Mukai, and A. Scherer, Nature Materials **3** (2004) 601.

Chapter 6

Nonlinear optical properties of Si nanocrystals embedded in SiO_2 prepared by a co-sputtering method

In this chapter, nonlinear optical properties of Si nanocrystals (Si-ncs) doped SiO_2 are studied by z-scan technique in a femtosecond regime at around 1.6 eV. The nonlinear refractive index (n_2) and nonlinear absorption coefficient (β) are strongly enhanced compared to those of bulk Si and found to be about $\sim 2 \times 10^{-13}$ cm^2/W and ~ 0.8 cm/GW, respectively. In the diameter range of 2.7 to 5.4 nm, the size dependence of n_2 coincided well with that calculated by a pseudoptential approach, suggesting that the discrete energy states of Si-ncs are responsible for the observed enhanced optical nonlinearity.

6.1 Introduction

Si-nc is a promising material towards the application of optical switching devices. Nonlinear optical refractive index (n_2) of Si-ncs has been reported to be enhanced more than two orders of magnitudes than that of bulk-Si in a relatively transparent energy range[2–5]. The elucidation of the origin of the large nonlinear optical response of Si-ncs has been attracting a great interest today.

There have been many reports on nonlinear optical response of various forms of Si-ncs. For example, a strong enhancement of the nonlinear optical response has been observed in chemically etched porous Si[6, 7], Si-ncs doped SiO_xN_y deposited by plasma enhanced chemical vapor deposition (PECVD)[8, 9], Si-ncs doped SiO_2 prepared by ion implantation[10], laser ablated Si-ncs deposited on quarts substrate[11, 12], Si-ncs doped

SiO_2 prepared by a sol-gel method[13], and so on. The nonlinear optical properties of Si-ncs depend strongly on the preparation method. The reported values of n_2 varied from $\sim 10^{-7}$cm^2/W to $\sim 10^{-13}$cm^2/W, and both positive and negative n_2 were reported for various forms of Si-ncs [6–13]. This implies that the origin of the enhancement may differ depending on the preparation methods and conditions. Therefore, further systematic studies for well-defined Si-nc samples are needed to elucidate the mechanism of large optical nonlinearity.

In this chapter, the nonlinear optical response of Si-ncs doped SiO_2 is studied for samples prepared by a conventional cosputtering method. Our samples are well-defined Si-ncs doped SiO_2, where the simple quantum size effect can explain its linear optical properties. For example, they show strong photoluminescence (PL) above the bandgap of bulk-Si (at around 1.4 eV). The origin of the PL is the band edge luminescence due to the recombination of quantum confined electron-hole pairs within Si-ncs, evidenced by the resonantly excited PL spectra[14], the temperature dependence of the PL lifetime [1], and resonant quenching of PL bands by energy transfer to nearby materials [15]. Since the quantum efficiency of the PL is rather high[16], the PL peak energy well coincides with the theoretically predicated band gap energy of Si-ncs[1]. The Si-nc samples are thus considered to be suitable for the systematic study to elucidate the mechanism of the nonlinear optical response of Si-ncs. In this paper, the size and photon-energy dependence of the nonlinear optical response of Si-ncs doped SiO_2 are discussed. These studies lead us to better understanding of the origin of the enhanced optical nonlinearity of Si-ncs.

6.2 Experimental details

Si-ncs doped SiO_2 was prepared by a co-sputtering method. Si and SiO_2 were simultaneously sputter-deposited in Ar gas on a quartz substrate and then the deposited SiO_x films were annealed in a N_2 gas (99.999 %) atmosphere for 30 min above 1100 °C to grow nanocrystals in the films. In this method, the size of Si-ncs can be controlled by changing the concentration of Si in the films or changing the annealing temperature (Ta). The size of Si-ncs was estimated by cross-sectional transmission electron microscopic (TEM) observations. The average diameter (D) was from 2.7 to 5.5 nm. The concentration of excess Si (C_{exSi}) ranges from 3 to 11 vol% , estimated by electron probe microscope analysis (EPMA). The thickness of the samples was estimated by a physical-contact-type surface roughness measurement and to be about 8 μm. PL spectra were measured by using a single grating monochromator and an InGaAs near-Infrared diode array. The spectral response of the detection system was calibrated with the aid of a reference spectrum of a standard tungsten lamp.

For the measurement of the nonlinear optical properties of Si-ncs, a Z-scan method was

used. Details of the z-scan method is found elsewhere[17]. Briefly, in the z-scan method, the tight focusing gaussian beam is vertically irradiated onto a sample and the sample is moved along the direction of the beam propagation (z axis). The transmitted light intensity is recorded as a function of the distance from the focal point (z). When whole transmitted light is detected (open aperture), the transmittance ($T_{op}(z)$) is determined by the nonlinear absorption coefficient (β), and its dependence on z is

$$T_{op}(z) = 1 + \frac{\beta I_0 L}{1 + (z/z_0)^2}, \tag{6.1}$$

where I_0, L, and z_0 are the peak intensity of the beam, sample thickness and the diffraction length of the beam, respectively. Note that T_{op} doesn't depend on the nonlinear refractive index (n_2) but does only on β, thus open aperture measurement provides the information on β.

When a small aperture is placed in front of the detector to cut peripheral region of the transmitted light (closed aperture), the transmittance (T_{cl}) depends both on n_2 and β . The information on n_2 is extracted by the division of T_{cl} by T_{op},

$$T_{cl}/T_{op}(z) = 1 + \frac{4\Delta\phi}{((z/z_0)^2 + 9)((z/z_0)^2 + 1)}, \tag{6.2}$$

where $\Delta\phi$ is the nonlinear phase change. n_2 is obtained from $\Delta\phi$ as,

$$n_2 = \frac{\lambda\alpha\Delta\phi}{2\pi I_0(1 - e^{-\alpha L})}, \tag{6.3}$$

where α and λ are the linear absorption coefficient and the wavelength of the beam, respectively.

For the gaussian beam, we used the mode-locked Ti:shaphire femtosecond laser with the pulse width of 70 fsec and the repetition frequency of 82 MHz. The photon energy was changed from 1.48 to 1.65 eV which overlaps PL emission energy bands of Si-ncs. The incident beam was focused on a sample by a lens with the focus length of 100 mm, and the beam waist and diffraction length determined by a knife edge method were 18 μm and 1.1 mm, respectively. The peak intensity of the beam was typically 10 GW/cm^2. No notable change of nolinear optical properties was observed in the intensity range of 0.5-20 GW/cm^2, suggesting that thermal effect is negligible in this measurement condition [8, 9]. The validity of the obtained data was checked by measuring a fused quarts plate as a reference.

6.3 Results and discussions

Figure 6.1 shows PL (left-hand axis) and absorption spectra (right-hand axis) of a typical sample (C_{exSi}=3.3 vol% , Ta=1100 °C, D=2.7 nm). A broad PL peak at around

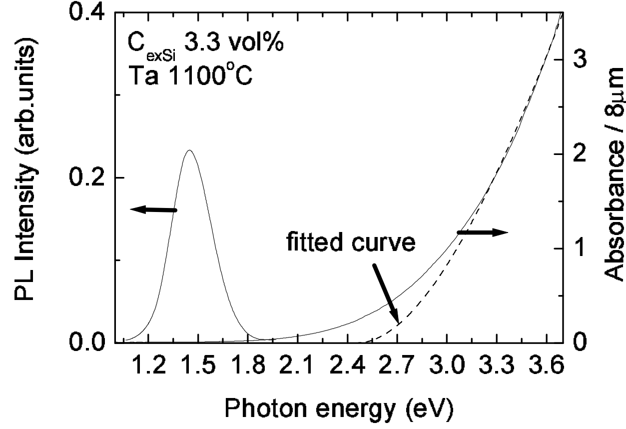

Figure 6.1: PL (left axis) and absorption (right axis) spectra of a typical sample (C_{exSi}=3.3 vol% , Ta=1100 °C, D=2.7 nm). The dashed line is a result of fitting by assuming an indirect bandgap semiconductor ($\sqrt{\alpha h\nu} \propto (h\nu - E_g)$). The optical bandgap is estimated to be 2.4 eV.

1.4 eV is assigned to the recombination of electron-hole pairs within Si-ncs. The optical bandgap (E_g) estimated from the absorption spectrum by using the $\sqrt{\alpha h\nu} \propto (h\nu - E_g)$ relation is around 2.4 eV. Therefore, in the energy range investigated in this paper (at around 1.6 eV), the samples are highly transparent.

Figure 6.2 shows typical results of z-scan measurements for (a) a closed aperture (T_{cl}) (b) an open aperture (T_{op}) and (c) the ratio (T_{cl}/T_{op}). Open squares and solid curves represent experimental data and fitted results, respectively. In Figs. 6.2(b) and 6.2(c), Eqs. (6.1) and (6.2), respectively, are used for the fittings. The solid curve in Fig. 6.2(a) is generated by using the parameters obtained by the fittings of Figs. 6.2(b) and 6.2(c). The agreement between the experimental data and the fitted curves is very good and the diffraction length estimated from the fitting well coincides with those measured by a knife edge method. The clear symmetrical valley to peak trace in Fig. 6.2(a) suggests that the sign of n_2 is positive and that the nonlinearity is mainly refractive. The analysis of the z-scan traces by equations (6.1)-(6.3) reveals that n_2 is $\sim 1.4 \times 10^{-13}$ cm^2/W and β is ~ 0.5 cm/GW, being similar values to previous reports [2, 8].

The observed n_2 is one order of magnitude larger than the bulk-Si value and 3 orders of magnitude than the amorphous SiO_2 value. In other words, addition of 3.3 vol% Si-ncs into SiO_2 results in as much as three orders of magnitudes enhancement of n_2 compared to SiO_2. It is worth noting that the linear refractive index of Si-ncs doped SiO_2 is explained simply by the volume ratio of Si and SiO_2 and is less than 1.6 in the present

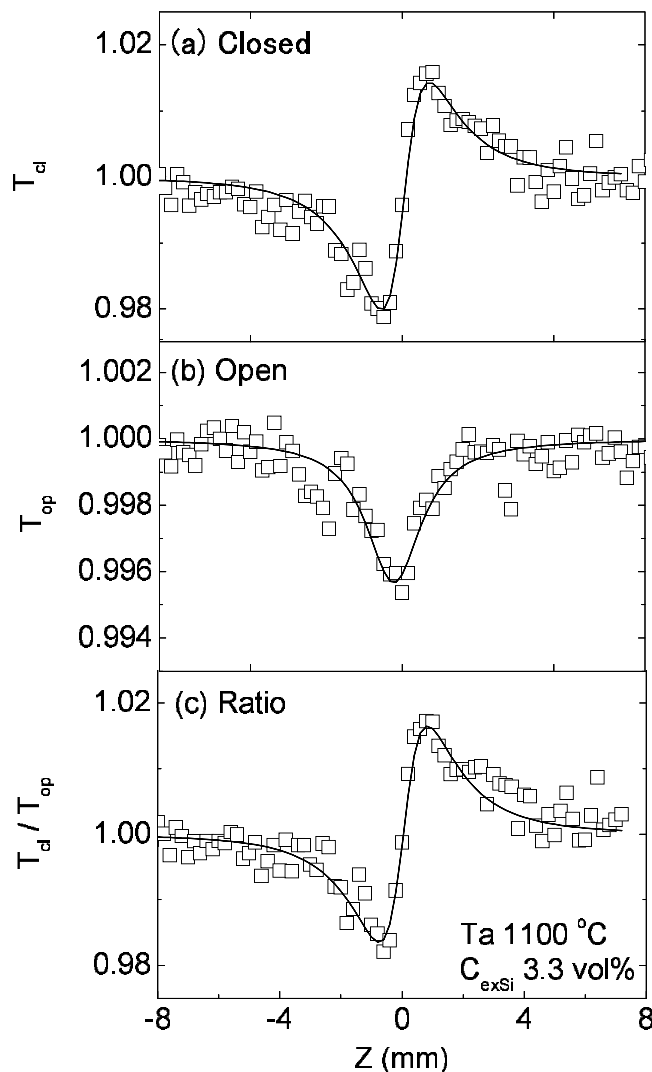

Figure 6.2: Results of z-scan measurements for (a) a closed aperture (T_{cl}), (b) an open aperature (T_{op}) and (c) the ratio of the two results (T_{cl}/T_{op}). The squares are experimental results and the solid curves are results of fittings.

case, being very close to that of amorphous SiO_2 . The small linear refractive index allows us to minimize the optical coupling loss with a conventional SiO_2 fiber. Therefore, both the linear and nonlinear refractive indices of Si-ncs doped SiO_2 are suitable for optical switching devices.

In order to elucidate the origin of the enhancement of n_2, the photon-energy dependence of n_2 and β is investigated. In Fig. 6.3, n_2(left-hand axis) and β(right-hand axis) are plotted as a function of photon energy. n_2 increases from 0.98×10^{-13} to 1.4×10^{-13}cm^2/W

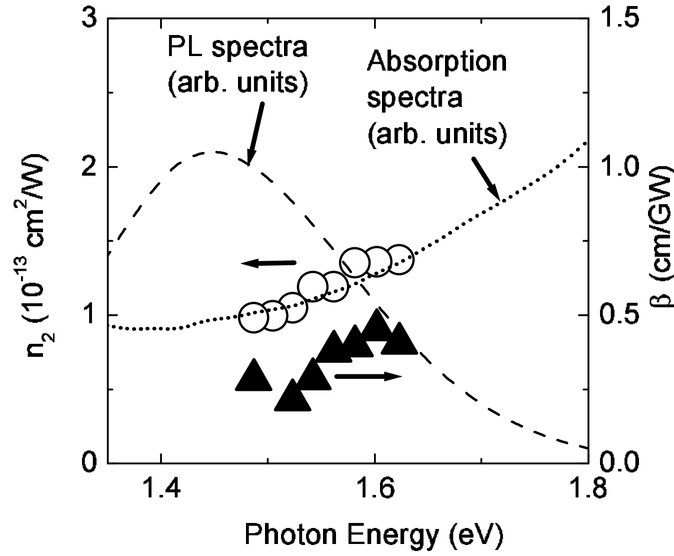

Figure 6.3: n_2 (left axis) and β (right axis) spectra of a typical sample (C_{exSi}=3.3 vol% , Ta=1100 °C, D=2.7 nm). The dashed and dotted curves are PL and absorption spectra, respectively.

with increasing the photon energy from 1.48 to 1.65 eV. Similarly, β increases from 0.3 to 0.5 cm/GW in the same range. The dashed and dotted lines are the PL and absorption spectra, respectively. A larger nonlinear optical response is obtained in a larger absorbance region, but not in a larger PL region. In the case of direct-bandgap semiconductors such as CuCl and CuBr, the nonlinear refractive index is the highest at the energy of the lowest level exciton absorption peak [18]. On the other hand, in absorption spectra of Si-ncs, clear features due to exciton absorption are not observed and the spectra are almost featureless [19]. The energy dependence of n_2 in Fig. 6.3 seems to follow the broad absorption spectra. Similar results were reported by Kanemitsu et.al. for porous Si [7]. They found by third harmonic generation measurements that third order nonlinear susceptibility ($\chi^{(3)}$) shows no enhancement in the PL spectrum region, and pointed out two possible mechanisms. First, phonon-assisted optical transitions and resultant small oscillator strength due to indirect bandgap nature of porous Si results in the small enhancement in the PL spectrum region. Second, the PL from porous Si may come not from the band-edge, but from surface or defect levels with small density of states. If the actual band-edge energy region is far from the PL spectrum region, the enhancement is not expected in the PL spectrum region.

Basically, the same discussion can be applied to understand the data in Fig. 6.3. However, in the present samples, as mentioned in the introduction, PL from Si-nc's can be

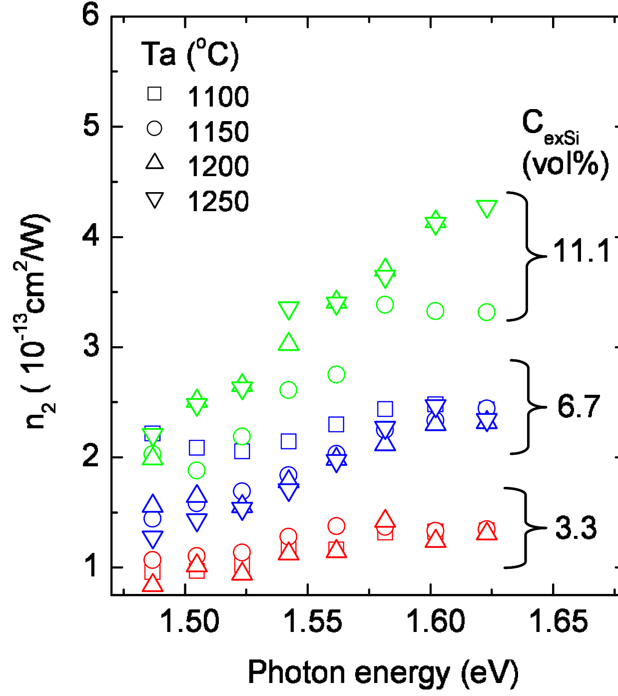

Figure 6.4: n_2 spectra of samples with different excess Si concentrations (C_{exSi}) and different annealing temperatures (Ta). The same colored (or shaped) symbols are used for the same C_{exSi} (or Ta) samples.

assigned to the band-edge luminescence due to the recombination of confined electron-hole pairs as evidenced by some kinds of experiments [1, 14, 15]. Thus the second hypothesis can be excluded. Probably, small oscillator strength due to the indirect bandgap nature causes the small enhancement at the PL energy.

The systematic control of the size and the concentration of Si-ncs provides further information to understand the mechanism of the large nonlinear response. In Fig. 6.4, the photon-energy dependence of n_2 for samples with different C_{exSi} and different Ta are shown. The same colored (or shaped) symbols are used for the samples with the same C_{exSi} (or Ta). For all the samples, n_2 is larger in higher photon energy. It is also interesting to note that n_2 strongly depends on C_{exSi}, while hardly does on Ta. In Fig. 6.5, C_{exSi} dependence of n_2 is shown. n_2 is nearly proportional to C_{exSi}, suggesting that C_{exSi} is a dominant factor to determine the nonlinear optical response of the samples.

From the experimentally obtained macroscopic nonlinear refractive index of the Si and SiO_2 composites, the microscopic nonlinear refractive index of Si-ncs ($\overline{n}_2$) is estimated by the relation $n_2 = pf^4\overline{n}_2$, where p is the Si volume fraction ($C_{exSi}/100$) and f is the local

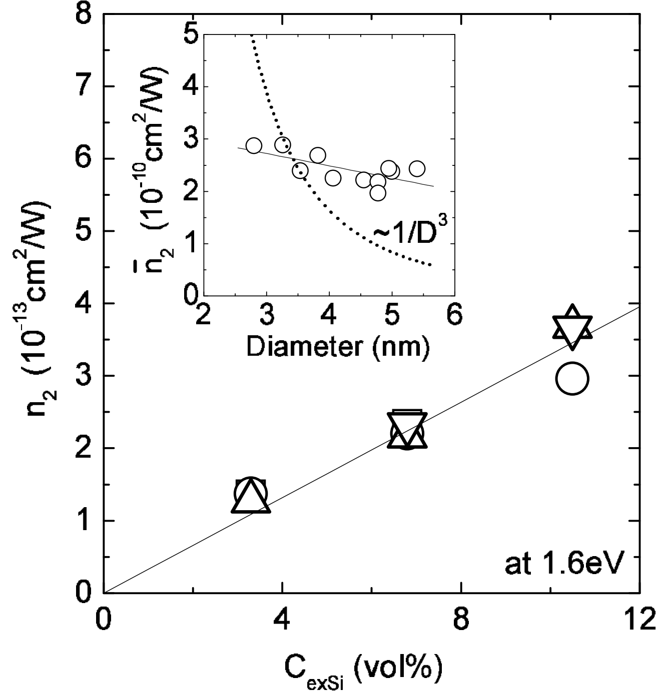

Figure 6.5: Si concentration dependence of n_2*. The inset shows the size dependence of the microscopic nonlinear refractive index of Si-ncs. The dotted line is a* $1/D^3$ *dependence predicted by a simple quantum confinment model*

field correction factor[20] given by $\frac{3\epsilon_{SiO_2}}{\epsilon_{SiO_2}+2\epsilon_{Si}}$, where ϵ_{SiO_2} and ϵ_{Si} are the real part of the dielectric constant of SiO_2 and Si. The estimated values of $\overline{n}_2$ are $2-3\times10^{-10}$ cm^2/W for all the samples and to be four orders of magnitudes larger than the bulk-Si value. In the inset of Fig. 6.5, the obtained $\overline{n}_2$ is plotted as a function of the diameter of Si-ncs. $\overline{n}_2$ increases slightly with decreasing the size of Si-ncs. This result is qualitatively consistent with other reports, where the modification of the band structure by the quantum confinement effect is suggested to be the origin of the enhancement of optical nonlinear response of Si-ncs[8, 9]. On the other hands, the result cannot quantitatively be explained by a simple quantum confinement model which predicts the enhancement with the $1/D^3$ dependence (D is the diameter of Si-ncs)[22] as shown by a dotted line in the inset of Fig. 6.5. While the model predicts as much as 8 times enhancement by the size reduction from 5.4 nm to 2.7 nm, the data shows the enhancement of only about 30% in the size range.

To our knowledge, quantitative discussion on the size dependence of nonlinear optical response of Si-ncs has been made only in limited number of papers [8, 9]. Vijaya, et. al. reported nonlinear optical response of Si-ncs doped SiO_xN_y prepared by PECVD

and demonstrated a strong enhancement of $\chi^{(3)}$ when the size of Si-ncs was very small (less than 1 nm) [9]. However, as they mentioned in the paper, the data were strongly scattered and thus the size dependence in the range of the present work was not very clear. Furthermore, the effect of Si concentration was not taken into account in the analysis. On the other hand, Hernandez et.al. discussed size dependence of $\chi^{(3)}$ by taking into account the Si concentration for similar Si-nc samples [8]. They observed $\sim 1/D^3$ dependence of $\chi^{(3)}$ and suggested that the modification of the band structure by the quantum confinement effect is responsible for the enhanced nonlinear optical response of Si-ncs. However, the discussion, i.e., the fitting of data points by the $\sim 1/D^3$ dependence, was based only on 3 experimental points, and thus the dependency is not very convincing.

The results of Fig. 6.5 shows for the first time detailed size dependence of the nonlinear optical response of Si-ncs. The observed deviation from $\sim 1/D^3$ dependence indicates that the nonlinear optical response of Si-ncs cannot be fully explained by the simple quantum confinement model. Recently, some investigations have revealed that the size dependence of the nonlinear optical response of semiconductor nanocrystals differs depending on the size range [21, 22]. In a strong confinement regime where the size is much smaller than that of the exciton Bohr radius (a_B), i.e., $D \ll 2a_B$, the nonlinear optical response increases with decreasing the size, while in a in a weak confinement regime ($D \gg 2a_B$), it increases with increasing the size [21–25]. The above mentioned simple quantum confinement model is the case of the strong confinement regime. Since the size range of Si-ncs studied in this work is comparable to the exciton Bohr radius of bulk Si, the competition of the two different size dependences may result in the observed small size dependence.

Very recently, H. Yilldirim. et.al. calculated the nonlinear optical properties of Si-ncs and Ge nanocrystals (Ge-ncs) in SiO_2 by an atomistic pseudopotential approach [26]. Their calculations focused on the third-order nonlinearities of Si-ncs by assuming no interface defects, no strain and thermal effects, and no compounding contribution of the excited carriers. They showed that $\chi^{(3)}$ of Si-ncs and Ge-ncs hardly depend on the size in the size range above 2.5 nm, while they significantly increase with decreasing the size in the size range below 2.5 nm. Since the size range of this work is 2.7 to 5.4 nm, the predicted small size dependence above 2.5 nm agree qualitatively with the present results. Furthermore, they predicted that $\chi^{(3)}$ of Si-ncs is about 4-5 orders of magnitudes enhanced compared to that of bulk-Si when the size is around 3.0 nm. This enhancement factor also coincides well with experimentally obtained ones (4 orders of magnitudes). These agreement may allow us to conclude that the discrete energy states of Si-ncs is responsible for the observed enhanced optical nonlinearity.

It should be mentioned here that defects within nanocrystals or at the surface can also cause the enhancement of the optical nonlinear response [27]. Takagahara, et.al. reported that localization of excitons at disorders or impurities enhances its oscillator strength, and

hence the nonlinear optical properties. They pointed out that sometimes this effect is more important than the dimensional confinement effect. In the model, the size dependence of the nonlinear optical response is expected to be very small. However, this model is considered to be not suitable to explain the observed enhanced nonlinear optical response of Si-ncs. As mentioned above, the nonlinear optical response of the present samples is hardly modified by annealing conditions. On the other hand, the quality, i.e, the defect density, of Si-ncs depends strongly on the annealing condition [16]. This inconsistency rules out the possibility of defect-related enhancement of the nonlinear response.

6.4 Conclusion

Nonlinear optical response of Si-ncs doped SiO_2 prepared by a co-sputtering method is studied by z-scan technique in a femtosecond regime at around 1.6 eV. An addition of a very small amount of Si-ncs into SiO_2 results in as much as three orders of magnitudes enhancement of n_2 compared to SiO_2 and one order of magnitude to bulk Si, while the linear refractive index is kept low (less than 1.6). The small index mismatch with a conventional SiO_2 fiber and the large nonlinear response make Si-ncs doped SiO_2 an ideal candidate for realizing Si-based optical switching devices. In order to elucidate the origin of the enhanced optical response, the size dependence of n_2 is studied in detail in the diameter range of 2.7 to 5.4 nm. We show that the size dependence is very small in the range, although small increase of n_2 with decreasing the size is observed. The observed size dependence agrees very well with that calculated by pseudoptential approach, suggesting that the discrete energy states of Si-ncs is responsible for the observed enhanced optical nonlinearity.

References

[1] S. Takeoka, M. Fujii, and S. Hayashi, Phys. Rev, B, **62**, 16820 (2000).

[2] S. Moon, A.Lin, B.H. Kim, P. R. Watekar, and Wan-Taek Han, J. Non-crystalline Solids, **354** (2008), 602.

[3] E. Koudoumas, O. Kokkinaki, M. Konstantaki, N. Kornilos, S. Couris S. Korovin, V. Pustovoi, V. E. Ogluzdin, Optical Materials, **30** (2007), 260.

[4] Fryad Z. Henari, Kai Morgenstern, and Werner J. Blau, Vladimir A. Karavanskii, and Vladimir S. Dneprovskii, Appl. Phys. Lett, **67** (1995), 323.

[5] Sudakshina Prusty, H.S. Mavi, and A. K. Shukla, Phys. Rev. B, **71**, 113313.

[6] S. Lettieri, and P. Maddalena, J. Appl. Physics, **91** (2002), 5564.

[7] Y. Kanemitsu, S. Okamoto, and A. Mito, Phys. Rev. B, **52** (1995), 10752.

[8] S. Hernandez, P. Pellegrino, A. Martinez, Y. lebour, B. Garrido, R. Spano, M. Cazzanelli, N. Daldosso, L. Pavesi, E. Jordana, and J. M. Fedeli, J. Appl. Phys., **103** (2008), 064309.

[9] G. Vijaya Prakash, M. Cazzaneli, Z. Gaburro, L. Pavesi, F. Lacona, G. Franzo, and F. Priolo., J. Appl. Phys., **91** (2002), 4607.

[10] S. Vijayalakshmi, H. Grebel, G. Yaglioglu, R. Pino, R. Dorsinville, C. W. White, J. Appl. Physics, **88** (2000), 6418.

[11] S. Vijayalakshmi, A. Lan, Z. lqbal, and H. Grebel, J. Appl. Phys. **92** (2002), 2490.

[12] S. Vijayalakshmi, M. A. George, and H. Grebel, Appl. Phys. Lett. **70** (1997), 708.

[13] E. Borsella, M. Falconieri, S. Botti, S. Martelli, F. Bignoli, L. Costa, S. Grandi, Luigi Sangaletti, B. Allieri, L. Depero, Materials Science and Engineering, B**79** (2001), 55.

[14] M. Fuji, D. Kovalev, J. Diener, F. Koch, S. Takkeoka, and S. Hayashi, J. Appl. Phys. **88** (200), 5772.

[15] K. Imakita, M. Fujii, and S. Hayashi, Phys. Rev. B, **71** (2006), 193301.

[16] S. Miura, T. Nakamura, M. Inui, and S. Hayashi, Phys. Rev. B, **73** (2006), 245333.

[17] M. Yin, H. P. Li, S. H. and Tang, W. Ji, Appl. Phys. **70** (2000), 587.

[18] Y. Li, M. Takata, and A. Nakamura, Phys. Rev. B **57** (1998), 9193.

[19] D. Kovalev, H. Heckler, G. Polisski, and F. Koch, Phys. stat. sol. (b) **215** (1999), 871

[20] C. Flytzanis, F. Hache, M. C. Klein, D. Ricard, and Ph. Roussignol, Progr. Opt. XXIX (1991), 323.

[21] E. Hanamura, Phys. Rev. B, **37** (1987), 1273.

[22] L. Banyai, Y. Z. Hu, M. Lindberg, and S. W. Koch, Phys. Rev. B, **38** (1988), 8142.

[23] S. V. Nair, and T. Takagahara, Phys. Rev. B, **55** (1997), 5153.

[24] S. Schumitt-Rink, D. A. B. Miller, and D. S. Chemla, Phys. Rev. B, **35** (1987), 8113.

[25] L. Belleguie, L. Banyai, Phys. Rev. B, **47** (1993), 4498.

[26] Hasan Yildirim, and Ceyhun Bulutay, Phys. Rev. B., **78** (2008), 115307.

[27] T. Takagahara, and E. Hanamura, Phys. Rev. Lett., **56** (1986), 2533.

Chapter 7

Nonlinear optical properties of Phosphorous-doped Si nanocrystals embedded in phosphosilicate glass thin films

In this chapter, nonlinear optical properties of phosphorus (P) -doped silicon (Si) nanocrystals are studied by z-scan technique in femtosecond regime at around 1.6 eV. The nonlinear refractive index (n_2) and nonlinear absorption coefficient (β) of Si-ncs are significantly enhanced by P-doping. The enhancement of n_2 is accompanied by the increase of the linear absorption in the same energy region, suggesting that impurity-related energy states are responsible for the enhancement of the nonlinear optical response.

7.1 Introduction

Silicon nanocrystal (Si-nc) is a topic of great interests in the field of optelectronics because of its high quantum efficiency of photoluminescence (PL) and relatively large nonlinear optical responses [1–6]. The large nonlinear optical response has been reported in various forms of Si-ncs such as porous Si prepared by electrochemical etching [7, 8], Si-ncs doped SiO_xN_y deposited by plasma enhanced chemical vapor deposition (PECVD) [9, 10], Si-ncs doped SiO_2 prepared by cosputtering [11], laser ablated Si-ncs deposited on quartz substrate [12, 13], and so on. In these literatures, dependence of the nonlinear optical response on the size and volume fraction of Si-ncs has been studied in detail.

Although the origin of the large nonlinear optical response is still not fully clarified, the quantum confinement effects are often believed to be responsible [9, 11].

It has been demonstrated experimentally [15–19] and theoretically [20–22] that the electronic band structure, and the resultant optical and electrical transport properties of Si-ncs are significantly modified by impurity doping. Experimentally, PL properties of Si-ncs were found to be very sensitive to the impurity doping [15–17]. The doping of either n- or p-type impurities results in strong quenching of the PL, due to efficient Auger process between photo-excited electron-hole pairs and impurity-supplied carriers [17]. The quenching can be suppressed by doping n- and p-type impurities simultaneously because of the compensation of carriers within Si-ncs. The PL of the codoped and compensated Si-ncs appears at very low energy; the PL peak reaches 0.9 eV in heavily-doped an compensated Si-ncs [15, 16]. These observed phenomena are successfully reproduced, at least qualitatively, by first principles calculations [20, 23].

In this chapter we study the effect of impurity doping on the nonlinear optical properties of Si-ncs by using the samples of phosphorus(P)-doped Si-ncs embedded in phosphosilicate glass (PSG) thin films. We show that P-doping further enhances the large nonlinear optical responses of Si-ncs and is thus an effective way to control the nonlinear optical properties of Si-ncs.

7.2 Experimental details

P-doped Si-ncs embedded in PSG thin films were prepared by a co-sputtering method. Si, SiO_2 and PSG were simultaneously sputter-deposited in Ar gas on a quartz substrate. Then the deposited films were annealed in a N_2 gas (99.999 %) atmosphere for 30 min at 1150 °C to grow nanocrystals in the films. The size of Si-ncs was estimated by cross-sectional transmission electron microscopy (TEM) observations [24]. The average diameter (D) was about 4.0 nm, and the standard deviation was about 1.0 nm. The concentration of excess Si (C_{exSi}) and P_2O_5 (C_P) were obtained by electron probe micro analysis (EPMA). C_{exSi} was about 6.7 vol% and P_2O_5 was changed from 0 to 1.2 mol% . The linear refractive indices were estimated from the volume ratio of Si and SiO_2 with the application of the Bruggeman effective medium theory [25] and was about 1.54 at 800 nm.

The thickness of the samples was estimated by physical-contact-type surface roughness measurement and was about 12μm. The evidence that P atoms are doped in substitutional sites of Si-ncs and are electrically active was shown in our previous work by infrared absorption and electron spin resonance (ESR) spectroscopy [19]. The nucleation of phosphorous particles can be ruled out because they are thermodynamically unstable in SiO_2 matrix.

PL spectra were measured by using a single grating monochromator and an InGaAs near-Infrared diode array. The spectral response of the detection system was calibrated with the aid of a reference spectrum of a standard tungsten lamp. For the measurement of the nonlinear optical properties, a z-scan method was used. Details of the z-scan method is discribed in seciton 6.2. For the gaussian beam, we used the mode-locked Ti:shaphire femtosecond laser with the pulse width of 70 fsec and the repetition frequency of 82 MHz. The photon energy was changed from 1.48 to 1.65 eV. The incident beam was focused on a sample by a lens with the focus length of 100 mm. The beam waist and diffraction length determined by a knife edge method were 18 μm and 1.1 mm, respectively. The peak intensity of the beam was typically 10 GW/cm^2. No notable change of nonlinear optical properties was observed in the intensity range of 0.5-20 GW/cm^2, suggesting that thermal effect was negligible in this measurement condition [9, 10]. The validity of the obtained data was checked by measuring a fused quartz plate as a reference.

7.3 Results and discussion

Figure 1 summarizes the PL and absorption properties of P-doped Si-ncs. Details of these properties are found in the literatures [17, ?]. In Figure 1(a), the absorption spectra of P-doped (C_P=0.8mol%) and pure Si-ncs are shown. In pure Si-ncs, absorption due to the valence-to-conduction-band transition starts at around 1.5 eV. In P-doped Si-ncs, in addition to the interband transition, intra-valence-band transitions appear below 1.3 eV. The observation of the intraband transitions evidences the doping of electrically active shallow impurities in Si-ncs [17, 19]. In Figure 1(a), we also notice that interband transition of P-doped Si-ncs near the band edge is larger than that of pure Si-ncs. This absorption enhancement is very similar to that observed in P-doped bulk Si [29, 30], and is probably due to the impurity-related states predicted by some theoretical calculations [31]; P-doping causes the formation of the energy state just below the conduction band of Si-ncs, and enhances the absorption near the band edge. It should be noted here that each Si-nc should have discrete impurity-related states, because the number of impurity atoms in Si-ncs is very small and hence the formation of an impurity band is not expected. Apparently, this seems to contradict with the observed very broad enhancement near the band edge. The broadness can be attributed to the inhomogeneities of the number- and position-distributions of P atoms within a Si-nc and the size- and shape-distributions of Si-ncs. It should be stressed here that the size of pure and P-doped Si-ncs is similar and thus the difference of the spectral shape cannot be attributed to the size difference.

The inset of Fig. 7.1(a) shows the PL spectra of pure and P-doped Si-ncs. Both samples exhibit a broad PL band at around 1.3 eV. The PL is assigned to the recombination of electron-hole pairs within Si-ncs. This is evidenced by the temperature and the photon-

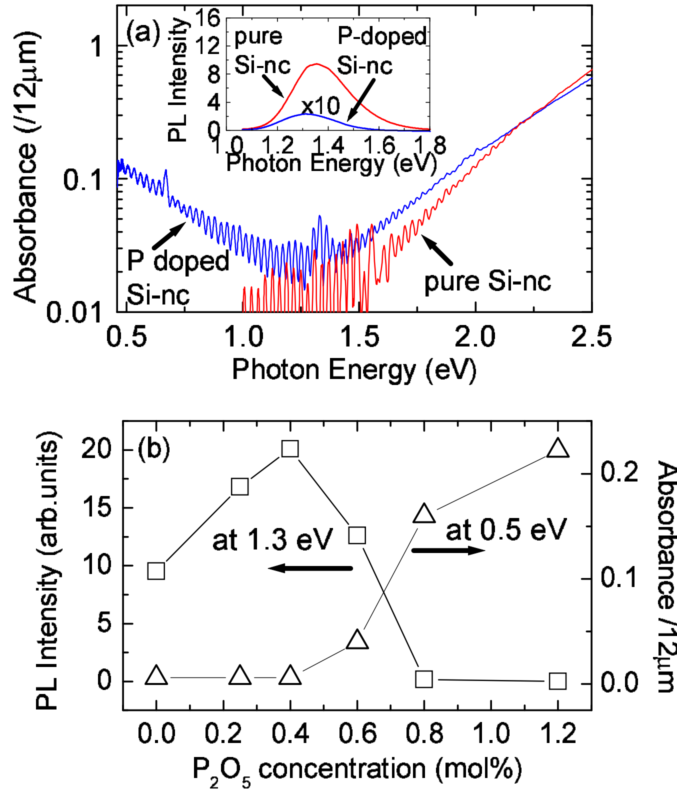

Figure 7.1: (a)Absorption spectra of pure and P-doped Si-ncs (C_P=0.8mol%). The inset shows the PL spectra of the same samples. (b)P_2O_5 concentration (C_P) dependence of PL intensity at 1.3 eV (Left axis) and absorbance at 0.5 eV (Right axis).

energy dependence of the PL-lifetime [2], and also by the resonantly excited PL spectra [27]. In Figure 7.1(b), PL intensity at 1.3 eV and absorbance at 0.5 eV are plotted as a function of C_P. In the lower C_P region (below 0.4mol%), no notable infrared absorption is observed, and PL intensity increases with increasing C_P. Carriers are thus not supplied within Si-ncs. The increase of the PL intensity in the C_P region is, as discussed in reference [28], considered to be due to the termination of dangling bond defects at the surface of Si-ncs by electrons supplied by doping. In the higher C_P region (above 0.6mol%), the infrared absorption increases and PL intensity decreases with increasing C_P. The PL quenching is accompanied by the shortening of the PL lifetime, and is considered to be nonradiative Auger recombination of photo-excited electron-hole pairs with the interaction with supplied carriers. It should be noted here that re-absorption by nearby clusters cannot explain the strong quenching because the samples are almost transparent in the energy range (optical transmittance $>$ 80%).

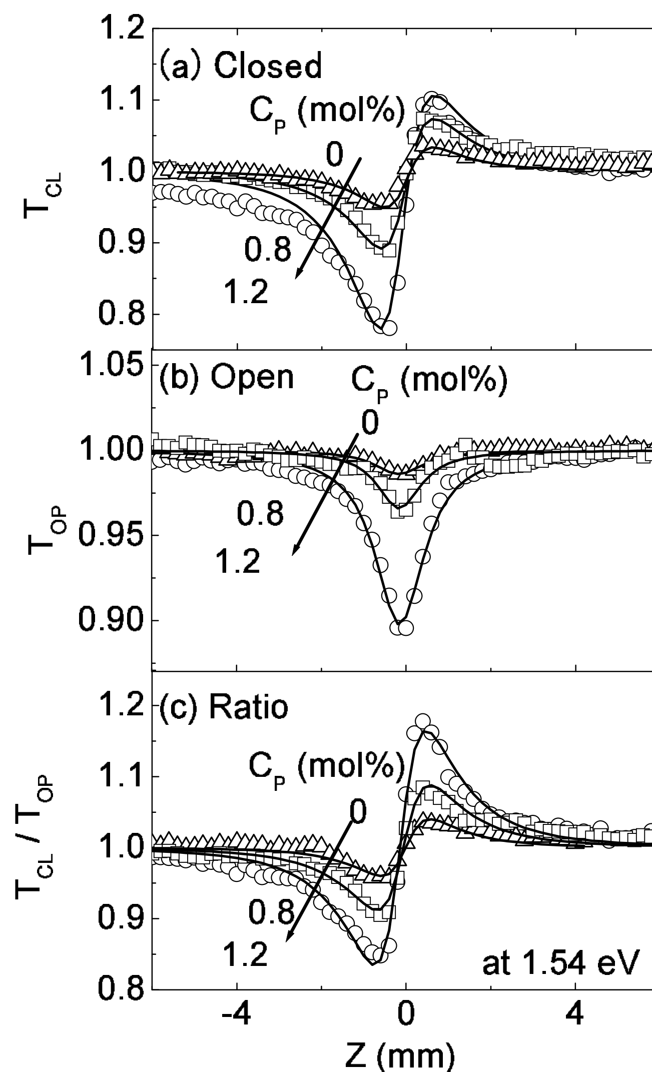

Figure 7.2: z-scan measurements for (a) a closed aperture (T_{cl}), (b) an open aperture (T_{op}) and (c) the ratio of the two results (T_{cl}/T_{op}). The squares are experimental results and the solid curves are results of fittings. P_2O_5 concentration (C_P) is changed from 0 to 1.2mol% .

Figure 7.2 shows the results of z-scan measurements for (a) a closed aperture (T_{cl}), (b) an open aperture (T_{op}), and (c) the ratio (T_{cl}/T_{op}). Open squares and solid curves represent experimental data and fitted results, respectively. In Figs. 7.2(b) and 7.2(c), Eqs. (6.1) and (6.2), respectively, are used for the fittings. The solid curve in Fig. 7.2(a) is generated by using the parameters obtained by the fittings of Figs. 7.2(b) and 7.2(c). The agreement between the experimental data and the fitted curves is very good and

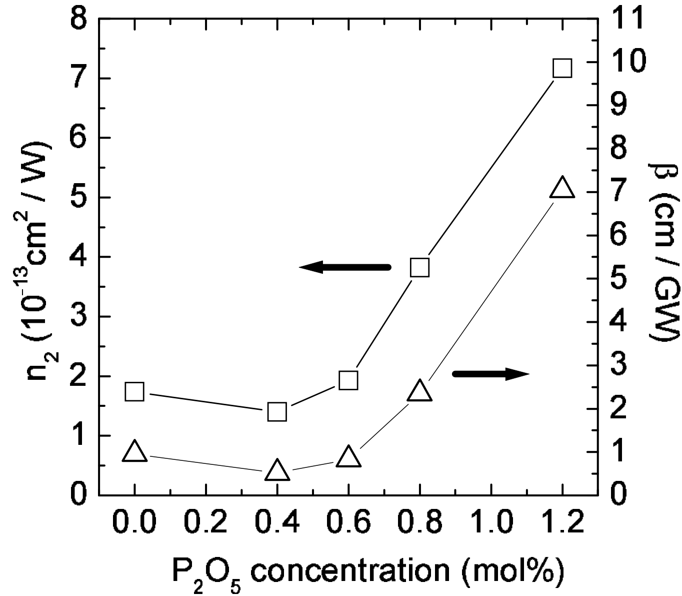

Figure 7.3: P_2O_5 concentration dependence of n_2 (left axis) and β (right axis).

the diffraction length estimated from the fitting coincides well with that measured by a knife edge method. In Fig. 7.2(c), all the z-scan spectra show valley to peak traces. This indicates that the sign of n_2 is positive for all the samples. We can see that the magnitude of the transmittance change depends on C_P. It increases with increasing C_P, suggesting that n_2 increases with increasing C_P.

Figure 7.3 shows the results of the analysis of the z-scan spectra. For the pure Si-ncs sample, i.e. C_P=0, the n_2 and β are $\sim 1.7\times10^{-13}$ cm^2/W and $\sim$ 1.0 cm/GW respectively. The observed n_2 is three orders of magnitudes larger than that of SiO_2, and one order of magnitude than that of bulk-Si.

Two different models have been proposed as the origin of the large n_2. The first one is a quantum confinement effect. This model has been proved by size-dependent n_2 enhancement [9]. The other one is that the surface state of Si-ncs is responsible for the large n_2. Klimov et al studied the transient absorption spectra of Si-ncs prepared by ion-implantation, and found a Si/SiO_2 interface state at around 1.6 eV, in addition to the size-dependent quantized states [32]. Vijayalakshumi et al showed that the surface state was responsible for the n_2 enhancement at around 1.6 eV in these samples [33, 34]. At present, no definite conclusion is obtained on the origin of the large n_2 and further intensive research is required to clarify the origin. However, since the investigation of pure Si-ncs is out of the scope of this work, we are going to focus on the effect of P-doping.

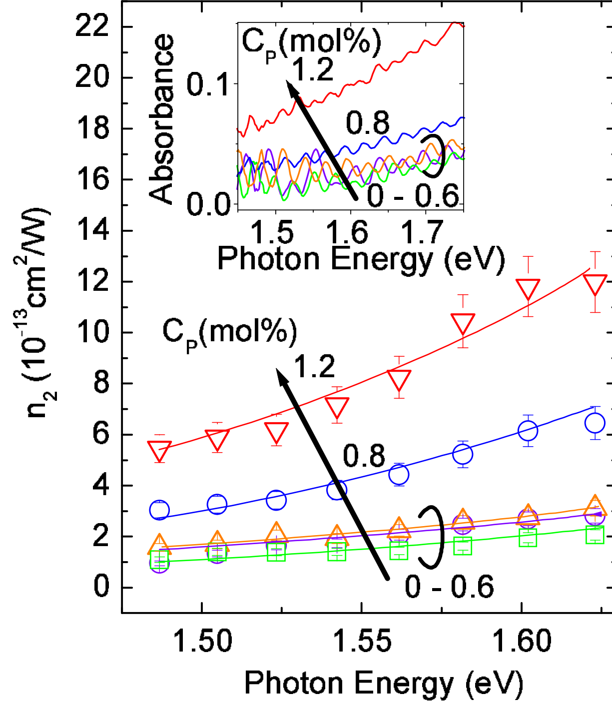

Figure 7.4: n_2 spectra of samples with different P_2O_5 concentration (C_P). The inset shows the absorption spectra of the same samples.

By P doping, n_2 increases from 1.7 to 7.0 $\times 10^{-13}$ cm^2/W, and β increases from 1.0 to 7.0 cm/GW. It is interesting to note that in the low C_P region, both n_2 and β are independent of C_P and are similar values to those of the pure Si-ncs sample. As shown in Figure 7.1, in the low C_P region, carriers are not generated within Si-ncs; supplied electrons are considered to be consumed for the termination of the dangling-bond-defects on the surface of Si-ncs. On the other hand, in the high C_P region, both n_2 and β increases with increasing C_P. One possible origin of this enhancement is the impurity-related state formed just below the conduction band of Si-ncs [31]. In the high C_P region, the states enhance optical absorption near the band edge of the Si-ncs. The enhanced absorption results in the enhancement of n_2.

In order to validate this possibility, we investigated the relation between n_2 and absorption. Figure 7.4 shows the photon-energy dependence of n_2. The error bars represents the fluctuation of average laser power and beam waist and also the estimation arising from the fitting procedure. For all the samples, n_2 increases with increasing the photon energy. The inset of Figure 7.4 shows the absorption spectra of the same samples. We

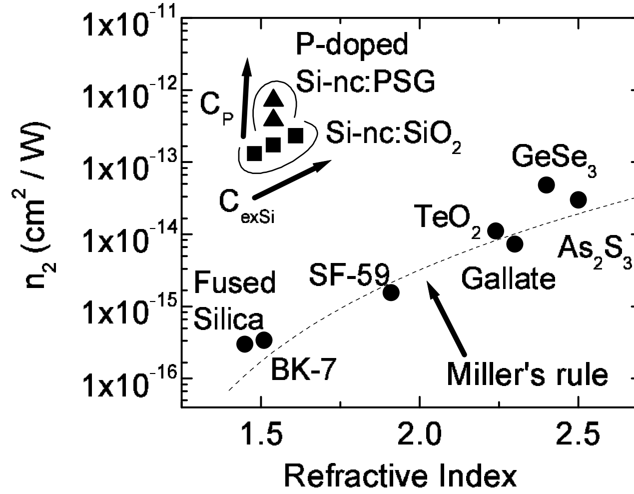

Figure 7.5: n_2 is plotted as a function of linear refractive index. The dashed line is the prediction of the Miller's rule. Circles, squares and triangles are the results of several kinds of typical glasses, P-doped Si-ncs embedded in PSG (P-doped Si-nc:PSG) and pure Si-ncs embedded in SiO_2 (Si-nc:SiO_2), respectively.

can see clear similarity between them. This suggests that the impurity-related state is responsible for the observed enhancement of the nonlinear optical response by P doping.

In Figure 7.5, n_2 is plotted as a function of a linear refractive index (n_0). The dashed line is the prediction of the Miller's rule [35, 36]. The circles, squares and triangles are the data of several kinds of glasses [37–40], P-doped Si-ncs embedded in PSG (P-doped Si-nc:PSG), and pure Si-ncs embedded in SiO_2 (Si-nc:SiO_2), respectively. C_{exSi} is changed from 3.3 to 10.5 vol% for Si-nc:SiO_2 and C_P is changed from 0 to 1.2mol% for P-doped Si-nc:PSG. The results of Si-nc:SiO_2 are quoted in our previous reports [11], where n_2 are obtained by the z-scan method with the same conditions as those of the present study. We can see that Si-nc:SiO_2 has relatively large n_2 and small n_0 compared to other typical glasses. For example, n_2 of Si-nc:SiO_2 is about three orders of magnitudes larger than that of a silica glass, while n_0 (=1.54) is similar to that of a silica glass. These properties are very suitable for the optical switching systems because smaller n_0 minimizes the optical coupling loss with the conventional SiO_2 fiber. As can be seen in Fig. 7.5, P-doping further enhances n_2 (at maximum 5 times) with no significant change of n_0. In this point, P-doped Si-ncs have great potential toward the realization of Si-based optical switching systems. It is definitely worth studying the n_2 of P-doped Si-ncs in other wavelength region, especially at around 1.5μm used in optical telecommunication industry.

7.4 Conclusion

Nonlinear optical properties of P-doped Si-ncs are studied by z-scan technique in femtosecond regime at around 1.6 eV. n_2 of Si-ncs is enhanced as much as 5 times by P-doping with no significant changes of n_0. This is a great improvement because generally the enhancement of n_2 is accompanied by the enhancement of n_0, which leads to the increase of the optical coupling loss with a conventional SiO_2 fiber. P-doped Si-nc is thus considered to be a promising candidate material for the realization of Si-based optical switching devices. We also showed that in the energy region of the n_2 enhancement, optical absorption is enhanced. This suggests that impurity-related energy states are responsible for the observed enhancement of the nonlinear optical response. The present results indicate that, in addition to the size and volume fraction of Si-ncs, impurity control is a parameter to control nonlinear optical responses of Si-ncs. Also, since this is, to our knowledge, the first report on the nonlinear optical properties of impurity-doped semiconductor nanocrystals, our study of P-doped Si-ncs will lead us to the better understanding of nonlinear optical properties of this kind of materials.

References

[1] L. T. Canham, Appl. Phys. Lett. **57,** 1046-1048 (1990).

[2] S. Takeoka, M. Fujii, and S. Hayashi, Phys. Rev. B **62,** 16820-16825 (2000).

[3] C. Delerue, M. Lannoo, G. Allan, and E. Martin, Thin Solid Films **255,** 27-34 (1995).

[4] P. Bettotti, M. Cazzanelli, L. Dal Negro, B. Danese, Z. Gaburro, C. J. Oton, G. Vijaya Prakash, and L. Pavesi, J. Phys:Condens. Matter, **14,** 8253-8281 (2002).

[5] L. Pavesi, Z. Gaburro, L. Dal Negro, P. bettotti, G. Vijaya Prakash, M. Cazzaneli, C. J. Oton, Opt. Lasers Eng., **39,** 345-367 (2003).

[6] S. Moon, A.Lin, B.H. Kim, P. R. Watekar, and Wan-Taek Han, J. Non-Cryst. Solids, **354,** 602-606 (2008).

[7] S. Lettieri, and P. Maddalena, J. Appl. Phys., **91,** 5564-5570 (2002).

[8] Y. Kanemitsu, S. Okamoto, and A. Mito, Phys. Rev. B, **52,** 10752-10755 (1995).

[9] S. Hemandez, P. Pellegrino, A. Martinez, Y. lebour, B. Garrido, R. Spano, M. Cazzanelli, N. Daldosso, L. Pavesi, E. Jordana, and J. M. Fedeli, J. Appl. Phys., **103,** 064309 (2008).

[10] G. Vijaya Prakash, M. Cazzaneli, Z. Gaburro, L. Pavesi, F. Lacona, G. Franzo, and F. Priolo., J. Appl. Phys., **91,** 4607-4610 (2002).

[11] K. Imakita, M. Ito, M. Fujii, and S. Hayashi, J. Appl. Phys. (to be published).

[12] S. Vijayalakshmi, A. Lan, Z. lqbal, and H. Grebel, J. Appl. Phys., **92,** 2490-2494 (2002).

[13] S. Vijayalakshmi, M. A. George, and H. Grebel, Appl. Phys. Lett., **70,** 708-710 (1997).

[14] M. Yin, H.P. Li, S.H. Tang, and W. Ji, Appl. Phys. B, **70,** 587-591 (2000).

[15] M. Fujii, Y. Yamaguchi, Y. Takase, K. Ninomiya, and S. Hayashi, Appl. Phys. Lett., **85,** 1158-1160 (2004).

[16] M. Fujii, Y. Yamaguchi, Y. Takase, K. Ninomiya, and S. Hayashi, Appl. Phys. Lett., **87,** 211919 (2005).

[17] A. Mimura, M. Fujii, S. Hayashi, D. Kovalev, and F. Koch, Phys. Rev. B, **62,** 12625-12627 (2000).

[18] B. J. Pawlak, T. Gregorkiewicz, C. A. J. Ammerlaan, W. Takkenberg, F. D. Tichelaar, and P. F. A. Alkemade, Phys. Rev. B, **64,** 115308 (2001).

[19] M. Fujii, A. Mimura, and S. Hayashi, Phys. Rev. Lett., **89,** 206805 (2002).

[20] G. Cantele, E. Degoli, E. Luppi, R. Magori, D. Ninno, G. Iadonisi, and S. Ossicini, Phys. Rev. B, **72,** 113303 (2005).

[21] G. Allan, C. Delerue, M. Lannoo, and E. Martin, Phys. Rev. B, **52,** 11982-11988 (1995).

[22] D. V. Melnikov, and J. R. Chelikowsky, Phys. Rev. Lett., **92,** 046802 (2004).

[23] S. Ossicini, F. Iori, E. Degoli, E. Luppi, R. Magri, R. Poli, G. Cantele, F. Trani, and D. Ninno, IEEE J. Sel. Top. Quantum Electron., **12,** 1585-1591 (2006).

[24] M. Fujii, S. Hayashi, and K. Yamamoto, J. Appl. Phys. **83,** 7953-7956 (1998).

[25] D. A. G. Bruggeman, Ann. Phys., **24,** 636-679 (1935).

[26] G. Lubberts, B. C. Burkey, F. Moser, and E. A. Trabka, J. Appl. Phys., **52,** 6870 (1981).

[27] M. Fuji, D. Kovalev, J. Diener, F. Koch, S. Takkeoka, and S. Hayashi, J. Appl. Phys. **88,** 5772-5776 (2000).

[28] M. Fujii, A. Mimura, and S. Hayashi, J. Appl. Phys., **87,** 1855-1857 (2000).

[29] P. E. Schmid, Phys. Rev. B, **23,** 5531-5536 (1981).

[30] V. Sa-yakanit, and H. R. Glyde, Phys. Rev. B, **22,** 6222-6232 (1980).

[31] E. L. de Oliveira, E. L. Albuquerque, J. S. de Sousa, and G. A. Farias, Appl. Phys. Lett., **94,** 103114 (2009).

[32] V. I. Klimov, Ch. J. Schwarz, and D. W. McBranch, and C. W. White, Appl. Phys. Lett., **73,** 2603-2605 (1998).

[33] S. Vijayalakshumi, H. Grebel, G. Yaglioglu, R. Pino, R. Dorsinville, and C. W. White, J. Appl. Phys., **88,** 6418-6422 (2000).

[34] S. Vijayalakshmi, H. Grebel, Z. lqbal, and C. W. White, J. Appl. Phys., **84,** 6502-6506 (1998).

[35] R. C. Miller, Appl. Phys. Lett., **5,** 17 (1964).

[36] C. C. Wang, Phys. Rev. B, **2,** 2045-2048 (1970).

[37] S. Kim, T. Yoko, S. Sakka, J. Am. Ceram. Soc. **76,** 2486-2490 (2005).

[38] N. Sugimoto, H. Kanbara, S. Fujiwara, K. Tanaka, Y. Shimizugawa, and K. Hirao, J. Opt. Soc. Am. B, **16,** 1904-1908 (1999).

[39] G. Lenz, J. Zimmermann, T. Katsufuji, M. E. Lines, H. Y. Hwang, S. Spalter, R. E. Slusher, S.-W. Cheong, J. S. Sanghera, and I. D. Aggarwal, Opt. Lett., **25,** 254-256 (2000).

[40] D. W. Hall, M. A. Newhouse, N. F. Borrelli, W. H. Dumbaugh, and D. L. Weidman, Appl. Phys. Lett., **54,** 1293 (1989).

Chapter 8

Conclusion

In this thesis, we studied Si nanocrystals-based photonics materials, such as Si nanocrystals doped SiO_2 (Si-ncs:SiO_2), P-doped Si-ncs:SiO_2, Er-doped Si-ncs:SiO_2 (Er:Si-ncs:SiO_2), and P- and/or B-doped Er:Si-ncs:SiO_2. All of these materials were found to have promising features for realizing Si-based photonics devices and the mechanisms were discussed.

In chapter 2, we studied Er:Si-ncs:SiO_2. In this material, Er^{3+} are known to show strong luminescence at room temperature due to the energy transfer from Si-ncs. Since the luminescence of Er^{3+} appears at 1.5μm, which is used as a standard wavelength in optical telecommunication, Er:Si-ncs:SiO_2 has attracted much attentions. In this chapter, the author tried to elucidate the energy transfer mechanism by analyzing the time resonse of the infrared luminescence from Er^{3+} just after short-time photo-excitation. After finishing the photo-excitation, the PL intensity of Er^{3+} continues to rise in several tens microseconds, due to the excitation by the energy transfer from Si-ncs. By analysing this rise part, it was found that there are two different energy transfer processes, i.e. slow and fast processes. The analysis also enable us to estimate the ratio of slow to fast processes, and energy transfer time of the slow process. The ratio and the energy transfer time is shown to depend on the Si-nc size and Er concentration. These give us a deep insight that the fast energy transfer is bulk-Si:Er-like, i.e., a trap-mediated energy transfer, and the slow one is a characteristic process occurring only in Er:Si-ncs:SiO_2 system.

In chapter 3, the energy transfer from Si-ncs to Er ions in Er:Si-ncs:SiO_2 was studied spectroscopically. At low temperatures, the author has shown that inhomogeneously broadened PL bands of Si-ncs are partially quenched due to resonant energy transfer to discrete electronic states of Er^{3+}. The observation of clear dips is the evidence that there is direct interaction between excitons in Si-ncs and Er^{3+}

In chapter 4, The interaction between Er^{3+} and shallow impurities in Si-ncs is studied for Er:Si-ncs:SiO_2. The luminescence property of Er^{3+} is strongly modified by shallow impurities in Si-ncs. The formation of excess carriers in Si-ncs by P or B doping results in the quenching of infrared PL of Er^{3+} and the shortening of the lifetime. When P and

B are doped simultaneously and carriers are compensated, the intensity and the lifetime are recovered. It is shown that the mechanism of the interaction is Auger de-excitation of excited Er^{3+} with the interaction of electrons or holes in Si-ncs. The estimated Auger coefficient is found to be two orders of magnitude smaller than that of Er doped bulk Si at low temperatures where carriers are bound to donor or acceptor ions, and four orders of magnitude smaller than that at room temperature. This small Auger coefficient makes Si-ncs immune from the impurity Auger de-excitation process compared to Er doped bulk Si and is considered to be responsible for temperature independent efficient PL of Er:Si-ncs:SiO_2 systems.

In chapter 5, by controlling the photonic mode density (PMD), we tried to improve the radiative recombination rate of electron-hole pairs within Si-ncs in Si-ncs:SiO_2 system. Time-resolved PL spectra of Si-ncs revealed that the radiative recombination rate of electron-hole pairs in spin-forbidden triplet states can be enhanced by the presence of Au half mirror, and that the degree of enhancement depends strongly on the emission photon energy. We showed that the observed enhancement can qualitatively be explained by that of PMD. The degree of the enhancement of the radiative recombination rate was larger than that predicted by theoretical calculations, suggesting that roughness on the Au mirror plays an important role for the enhancement, and by properly controlling the roughness, larger enhancement factor will be obtained.

In chapter 6, nonlinear optical response of Si-ncs:SiO_2 is studied by z-scan technique in a femtosecond regime at around 1.6 eV. An addition of a very small amount of Si-ncs into SiO_2 results in as much as three orders of magnitudes enhancement of n_2 compared to SiO_2 and one order of magnitude to bulk Si, while the linear refractive index is kept low (less than 1.6). The small index mismatch with a conventional SiO_2 fiber and the large nonlinear response make Si-ncs doped SiO_2 an ideal candidate for realizing Si-based optical switching devices. In order to elucidate the origin of the enhanced optical response, the size dependence of n_2 is studied in detail in the diameter range of 2.7 to 5.4 nm. We show that the size dependence is very small in the range, although small increase of n_2 with decreasing the size is observed. The observed size dependence agrees very well with that calculated by pseudoptential approach, suggesting that the discrete energy states of Si-ncs is responsible for the observed enhanced optical nonlinearity.

In chapter 7, nonlinear optical properties of P-doped Si-ncs:SiO_2 are studied by z-scan technique in femtosecond regime at around 1.6 eV. n_2 of Si-ncs:SiO_2 is enhanced as much as 5 times by P-doping with no significant changes of n_0. This is a great improvement because generally the enhancement of n_2 is accompanied by the enhancement of n_0, which leads to the increase of the optical coupling loss with a conventional SiO_2 fiber. P-doped Si-ncs:SiO_2 is thus considered to be a promising candidate material for the realization of Si-based optical switching devices. We also showed that in the energy region of the n_2

enhancement, optical absorption is enhanced. This suggests that impurity-related energy states are responsible for the observed enhancement of the nonlinear optical response. The present results indicate that, in addition to the size and volume fraction of Si-ncs, impurity control is a parameter to control nonlinear optical responses of Si-ncs.

Acknowledgment

The author would like to express his sincere gratitude to Professor Minoru Fujii for the critical reading of this thesis and the stimulating discussions leading to theoritical and experimental ideas implemented in this thesis. The author would like to thank Professor Shinji Hayashi for his enormous support and insightful comments throughout the course of this study. The author would like to express his profound gratitude to Professor Hidehiro Yasuda and Professor Takashi Kita for their fruitful discussions and valuable comments on this thesis.

The author want to make his deep acknowledgment to Associate Professor Kazuyuki Moriwaki for his continuous support and encouragement throughout the course of this study.

The author would like to express his heartfelt gratitude to Dr. Naoki Sugimoto (Asahi Glass. co. ltd.) for his continuous encouragement. The author would like to thank to Dr. Tomoharu Hasegawa (Asahi Glass. co. ltd.) and Dr. Madoka Ono(Asahi Glass. co. ltd.) for their experimental supports and excellent discussions.

This work has been done at Mesoscopic Material Laboratory, Department of Electrical and Electronics Engineering, Faculty of Engineering, Kobe University under the direction of Professor Minoru Fujii. The author wish to give his highest appreciation to his co-workers in the laboratory who have contributed to this work, particularly, to Mr. Masahiko Ito for his excellent technical assistance on the study of the nonlinear optical response of Si-ncs. The author greatfully thanks all collegues in the Mesoscopic Material Laboratory. In particular, usual and enjoyable discussions with Mr. Yasuhiro Yamaguchi, Mr. Nobuto Managaki, and Shingo Minobe are much appreciated.

Finally, the author is deeply indebted to his father, Tomio, to his mother, Terumi, to his brother, Yoshinori, and to all his friends for all their hearty support and endless encouragement till now, without which the author could not be able to achieve this work.

List of Publications

Journal Papers

[1] Kenji Imakita, Minoru Fujii, Yasuhiro Yamaguchi, and Shinji Hayashi "Interaction between Er ions and shallow impurities in Si nanocrystals" Physical Review B, Physical Review B Vol. 71, pp. 115440-1-7, (2005).

(Chapter 4)

[2] Kenji Imakita, Minoru Fujii, and Shinji Hayashi "Spectrally resolved energy transfer from excitons in Si nanocrystals to Er ions", Physical Review B Vol. 71, pp. 193301-1-4, (2005).

(Chapter 3)

[3] Kenji Imakita, Minoru Fujii, Toshihiro Nakamura, Satoru Miura, Eiji Takeda and Shinji Hayashi, "Enhancement of Radiative Recombination Rate of Excitons in Si Nanocrystals on Au Film", Japanese Journal of Applied Physics, Vol. 45, No. 8A, pp. 6132-6136, (2006).

(Chapter 5)

[4] Kenji Imakita, Masahiro Ito, Minoru Fujii, and Shinji Hayashi, "Nonlinear optical properties of Si nanocrystals embedded in SiO_2 prepared by a co-sputtering method", Journal of Applied Physics, Vol. 105, pp. 093531-093536, (2009).

(Chapter 6)

[5] Kenji Imakita, Masahiro Ito, Minoru Fujii, and Shinji Hayashi, "Nonlinear optical properties of Phosphorous-doped Si nanocrystals embedded in phosphosilicate glass thin films", Optics Express, Vol. 17, Issue 9, pp. 7368-7376, (2009).

(Chapter 7)

Conference Papers

[1] Kenji Imakita, Minoru Fujii, and Shinji Hyashi ”The mechanism of energy transfer from Si nanocrystals to Er ions in SiO_2 -Different mechanisms depending on Er concentration-” The European Physical Journal D, Vol. 34, pp. 161-163 (2005).

(Chapter 2)

Articles to which the auther also contributed

[1] Minoru Fujii, Kenji Imaktia, Kei Watanabe, and Shinji Hayashi ”Co-existence of two different energy transfer processes in SiO_2 films containing Si nanocrystals and Er” Journal of Applied Physics, Vol. 95, pp. 272-280 (2004).

[2] Toshihiro Nakamura, Minoru Fujii, Kenji Imaktia, and Shinji Hayashi ”Modification of energy transfer from Si nanocrystals to Er^{3+} near a Au thin film” Physical Review B, Vol. 72, pp. 235412 (2005).

[3] Kimihisa Matsumoto, Kenji Imakita, Minoru Fujii, and Shinji Hyashi ”Optical properties of Er and Si-nanocrystal co-doped SiO_2 films at a high Er concentration regime” International Journal of Modern Physics B, pp. 2598-2603 (2005).

[4] Kimihisa Matsumoto, Kenji Imakita, Minoru Fujii, and Shinji Hyashi ”Photoluminescence from Si Nanocrystals Embedded in SiOxNy Thin Films” Japanese Journal of Applied Physics, 2005, Vol. 44, L1547-L1549(2005).